



## UvA-DARE (Digital Academic Repository)

### Towards greater selectivity and peak capacities in multidimensional separations of complex samples

Roca, L.S.

**Publication date**

2022

**Document Version**

Final published version

[Link to publication](#)

**Citation for published version (APA):**

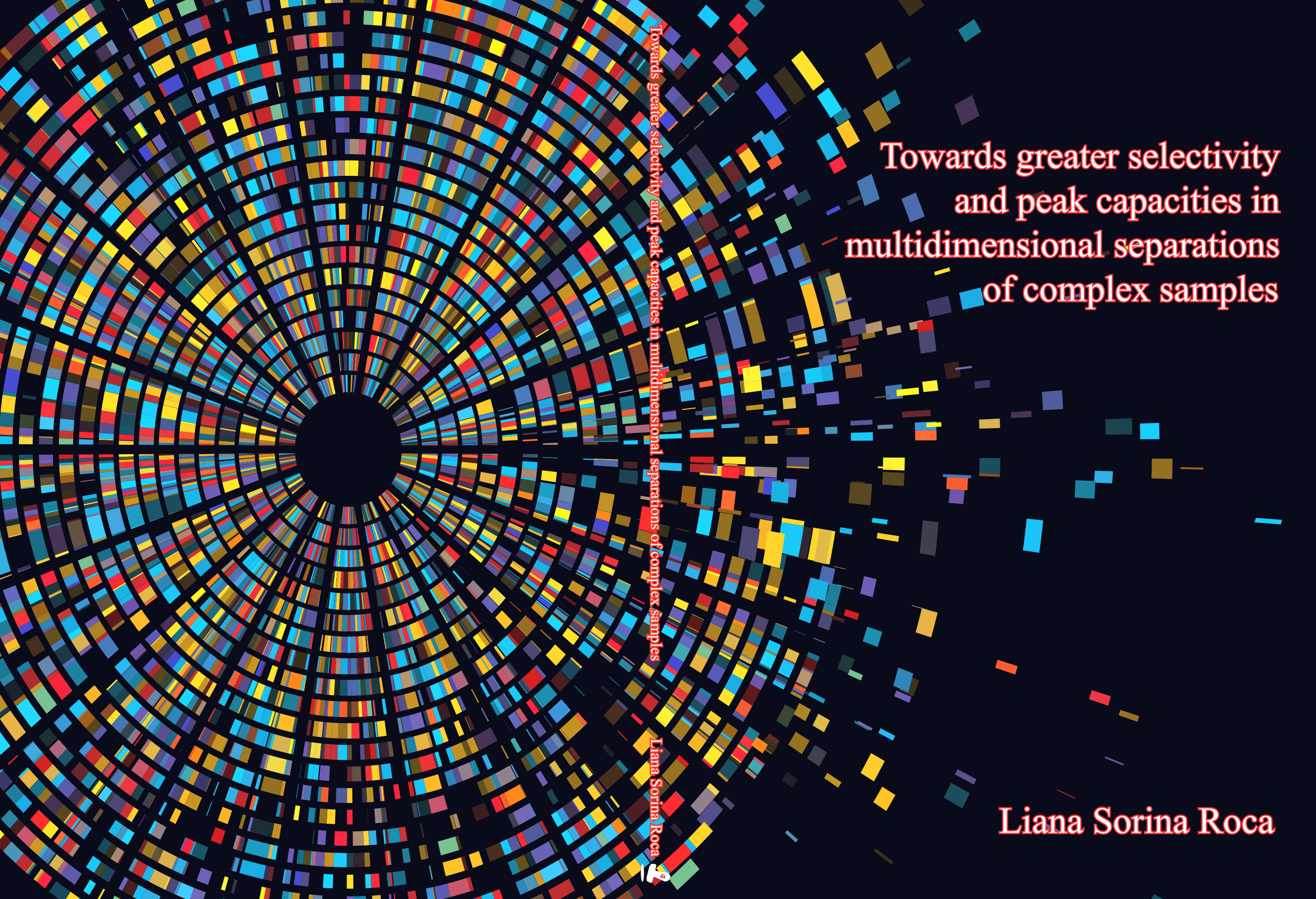
Roca, L. S. (2022). *Towards greater selectivity and peak capacities in multidimensional separations of complex samples*. [Thesis, fully internal, Universiteit van Amsterdam].

**General rights**

It is not permitted to download or to forward/distribute the text or part of it without the consent of the author(s) and/or copyright holder(s), other than for strictly personal, individual use, unless the work is under an open content license (like Creative Commons).

**Disclaimer/Complaints regulations**

If you believe that digital publication of certain material infringes any of your rights or (privacy) interests, please let the Library know, stating your reasons. In case of a legitimate complaint, the Library will make the material inaccessible and/or remove it from the website. Please Ask the Library: <https://uba.uva.nl/en/contact>, or a letter to: Library of the University of Amsterdam, Secretariat, P.O. Box 19185, 1000 GD Amsterdam, The Netherlands. You will be contacted as soon as possible.



Towards greater selectivity  
and peak capacities in  
multidimensional separations  
of complex samples

Towards greater selectivity and peak capacities in multidimensional separations of complex samples

Liana Sorina Roca



Liana Sorina Roca

Towards greater selectivity and peak capacities in multidimensional separations  
of complex samples

## ACADEMISCH PROEFSCHRIFT

ter verkrijging van de graad van doctor  
aan de Universiteit van Amsterdam  
op gezag van de Rector Magnificus  
prof. dr. ir. P.P.C.C. Verbeek

ten overstaan van een door het College voor Promoties ingestelde commissie,  
in het openbaar te verdedigen in de Agnietenkapel  
op donderdag 27 oktober 2022, te 16.00 uur

door Liana Sorina Roca  
geboren te Boekarest

**Promotiecommissie**

<i>Promotor:</i>	prof. dr. ir. P.J. Schoenmakers	Universiteit van Amsterdam
<i>Copromotor:</i>	dr. A. Gargano	Universiteit van Amsterdam
<i>Overige leden:</i>	prof. dr. A.C. van Asten	Universiteit van Amsterdam
	prof. dr. G.W. Somsen	Vrije Universiteit Amsterdam
	prof. dr. G.L. Corthals	Universiteit van Amsterdam
	dr. B.W.J. Pirok	Universiteit van Amsterdam
	dr. ir. M.T. Ackermans	Universiteit van Amsterdam
	prof. dr. G.E. Morlock	Justus-Liebig-Universität Giessen
	prof. dr. D.V. McCalley	University of the West of England - UWE Bristol

Faculteit der Natuurwetenschappen, Wiskunde en Informatica

The work in this thesis was financially supported by the STAMP Separation Technology for A Million Peaks (Grant agreement ID: 694151) project which is funded by the European Research Council (ERC) and the European Commission in the framework of Horizon 2020





Chapter 1 Introduction

Chapter 2 How two-dimensional liquid chromatography can benefit from recent technological advances

Chapter 3 Accurate modelling of the retention behavior of peptides in gradient-elution hydrophilic interaction liquid chromatography

Chapter 4 Development of comprehensive two-dimensional low-flow liquid-chromatography setup coupled to high- resolution mass spectrometry for shotgun proteomics

Chapter 5 Introduction of octadecyl-bonded porous particles in 3D-printed transparent housings with multiple outlets

Chapter 6 Conclusion/ future outlook

# Chapter 1

## Introduction

### Contents

1.	Need for high resolving power .....	5
2.	Retention mechanisms in LC .....	7
3.	Separation power .....	12
4.	Orthogonality .....	16
5.	Implementations of multidimensional separations .....	19
6.	Conclusion .....	26
7.	Scope of this thesis .....	27
8.	References .....	28

## 1. Need for high resolving power

Liquid chromatography (LC) is one of the most-used tools in analytical chemistry [1]. Its great separation power can be used for sample analysis, sample fractionation or sample purification. In recent years the attainable speed of separation has been enhanced by the introduction of smaller (sub-2- $\mu\text{m}$ ) particles, while the attainable separation efficiency has grown, due to the development of ultra-high performance liquid chromatography (UHPLC; pressures exceeding 100 MPa) and longer columns and by the application of elevated temperatures. However, the separation efficiency obtainable with one dimensional separation (1D-LC) is not always enough.

It has been shown that with 1D-LC a maximum peak capacity of little more than 1000 can be obtained [2,3]. In the case of complex samples of more than 1000 components a very much higher peak capacity is needed. If the peaks are randomly distributed across the chromatogram, a required excess peak capacity of a factor 20 has been estimated [4]. One of the fields in which we encounter samples with a high degree of complexity, which current separation techniques cannot fully resolve, is proteomics. The human proteome comprises of about 100 000 proteins encoded by over 20 000 genes [5]. The samples can gain even higher levels of complexity due to post-translational modifications and/or digestion prior to analysis. The most used workflow for proteomics samples is digestion of proteins [6], peptide separation using liquid chromatography (LC), detection with high-resolution mass spectrometry (HRMS), and identification based on spectral matching using peptide data bases. The current limitation for elucidating proteomics samples are the LC and MS technologies that lack the needed resolving power [7].

## Chapter 1

In the last years, multidimensional liquid-chromatographic systems were introduced as a way of gaining separation power. These can be either time-based separations or spatial separations that can be performed online or offline. In offline 2D-LC fractions are collected first and then analysed on an independent second-dimension system. Two-dimensional liquid chromatography (2D-LC) is the most established multidimensional technique. It can be either comprehensive (LC×LC), where all components are transferred from one dimension to the other, or “heart-cut” separations, where only some analytes of interest are separated in the second dimension. The best example of a spatial comprehensive two-dimensional separation system is poly(acryl amide) gel electrophoresis (2D-PAGE). It employs iso-electric focussing in the first dimension and a size-based gel-electrophoretic separation in the second dimension. 2D-PAGE provides very high separation power, but it is very slow, lacks reproducibility, and is notoriously difficult to combine with the all-important mass spectrometry [8]. Recent studies, have described the development of chip-based separations that in the future may provide much faster and high-efficiency separations by employing spatial separations [9–13].

Challenges encountered when developing multidimensional separations include the selection of appropriate separation mechanisms that can provide different types of retention in each dimension. Additional obstacles encountered in time-based LC×LC include sample transfer and dealing with solvent incompatibilities between the dimensions. In the case of chip-based separations, the design can allow for multiple channels in the second (<sup>2</sup>D) or third dimension (<sup>3</sup>D), or a continuous bed of stationary phase. Fundamentally, spatial separations reduce the analysis time, thanks to the simultaneous development in the <sup>2</sup>D or <sup>3</sup>D. To make such novel spatial 2D separations successful, additional aspects must be considered, such as appropriate design

and material of the device, flow confinement between the dimensions, implementation of stationary phases, and appropriate means of detection.

Some of these challenges and ways in which they may be overcome will be discussed in the following sections of this chapter.

## 2. Retention mechanisms in LC

An advantage of LC over gas chromatography (GC) and capillary electrophoresis (CE) is the possibility of employing very different retention mechanisms to meet the requirements of the desired application. For choosing an appropriate selectivity we need to consider the sample properties, the stationary-phase chemistry, the mobile-phase composition and, in case of large molecules, the pore size. Some key characteristics of the sample that can be exploited to achieve separation, also known as sample dimensions [14], can be the carbon-chain length, polarity, size, *etc.* Based on the sample, an appropriate stationary-phase can be selected that provides the needed interaction. The separation can be tuned by adapting the mobile-phase composition, pH buffers, and additives. Some of the main separation mechanisms are described in *Table 1*.

The most-used separation mode is reversed-phase liquid chromatography (RPLC), where – by definition – the mobile phase is more polar than the stationary phase. The stationary phase is typically formed of porous-silica particles, modified with aliphatic (most commonly octadecyl, C<sub>18</sub>, chains) or aromatic ligands to obtain a hydrophobic surface [15]. The retention mechanism is partition between the solvated hydrophobic surface and the mostly polar mobile phase. The separation can be performed either in isocratic (constant mobile-phase composition) or gradient (varying mobile-phase composition) mode. In the latter case the mobile phase initially contains a

## Chapter 1

large fraction of water and has the concentration of an organic solvent (“modifier”) increase during the run to facilitate elution. When silica particles are used for the stationary-phase support, residual (ionizable) silanol groups can interact with the analytes. Electrostatic interactions with silanols can be minimized by using acidic additives to lower the pH below 4, where the silanol groups are protonated. However, the use of high pH in RPLC has shown to exhibit higher retention and better separation of basic analytes, while a low pH yields higher retention for acidic compounds.

Another separation mechanism that is still widely used is ion-exchange chromatography (IEC). The advantage of this technique is that mostly aqueous mobile phases can be used [16]. Salts are added to the mobile phase and elution can be achieved by increasing the ionic strength, by a pH gradient or a combination of the two [17]. Depending on the ligands used on the stationary phase, the separation mode can be either cation exchange (negatively charged ligands) or anion exchange (positively charged ligands), with either strong (permanently charged) or weak (pH-dependent) charged groups. Occasionally, hydrophobic interactions may also occur in IEC, but they can be suppressed by adding organic modifiers, such as acetonitrile to the mobile phase [18]. Limitations of the technique are the need to detect the analytes in effluents containing high salt concentrations, and limited selectivity for the separation of similar analytes (*e.g.* peptides eluting in clusters based on their charge state) [15].

Hydrophilic-interaction liquid chromatography (HILIC) was named in 1990 [19] and is based on highly polar (normal-phase) stationary-phases. The mobile phase is largely organic, but always contains a fraction of water, which is thought to form an aqueous immobilized layer on the stationary phase. In the case of HILIC, polar groups will play a major role in the retention of the analytes on the column. The mobile phase usually contains at least 3% water

initially. Addition of acids (*e.g.* trifluoroacetic acid, TFA, or formic acid, FA) or salts (*e.g.* volatile salts, such as ammonium acetate or formate) have been shown to lead to improved peak shapes [20,21]. The perceived water layer on the surface of the polar stationary phase allows for the analytes to partition from the mostly organic bulk mobile-phase. However, electrostatic interactions can also influence the retention. Elution is facilitated by increasing the polarity of the mobile phase, hence the water content.

*Table 1: Summary of retention mechanisms and possible favourable combinations*

<b>LC separation mode</b>	<b>Acronym</b>	<b>Favourable combinations</b>	<b>Separation conditions</b>
Reversed phase	RPLC	HILIC, IEC, HIC, RPLC, SECaq	Retention at highly aqueous conditions and elution at increasing organic-solvent concentrations. Retention based on the hydrophobic character of analytes
Hydrophilic interaction	HILIC	RPLC, SECaq	Retention at high organic-solvent concentrations and elution at increasing water concentrations. Usually salts, such as ammonium formate/acetate are used (5-100 mM). Retention based on partitioning in water layer on stationary-phase surface, with possible strong H-bonding and electrostatic interactions
Ion exchange	IEC	RPLC, SECaq	Salts gradients or pH gradients are used to elute analytes. Basic conditions are common for anion-exchange and acidic conditions for cation-exchange chromatography.  Retention is based on electrostatic interactions
Hydrophobic interaction	HIC	RPLC	Retention at very high salt concentrations and elution upon decreasing salt concentration. The stationary phase is less retentive

## Chapter 1

Table 1: Summary of retention mechanisms and possible favourable combinations

LC separation mode	Acronym	Favourable combinations	Separation conditions
Size exclusion	SECaq SECorg	RPLC, HILIC, IEC; NPLC	then those used in RPLC ( <i>e.g.</i> short alkyl ligands). Either aqueous (aq) or organic (org) eluents. Separation based on size, due to (partial) penetration into the pores, without interaction with the stationary-phase surface.
Normal phase	NPLC	SECorg	Non-polar or moderately polar mobile-phase, with more-polar stationary phase. Retention based on polar interactions.
Immobilized-metal-ion affinity	IMAC	RPLC, HILIC, SECaq	Retention based on selected affinity ( <i>e.g.</i> TiO <sub>2</sub> for enriching phosphopeptides)

Peptide mixtures have been analysed using many different LC retention mechanisms. All of these may potentially be useful, due to the high sample dimensionality. The sample dimensionality, as introduced by Giddings in 1995 [14], considers the sample properties, which ideally should be correlated with the retention mechanism (separation dimensions). As an example a homologous series (*e.g.* *n*-alkanes) or a sample of a linear homopolymer with given end-groups (*e.g.* polystyrene) has only one sample dimensionality, the chain length. In this case the use of multidimensional separations is anticipated to provide no improvement compared to a one-dimensional separation. When considering peptides, among the many dimensions (including the numbers and types of the various amino acids, their sequence, *etc.*) two overall characteristics may be dominant, *viz.* hydrophobicity and charge. We can exploit the various dimensions and separate complex peptide samples using either reversed-phase LC [22] (RPLC, hydrophobicity), ion-exchange

chromatography [18] (IEC, charge), size-exclusion chromatography [23] (SEC, molecular size), hydrophilic-interaction LC [24] (HILIC, hydrophilicity), or metal-affinity chromatography (post-translational modifications, *e.g.* phosphorylation [25]). Some retention mechanisms and favourable combinations are summarized in Table 1.

One-dimensional liquid chromatography (1D-LC) offers great possibilities for determining the composition of samples in a variety of fields. However, in case of complex mixtures 1D-LC does not suffice to characterize all the components present. Proteomics samples are a case in point. To increase the number of components that are resolved, extra selectivity is needed. One solution for proteomics samples has been the use of mass spectrometry (MS), adding separation based on mass-to-charge ratio. In most cases the coupling between LC and MS can be easily accomplished. However, there are also limitations, for example, the analytes should be present at similar concentrations, a limited number of analytes should be introduced into the MS at any one time, and the analytes and mobile phase should be compatible with the MS. MS is of enormous value for protein analysis and it should always be used if at all possible. However, given the large number of sample dimensions and the limitations of LC-MS, more separation dimensions are needed.

A good way to introduce more separation power is to use multidimensional systems, with different selectivities and high separation efficiencies in each dimension. Two-dimensional separations are the most established, but some three-dimensional separations have also been reported [26]. The step from 1D-LC to on-line comprehensive 2D-LC (LC $\times$ LC) offers a great leap in peak capacity and peak-production rate (*i.e.* peak capacity per unit time). By now LC $\times$ LC is well-developed, robust and automated. The columns in the two dimensions are commonly coupled using a 10-port or an 8-port two-position valve, equipped with two identical loops or trap columns. This allows the

entire <sup>1</sup>D effluent to be divided in many fractions, all of which are submitted to the <sup>2</sup>D column for additional separation. To maximize the gain in selectivity the two columns need to employ very different retention mechanisms. Moreover, the phase systems used need to be compatible, with the <sup>1</sup>D effluent typically acting as the <sup>2</sup>D injection solvent.

Pirok *et al.* discussed many different separation mechanisms and speculated on favourable combinations based on potential peak capacity, phase-system compatibility, independence of retention mechanisms, and time needed for equilibration [27]. The most-important and most-favourable combinations are included in *Table 1*. However, less-favourable combinations are still possible, depending on applications or setups used. For instance, combining RPLC and NPLC, which is generally deemed unfavourable, would be a highly attractive combination in terms of selectivity if the issue of solvent incompatibility can be rigorously dealt with [28].

Below, the most-important aspects of multidimensional LC will be discussed, *i.e.* separation power (efficiency and peak capacity), selectivity (orthogonality), and the various possible implementations.

### 3. Separation power

The concept of peak capacity was introduced to quantify the maximum number of components that can be separated in a chromatographic measurement [29]. When separations of complex samples are involved, resolution is not a good measure of separation efficiency, due to inevitable coelution. Instead, peak capacity can be used and it can be described by the following equation

$$n_c = 1 + \int_{t_0}^{t_R} \frac{1}{4\sigma} dt \quad (1)$$

where  $t_0$  represents the elution time of an unretained compound [30].

In practice, complex mixtures are invariably eluted under programmed conditions (temperature programming in GC or gradient-elution in LC). In the latter case the peak capacity can be calculated based on the gradient time ( $t_g$ ) and the average peak width at the base ( $w$ ) of analytes ( $n$ )

$$n_c = 1 + \frac{t_g}{(1/n) \sum_1^n w} \quad (2)$$

A separation of  $n_c$  peaks in a one-dimensional chromatogram can only be achieved if all the analytes give rise to a series of equidistant peaks throughout the separation. Conceptually, this may be achieved for a homologues series, but never for more-complex samples. In practice a random distribution of peaks is expected. Assuming a Poisson distribution of peaks, Davis and Giddings have shown that the number of compounds that can be fully resolved is only a fraction of the calculated peak capacity [4]. Nevertheless, the peak capacity is a very good indication of the separation power of a chromatographic system.

In packed-column LC the peak capacity can be increased by decreasing the particle size (keeping the column length constant), increasing the column length, or using longer, shallower gradients. However, the total peak capacity of a 1D separation has been found to be limited to about 1500, using a very long gradient [3]. When using comprehensive two-dimensional LC (LC×LC) or multidimensional separations, the total peak capacity can be approximated by the product of the peak capacities in each dimension.

$${}^{3D}n_c \approx {}^1n_c \times {}^2n_c \times {}^3n_c \quad (3)$$

To make full use of this peak capacity, it is essential that the retention mechanisms employed in the individual dimensions are extremely different ('orthogonal').

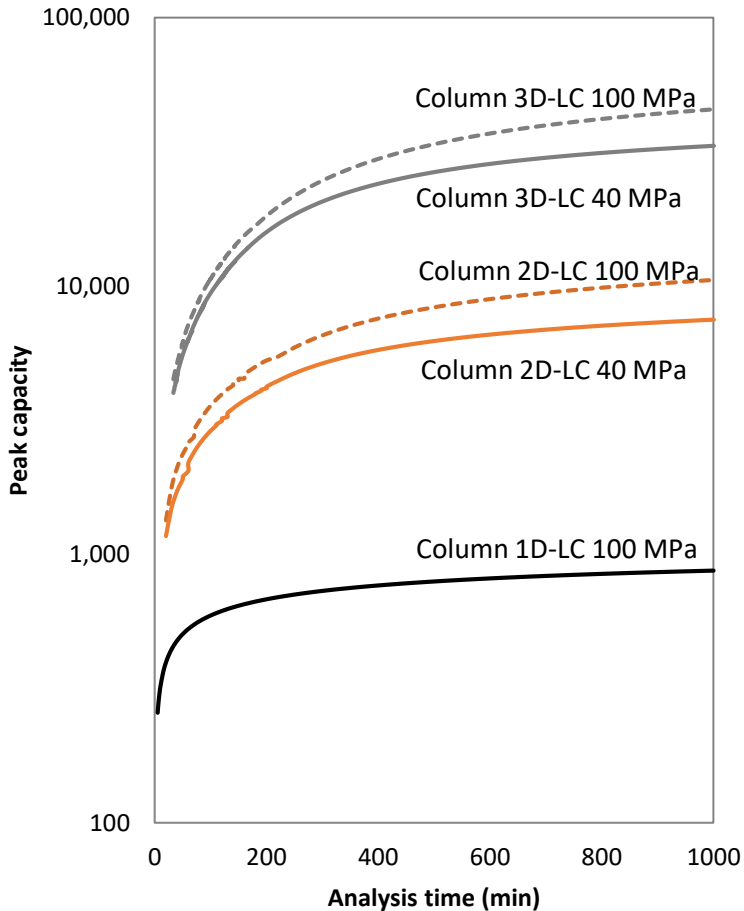


Figure 1 The theoretical peak capacity that can be achieved with different systems as a function of the analysis time, assuming a gradient duration equal to ten times the column hold-up time.

One way of increasing the peak capacity is by increasing the plate number in 1D-LC. This can be achieved by using a longer column or smaller particles. This can be made possible by increasing the operating pressure (*i.e.* ultra-high-pressure liquid chromatography, UHPLC), by using column with higher permeability (*e.g.* monolithic columns), or by operating the columns at higher temperatures, so as to decrease the solvent viscosity [31]. However, there is a limit in the gains that can be attained for 1D-LC. In figure 1, the theoretical peak capacity can be observed for different systems as a function of the

analysis time [32]. It can be seen that even at very long analysis times and operating at a very high pressure, 1D-LC cannot compete with the separation powers offered by LC×LC operated at a more-modest pressure.

The peak capacity can be correlated to the efficiency of the system by considering the number of plates.

$$N = \left(\frac{t_R}{\sigma_t}\right)^2 = \frac{L}{H} \quad (4)$$

Where  $t_R$  is the retention time of the analyte,  $\sigma_t$  is the standard deviation in time units, usually derived from the peak width at half height,  $L$  represents the column length, and  $H$  is the plate height. Equivalently, the plate height is equal to

$$H = \frac{L \times \sigma_t^2}{t_R^2} \quad (5)$$

Whether the separation is performed in isocratic mode or using a solvent gradient, the plate height can be related to peak capacity using equation 6, 7 or 8, assuming a resolution of 1 (four standard deviations between the peak maxima).

$$n_{iso} = 1 + \frac{\sqrt{N}}{4} \ln \frac{t_{R,n}}{t_{R,1}} \quad (6)$$

$$n_{grad} \approx 1 + \frac{t_g}{4\sigma_t} \approx \frac{t_g \sqrt{N}}{4t_0(1+k_e)} \quad (7)$$

or

$$n_{grad} \approx 1 + \frac{t_g}{4\sigma_t} \approx \frac{(t_{R,n} - t_{R,1})\sqrt{N}}{4t_0(1+k_e)} \quad (8)$$

if only a limited part of the gradient can effectively be used.

Here  $t_{R,1}$  and  $t_{R,n}$  represent the elution time of the first and last eluting compounds considered to be of relevance for the analysis [33],  $t_g$  is the duration of the gradient and  $k_e$  is the retention factor at the moment of elution, which in this equation is assumed equal for all analytes [31]. When applying the LSS theory, equation 7 may be written as

$$n_{grad} \approx \frac{t_g \sqrt{N}}{4(t_0 + 1/SB)} \quad (9)$$

where  $S$  is the slope of the  $\ln k$  vs.  $\varphi$  relationship and  $B$  is the slope of the gradient (in volume-fraction-per-time units). Since  $k_e$  (and  $S$ ) are not equal for all analytes, the average value of  $k_e$  or the average value of  $1/S$  may be used.

## 4. Orthogonality

With the introduction of multidimensional separations came the need to measure the performance of different combinations in terms of selectivity, which resulted in the development of orthogonality metrics. By definition, two systems are orthogonal if the first-dimension retention time ( $^1t_R$ ) is totally unrelated to the second-dimension retention time ( $^2t_R$ ). If this is the case, peaks may appear everywhere in the two-dimensional separation space. Thus, the degree of orthogonality in 2D-LC can be related to the extent of coverage of the separation space and this parameter can be used as a guideline for column selection or method optimization. Several orthogonality metrics have been introduced [34], but until now no consensus has been reached on an optimal metric for multidimensional chromatography.

Gilar *et al.* presented a way of calculating orthogonality based on division of the separation space into bins [35]. This approach utilizes normalized

retention data plotted in a 2D separation space as seen in figure 2A. The separation space is divided into square bins. The total number of bins should be equal or very close to the number of peaks observed in the chromatogram. The coverage of the separation space is calculated based on the total area of the occupied bins. From a probabilistic point of view, a 100% coverage is unlikely. Assuming a random distribution of peaks following Poisson statistics, Gilar et al. suggested that a coverage 63% would represent fully orthogonal separations [35].

Semard *et al.* introduced the convex hull metric for calculating the orthogonality [36]. In this case, the separation space is limited to the usable space, delimited by  $t_0$  and the  $t_R$  of the last eluting compound. The retention space used is determined by the Delauney triangulation method [37]. The area of the convex hull is the sum of the areas of the triangles. When calculating the orthogonality, the percentage “synentropy” is considered. This is calculated by dividing the informational entropy of data aligned on the diagonal by the total informational entropy of the 2D system.

Another orthogonality metric, called the asterisk method, was introduced by Camenzuli *et al.* [38]. In this case the retention time is normalized and a 2D plot is created. The 2D separation space is crossed by 4 axes, one vertical ( $Z_1$ ), one horizontal ( $Z_2$ ) and the two diagonals ( $Z_+$ ,  $Z_-$ ) (see figure 2B). The orthogonality is determined by considering the distance of each peak to the four axes. In the case of full orthogonality, the peak spreading would be maximal.

In a recent review, Schure and Davis [39] concluded that none of 20 published orthogonality metrics accounted for all the variance and none of them fully matched with visual interpretation of the data by experts. By using the product of several metrics a more reliable indication on orthogonality was said to be

obtained. By considering multiple metrics and visual assessment of the data the best combinations of separation modes could be selected.

Orthogonality metrics have been used to characterize two-dimensional separations of peptides. In 2005, Gilar *et al.* [35] showed the separation of peptides (196 were considered) in one-dimensional LC using different separation mechanisms (RPLC, HILIC, SCX, SECaq). The resulting retention times were normalized and plotted against the RPLC separation at pH=2.6. They concluded that HILIC×RPLC would be the best combination in terms of peak spreading followed by RPLC(pH 10)×RPLC(pH 2.6) and SCX×RPLC. This is a good first step in choosing the most-promising retention mechanisms needed to create a multidimensional separation setup, without needing complex instrumentation and experimentation. In the following section the different implementations of multidimensional separations are discussed.

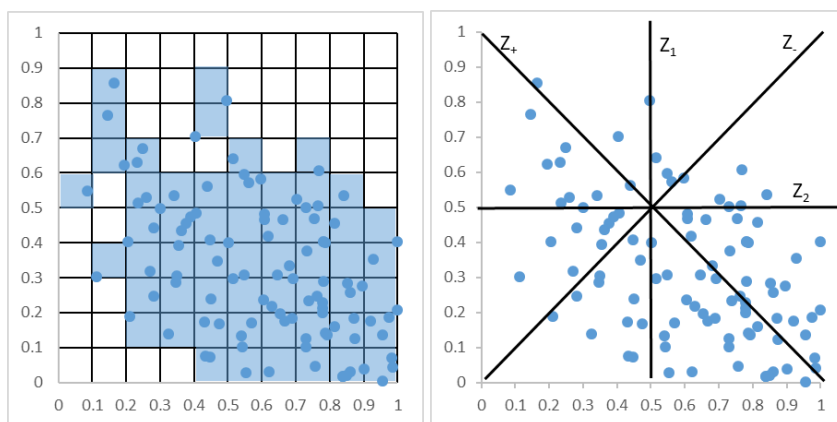


Figure 2 Normalized retention time of 100 peptides separated in HILIC and RPLC plotted in a two-dimensional space [40]. On the left (A) the separation space was divided in 100 bins (10x10) and the occupied bins were highlighted [41]. On the right (B) the same separation space is crossed by four lines used to calculate the asterisk criterion [38].

## 5. Implementations of multidimensional separations

Multidimensional separations can be either time-based (LC) or spatial (<sup>x</sup>LC). In time-based separations, the analytes will exit the column or separation space. Therefore, they are easier to couple with conventional detection methods, such as UV or MS. In the case of spatial separations, analytes are distributed along the distance of the separation space. Detection can rely on imaging or the analytes need to be extracted from the separation space (e.g. polyacrylamide gel electrophoresis, PAGE).

The advantage of spatial separations is the simultaneous development in the second and third dimensions, leading to faster separations overall. For example, we may imagine a 3D separation cube with a channel as the first dimension, a perpendicular separation space as the second dimension and a third dimension separation cube under the second dimension plane. In this case the sample would be separated in the first dimension column space, with the entire separated sample being transferred to the second dimension simultaneously, before the analytes could exit the column. After separation in the 2D plane all analytes would simultaneously be sent to the 3D cube. The third dimension could be either a spatial separation or time based separation, with the compounds being eluted at the end of the cube. Among the challenges still faced to realize such a device are the flow control and confinement for each dimension, introduction of different stationary phases in each dimension and detection either within the device or simultaneously for multiple outlet points at the exit of the cube.

Two-dimensional liquid chromatography (2D-LC) methods – either off-line or on-line – have already been applied in many fields (e.g. food science, proteomics, metabolomics, lipidomics, etc.). Off-line combinations are easily implemented and the fractions collected from the first-dimension effluent can be processed before their injection in the second-dimension

## Chapter 1

system to address issues such as solvent incompatibility or dilution. Off-line LC×LC can be a highly time-consuming process. On-line 2D-LC separations (<sup>1</sup>LC×<sup>1</sup>LC) require more-complex setups and method development. The conventional setup is based on a valve system with two identical loops that are alternately filled and emptied towards the second-dimension (<sup>2</sup>D) column. A limitation of these on-line <sup>1</sup>LC×<sup>1</sup>LC techniques is that the <sup>2</sup>D separation needs to be completed in a very short time, while the alternate loop is getting filled. The loops must be large enough to hold the entire fraction for each modulation without sample loss. Due to the Poiseuille flow profile this implies that the loop volume should exceed the fraction volume by up to 100% [27]. The conventional setup can give rise to incompatibility issues. Due to the combination of orthogonal separation mechanisms, the <sup>1</sup>D solvent is often not compatible with the initial <sup>2</sup>D conditions (“solvent-strength mismatch”). This can cause peak splitting, peak deformation, or elution of the analytes with the <sup>1</sup>D plug (“breakthrough”). Transfer of very small volumes can overcome the solvent mismatch [42]. However, in combination with dilution of the analytes during the two chromatographic separations, this makes detection more difficult. To overcome these issues active modulation has been developed to perform desalting, focussing on trapping columns, solvent exchange, or evaporation under vacuum [43].

For relatively compatible mobile phases, a setup containing a 2-position 10-port or 8-port valve can be used and the effluent from the first dimension can be diluted before injection in the second dimension, so as to yield a solvent strength equal to or weaker than that of the initial solvent composition of the <sup>2</sup>D run. In this way the analytes will be focused at the inlet of the <sup>2</sup>D column. One way to achieve such active solvent modulation employs two loops and a third pump to generate a make-up flow. Another way to achieve this is the co-called fixed solvent modulation (FSM). In this setup no additional pump is needed. Instead, the <sup>2</sup>D pump is used to dilute the <sup>1</sup>D fractions. The <sup>2</sup>D-pump

flow is split prior to the modulator valve, creating a bypass connection to the  $^2\text{D}$  column. The extent of dilution is determined by the ratio of the flow restrictions through the two paths. If these are equal, a 1:1 dilution is achieved. The main limitations of this technique are the lower flow rate in the modulator loop and the complex flow profile when the two streams are recombined. To overcome these limitations, Stoll *et al.* introduced active solvent modulation (ASM) [44]. An 8-port valve was modified to have two more ports and two extra rotational positions. This allowed the bypass loop to be connected only while the sample was transferred and not during the separation.

Another type of active modulation, called stationary-phase-assisted modulation (SPAM) [45], was achieved using small columns (“traps”) instead of loops for the sample transfer. The analytes are focused on the traps before the  $^2\text{D}$  separation. If necessary, adsorption may be enhanced by dilution of the  $^1\text{D}$  effluent with a make-up flow. The trap can be overfilled (*i.e.* flushed with much more effluent than their own volume) and the analytes can be focused in a much smaller volume. The  $^1\text{D}$  solvent can be almost completely removed, detection is improved due to focusing on the trap, and the  $^2\text{D}$  injection volume is decreased (to the volume of the trap). In order to apply this technique, all analytes in the sample need to be retained on the trapping column and the solvents in the two dimensions should be miscible. Another limitation arises from the more-complex timing for the valve switch and the start of the  $^2\text{D}$  gradient. Also, the two trapping columns must perform identically and robustly during many cycles.

An alternative approach to those discussed above is vacuum-evaporation modulation. For this approach, solvent miscibility is no longer a requirement. The modulation valve is equipped with two loops containing heating elements to aid evaporation. The loops are connected to vacuum during the evaporation step. The setup has been developed for a  $^1\text{D}$  (NPLC) separation with a fully

## Chapter 1

organic (low polarity) mobile phase and a <sup>2</sup>D (RPLC) separation with a water-based mobile phase. Many parameters need to be considered, such as the time needed to remove all the solvent, the volatility of the analytes, and the re-dissolution of the precipitated analytes during the modulation.

A number of other modulators have been proposed, including several thermal modulators, which rely on the effect of temperature on retention [46–49]. These are less commonly used for LC×LC than for GC×GC, because the effect of temperature on retention is much-more modest in LC. The principle is most attractive for high-molecular-weight analytes, such as polymers [50].

All these types of modulators have helped make LC×LC an indispensable technique with great separation power and a broad range of applications. However, the setups are complicated and the sequential separations in the second dimension make column-based (temporal) LC×LC time-consuming. An alternative method of analysis that may offer a greater separation power per unit time is spatial two-dimensional LC.

The best-known technique for spatial separation is thin-layer chromatography (TLC), introduced in 1938 by Izmailov and Shraiber [51]. Conventionally, separations were performed in normal-phase mode, utilizing a polar stationary phase and a non-polar mobile phase. Since then, the technique has been improved, with the introduction of high-performance TLC (HPTLC)[52], using smaller particles and smoother surfaces, and over-pressured TLC (OPTLC) [53], using a pressurized chamber and flow delivered by a pump. For TLC and HPTLC the progression of the solvent front is controlled by capillary forces, while in OPTLC a combination of capillary forces and pump-delivered flow determines the migration of the front. The efficiencies achievable by TLC and HPTLC are limited due to the long development times needed for longer beds. OPTLC has the advantage over TLC and HPTLC of

faster separations (5 to 20 times faster), while the precision is comparable to that of HPLC [53].

A well-established electrophoretic 2D-spatial separation is two-dimensional poly(acryl amine) gel electrophoresis (2D-PAGE). This technique combines isoelectric focusing in the first dimension, a separation that is based on the isoelectric point (pI) of the analytes, and separation based on molecular weight and charge in the second dimension (using sodium dodecyl sulphonate in the carrier liquid, SDS-PAGE) [54]. 2D-PAGE has become a vital technique for protein separation with great resolution (over 10 000 proteins were separated using a  $200 \times 200$  mm gel [55]). The limitations of the technique include difficulties with the separation of compounds with extreme pI or molecular weight and with proteins present in low abundance. Also, 2D-PAGE separations are very slow and laborious. Detection is typically performed through staining, but this further complicates the combination of 2D-PAGE with MS.

Detection is generally a challenge encountered with the spatial separations discussed above. Coupling with detectors used in HPLC is not possible without additional steps. In open-bed systems compounds that are – or can be made – UV/Vis active or fluorescent can be visualized, detected and quantified. However, in comparison with HPLC the options for detection are limited.

Over the last decades, microfluidic devices for multidimensional separations have been introduced. In some cases, microfluidic devices offer high separation efficiencies, while analysis times tend to be short and low sample quantities are required. Also, due to the freedom in creating various designs, dead volumes can be minimized, making the coupling of multiple separation channels possible [56].

## Chapter 1

The earliest micro-fabricated device for multidimensional separation was introduced by Becker *et al.* [57]. The device was used to perform two-dimensional electrophoresis with 500 parallel micro-channels in the second dimension. Other electro-driven separations were later developed and implemented by other groups, such as isoelectric focusing (IEF), capillary gel electrophoresis (CGE), micellar electrokinetic chromatography (MEKC), sodium-dodecyl-sulphate polyacrylamide-gel electrophoresis (SDS-PAGE), *etc.* [58]. Devices were fabricated in quartz, glass, silicon or polymeric materials using various microfabrication processes [59]. The devices showed a very low reagent consumption, possibilities for rapid analysis, and also for hyphenation to detectors either on chip (*e.g.* UV, fluorescence, C4D) or after elution (*e.g.* MS).

Integration of HPLC in microfluidic chips presented researchers with additional challenges, such as the need for high-pressure resistance of the devices and for the introduction of stationary phases. In 2010, the first microfluidic device combining an electrophoretic separation (IEF) and a reversed-phase liquid-chromatography separation (RPLC) was introduced [60]. The first-dimension separation was a single channel, where the sample was separated using IEF, and the second dimension was formed by multiple RPLC columns. The sample transfer was enabled by the integration of high-pressure micro-valves on the chip. Detection was performed either with on-chip fluorescence detection or by matrix-assisted laser-desorption/ionization mass spectrometry (MALDI-MS) detection following droplet deposition on a MALDI plate. The authors showed an increased peak capacity for the separation of peptides compared to one-dimensional micro-RPLC operated under the same conditions.

In 2011, a spatial multidimensional device, for CE×LC or LC×LC separations was presented [13]. The device was formed of two Borofloat glass disks with

six nano-ports in the bottom disk. A polyethylene spacer was used in between to allow the introduction of a polymerization mixture for the formation of the stationary phase. A sample-introduction channel and two flow distributors were created by incorporating a copper wire and two copper plates before polymerization. Which were removed by etching with nitric acid after the stationary phase was formed, leaving empty spaces. The authors showed the applicability of the monolithic bed in RPLC separations, but the device presented a low efficiency and an uneven flow-profile.

Another device for LC×LC was introduced by Wouters *et al.* [10]. The proposed device was created in cyclic-olefin copolymer (COC) and it contained a single channel for the first dimension and 21 parallel channels for the second dimension. Flow control and confinement were achieved by the use of a diamond-shaped flow distributor and the implementation of physical barriers around the first dimension channel. A monolithic stationary phase was created by UV-polymerization and confined to the second-dimension channels using photo-masks. Later, Wouters *et al.* showed the addition of a third dimension separation module, comprising of an array of channels perpendicular to the second dimension channels [61]. The device was intended to provide a three-dimensional separation, with first IEF, followed by a spatial RPLC separation and a time-based RPLC separation (<sup>x</sup>IEF×<sup>x</sup>LC×<sup>l</sup>LC). By using RPLC in the second and third dimension only one stationary-phase type needed to be created and the separations could feasibly be run at different pH (*e.g.* pH=2 and pH=10) to provide orthogonal separations of peptides. Actual three-dimensional separations were not yet demonstrated.

## 6. Conclusion

In this chapter I presented the challenges and improvements associated with multidimensional separations. Keeping the goal of comprehensive analysis of complex samples in mind, multidimensional LC seems to be the best tool, due to its higher separation power and the possibility of fast analysis.

The desire to enhance the capability of conventional separation technologies does come with challenges. The main challenges considered here were the selection of appropriate retention mechanisms, sample transfer between dimensions and developments towards spatial separation devices.

To take full advantage of separation power of multidimensional separations, all dimension need to be orthogonal. When choosing the appropriate separation modes or retention mechanisms, multiple approaches have been presented to determine the orthogonality for a class of analytes. Completely orthogonal separation cannot be achieved in practice, but a great gain in separation power has been demonstrated for favourable combinations.

Implementation of such favourable retention mechanisms in multidimensional approaches, such as column-based comprehensive two-dimensional liquid chromatography  $^1\text{LC}\times^1\text{LC}$ , have already been widely investigated. Separations can be performed on-line or offline, with direct transfer to the second dimension with or without active modulation, and with hyphenation to a variety of detectors.

The desire to further enhance separation power, without an increase in analysis time, has driven the investigations towards spatial separations. Spatial separations discussed in this chapter range from the well-known TLC plates, to more advanced OPTLC, and ultimately to microfluidic devices. Separation powers comparable to those reported for column-based 2D separations have not been obtained yet for spatial separations. However, the great interest in

microfluidics and the advances in 3D-printing technology offer hope for progress in spatial separations.

## **7. Scope of this thesis**

Chapter 1 provides a general introduction into the need of employing multidimensional separations for complex samples encountered in life science fields (*e.g.* proteomics, metabolomics, lipidomics, bio-pharmaceuticals). It also provides an overview of attempts by other groups to realize microfluidic multidimensional separation devices.

Chapter 2 addresses recent developments in the technology of high-pressure liquid chromatography that have implications for two- and three-dimensional separations. Especially ways to realize very fast separations are shown to be relevant in the context.

In the study described in Chapter 3 we investigated the possibility of retention modelling for peptides in one-dimensional hydrophilic-interaction liquid chromatography. We show an effective way of retention-time prediction of peptides from the use of at least two scanning gradients.

Chapter 4 describes the development of a two-dimensional low-flow hydrophilic-interaction liquid chromatography separation, hyphenated to reversed-phase liquid chromatography for the separation of peptides. Detection and identification of the analytes were realized with a high-resolution mass spectrometer. An increase in peak capacity was shown with the developed 2D-LC method when compared to 1D separation.

Chapter 5 describes the development of particle-packed 3D-printed devices that may serve as a third-dimension separation space in a three-dimensional

## Chapter 1

separation device. The operation of the device was verified with a separation of peptide standards and detection with mass spectrometer.

Chapter 6 summarizes some possible directions for future work in the field of this thesis.

## 8. References

- [1] V. Gupta, A.D.K. Jain, N.S. Gill, K. Gupta, Development and validation of HPLC method - a review, *Int. Res. J. Pharm. Appl. Sci.* 2 (2012) 17–25.
- [2] S. Eeltink, S. Dolman, F. Detobel, R. Swart, M. Ursem, P.J. Schoenmakers, High-efficiency liquid chromatography-mass spectrometry separations with 50mm, 250mm, and 1m long polymer-based monolithic capillary columns for the characterization of complex proteolytic digests, *J. Chromatogr. A.* 1217 (2010) 6610–6615. doi:10.1016/j.chroma.2010.03.037.
- [3] Y. Shen, R. Zhang, R.J. Moore, J. Kim, T.O. Metz, K.K. Hixson, R. Zhao, E.A. Livesay, H.R. Udseth, R.D. Smith, Automated 20 kpsi RPLC-MS and MS/MS with chromatographic peak capacities of 1000-1500 and capabilities in proteomics and metabolomics, *Anal. Chem.* 77 (2005) 3090–3100. doi:10.1021/ac0483062.
- [4] J.M. Davis, J.C. Giddings, Statistical Theory of Component Overlap in Multicomponent Chromatograms, *Anal. Chem.* 55 (1983) 418–424. doi:10.1021/ac00254a003.
- [5] B. Zhan, J.R. Yates, M.-C. Baek, Y. Zhang, B.R. Fonslow, Protein Analysis by Shotgun/Bottom-up Proteomics, *Chem. Rev.* 113 (2013) 2343–2394. doi:10.1021/cr3003533.
- [6] L. Switzar, M. Giera, W.M.A. Niessen, Protein digestion: An overview of the available techniques and recent developments, *J. Proteome Res.* 12 (2013) 1067–1077. doi:10.1021/pr301201x.
- [7] M. Gilar, A.E. Daly, M. Kele, U.D. Neue, J.C. Gebler, Implications of column peak capacity on the separation of complex peptide mixtures in single- and two-dimensional high-performance liquid chromatography, *J. Chromatogr. A.* 1061 (2004) 183–192. doi:10.1016/j.chroma.2004.10.092.
- [8] P.H. O'Farrell, High Resolution Two-Dimensional Electrophoresis of Proteins, *J. Biol. Chem.* 250 (1975) 4007–4021. <http://www.jbc.org/content/250/10/4007.short>.
- [9] S.M. Scott, Z. Ali, Fabrication methods for microfluidic devices: An overview, *Micromachines.* 12 (2021). doi:10.3390/mi12030319.

- [10] B. Wouters, J. De Vos, G. Desmet, H. Terryn, P.J. Schoenmakers, S. Eeltink, Design of a microfluidic device for comprehensive spatial two-dimensional liquid chromatography, *J. Sep. Sci.* 38 (2015) 1123–1129. doi:10.1002/jssc.201401192.
- [11] T. Adamopoulou, S. Deridder, G. Desmet, P.J. Schoenmakers, Two-dimensional insertable separation tool (TWIST) for flow confinement in spatial separations, *J. Chromatogr. A.* 1577 (2018) 120–123. doi:10.1016/j.chroma.2018.09.054.
- [12] M. Gilar, T.S. McDonald, F. Gritti, G.T. Roman, J.S. Johnson, B. Bunner, J.D. Michienzi, R.A. Collamati, J.P. Murphy, D.D. Satpute, M.P. Bannon, D. DellaRovere, R.A. Jencks, T.A. Dourdeville, K.E. Fadgen, G.C. Gerhardt, Chromatographic performance of microfluidic liquid chromatography devices: Experimental evaluation of straight versus serpentine packed channels, *J. Chromatogr. A.* 1533 (2018) 127–135. doi:10.1016/j.chroma.2017.12.031.
- [13] D.J.D. Vanhoutte, S. Eeltink, W.T. Kok, P.J. Schoenmakers, Construction and initial evaluation of an apparatus for spatial comprehensive two-dimensional liquid-phase separations, *Anal. Chim. Acta.* 701 (2011) 92–97. doi:10.1016/j.aca.2011.06.004.
- [14] J.C. Giddings, Sample dimensionality: A predictor of order-disorder in component peak distribution in multidimensional separation, *J. Chromatogr. A.* 703 (1995) 3–15. doi:10.1016/0021-9673(95)00249-M.
- [15] S. Di Palma, M.L. Hennrich, A.J.R. Heck, S. Mohammed, Recent advances in peptide separation by multidimensional liquid chromatography for proteome analysis, *J. Proteomics.* 75 (2012) 3791–3813. doi:10.1016/j.jprot.2012.04.033.
- [16] E. Hallgren, Prediction of protein retention at gradient elution conditions in ion-exchange chromatography, *J. Chromatogr. A.* 852 (1999) 351–359. doi:10.1016/S0021-9673(99)00646-9.
- [17] C. Hou, H. Yuan, X. Qiao, J. Liu, Y. Shan, L. Zhang, Z. Liang, Y. Zhang, Weak anion and cation exchange mixed-bed microcolumn for protein separation, *J. Sep. Sci.* 33 (2010) 3299–3303. doi:10.1002/jssc.201000440.
- [18] T.W. Lorne Burke, C.T. Mant, J.A. Black, R.S. Hodges, Strong cation-exchange high-performance liquid chromatography of peptides. Effect of non-specific hydrophobic interactions and linearization of peptide retention behaviour, *J. Chromatogr. A.* 476 (1989) 377–389. doi:10.1016/S0021-9673(01)93883-X.
- [19] A.J. Alpert, Hydrophilic-interaction chromatography for the separation of peptides, nucleic acids and other polar compounds, *J. Chromatogr. A.* (1990). doi:10.1016/S0021-9673(00)96972-3.

## Chapter 1

- [20] D. V. McCalley, Understanding and manipulating the separation in hydrophilic interaction liquid chromatography, *J. Chromatogr. A.* 1523 (2017) 49–71. doi:10.1016/j.chroma.2017.06.026.
- [21] J.C. Heaton, J.J. Russell, T. Underwood, R. Boughtflower, D. V. McCalley, Comparison of peak shape in hydrophilic interaction chromatography using acidic salt buffers and simple acid solutions, *J. Chromatogr. A.* 1347 (2014) 39–48. doi:10.1016/j.chroma.2014.04.026.
- [22] S. Fekete, J.L. Veuthey, D. Guillarme, New trends in reversed-phase liquid chromatographic separations of therapeutic peptides and proteins: Theory and applications, *J. Pharm. Biomed. Anal.* 69 (2012) 9–27. doi:10.1016/j.jpba.2012.03.024.
- [23] G.B. Irvine, High-performance size-exclusion chromatography of peptides, *J. Biochem. Biophys. Methods.* 56 (2003) 233–242. doi:10.1016/S0165-022X(03)00061-7.
- [24] P.J. Boersema, S. Mohammed, A.J.R. Heck, Hydrophilic interaction liquid chromatography (HILIC) in proteomics, *Anal. Bioanal. Chem.* 391 (2008) 151–159. doi:10.1007/s00216-008-1865-7.
- [25] A.B. Iliuk, J. V. Arrington, W.A. Tao, Analytical challenges translating mass spectrometry-based phosphoproteomics from discovery to clinical applications, *Electrophoresis.* 35 (2014) 3430–3440. doi:10.1002/elps.201400153.
- [26] N. Abdulhussain, S. Nawada, P. Schoenmakers, Latest Trends on the Future of Three-Dimensional Separations in Chromatography, *Chem. Rev.* 121 (2021) 12016–12034. doi:10.1021/acs.chemrev.0c01244.
- [27] B.W.J. Pirok, A.F.G. Gargano, P.J. Schoenmakers, Optimizing separations in online comprehensive two-dimensional liquid chromatography, *J. Sep. Sci.* 41 (2018) 68–98. doi:10.1002/jssc.201700863.
- [28] G. Groeneveld, M.N. Dunkle, M. Pursch, E.P.C. Mes, P.J. Schoenmakers, A.F.G. Gargano, Investigation of the effects of solvent-mismatch and immiscibility in normal-phase  $\times$  aqueous reversed-phase liquid chromatography, *J. Chromatogr. A.* 1665 (2022) 462818. doi:10.1016/j.chroma.2022.462818.
- [29] J. Calvin Giddings, Maximum Number of Components Resolvable by Gel Filtration and Other Elution Chromatographic Methods, *Anal. Chem.* 39 (1967) 1027–1028. doi:10.1021/ac60252a025.
- [30] U.D. Neue, Theory of peak capacity in gradient elution, *J. Chromatogr. A.* 1079 (2005) 153–161. doi:10.1016/j.chroma.2005.03.008.
- [31] G. Vivó-Truyols, S. Van Der Wal, P.J. Schoenmakers, Comprehensive study on the optimization of online two-dimensional liquid chromatographic systems considering losses in

theoretical peak capacity in first- and second-dimensions: A pareto-optimality approach, *Anal. Chem.* 82 (2010) 8525–8536. doi:10.1021/ac101420f.

[32] E. Davydova, P.J. Schoenmakers, G. Vivó-Truyols, Study on the performance of different types of three-dimensional chromatographic systems, *J. Chromatogr. A.* 1271 (2013) 137–143. doi:10.1016/j.chroma.2012.11.043.

[33] G. Guiochon, N. Marchetti, K. Mriziq, R.A. Shalliker, Implementations of two-dimensional liquid chromatography, *J. Chromatogr. A.* 1189 (2008) 109–168. doi:10.1016/j.chroma.2008.01.086.

[34] J. Mommers, S. van der Wal, Two metrics for measuring orthogonality for two-dimensional chromatography, *J. Chromatogr. A.* 1586 (2019) 101–105. doi:10.1016/j.chroma.2018.11.081.

[35] M. Gilar, P. Olivova, A.E. Daly, J.C. Gebler, Orthogonality of separation in two-dimensional liquid chromatography, *Anal. Chem.* 77 (2005) 6426–6434. doi:10.1021/ac050923i.

[36] G. Semard, V. Peulon-Agasse, A. Bruchet, J.P. Bouillon, P. Cardinaël, Convex hull: A new method to determine the separation space used and to optimize operating conditions for comprehensive two-dimensional gas chromatography, *J. Chromatogr. A.* 1217 (2010) 5449–5454. doi:10.1016/j.chroma.2010.06.048.

[37] D.T. Lee, A.K. Lin, Generalized delaunay triangulation for planar graphs, *Discrete Comput. Geom.* 1 (1986) 201–217. doi:10.1007/BF02187695.

[38] M. Camenzuli, P.J. Schoenmakers, A new measure of orthogonality for multi-dimensional chromatography, *Anal. Chim. Acta.* 838 (2014) 93–101. doi:10.1016/j.aca.2014.05.048.

[39] M.R. Schure, J.M. Davis, Orthogonality measurements for multidimensional chromatography in three and higher dimensional separations, *J. Chromatogr. A.* 1523 (2017) 148–161. doi:10.1016/j.chroma.2017.06.036.

[40] L.S. Roca, A.F.G. Gargano, P.J. Schoenmakers, Development of comprehensive two-dimensional low-flow liquid-chromatography setup coupled to high-resolution mass spectrometry for shotgun proteomics, *Anal. Chim. Acta.* 1156 (2021) 338349. doi:10.1016/j.aca.2021.338349.

[41] M. Gilar, J. Fridrich, M.R. Schure, A. Jaworski, Comparison of orthogonality estimation methods for the two-dimensional separations of peptides, *Anal. Chem.* 84 (2012) 8722–8732. doi:10.1021/ac3020214.

## Chapter 1

- [42] P. Dugo, M. del M.R. Fernández, A. Cotroneo, G. Dugo, L. Mondello, Optimization of a comprehensive two-dimensional normal-phase and reversed-phase liquid chromatography system, *J. Chromatogr. Sci.* 44 (2006) 561–565. doi:10.1093/chromsci/44.9.561.
- [43] Y. Chen, L. Montero, O.J. Schmitz, Advance in on-line two-dimensional liquid chromatography modulation technology, *Trends Anal. Chem.* 120 (2019) 115647. doi:10.1016/j.trac.2019.115647.
- [44] D.R. Stoll, K. Shoykhet, P. Petersson, S. Buckenmaier, Active Solvent Modulation: A Valve-Based Approach to Improve Separation Compatibility in Two-Dimensional Liquid Chromatography, *Anal. Chem.* 89 (2017) 9260–9267. doi:10.1021/acs.analchem.7b02046.
- [45] R.J. Vonk, A.F.G. Gargano, E. Davydova, H.L. Dekker, S. Eeltink, L.J. de Koning, P.J. Schoenmakers, Comprehensive Two-Dimensional Liquid Chromatography with Stationary-Phase-Assisted Modulation Coupled to High-Resolution Mass Spectrometry Applied to Proteome Analysis of *Saccharomyces cerevisiae*., *Anal. Chem.* 87 (2015) 5387–5394. doi:10.1021/acs.analchem.5b00708.
- [46] M. Verstraeten, M. Pursch, P. Eckerle, J. Luong, G. Desmet, Thermal modulation for multidimensional liquid chromatography separations using low-thermal-mass liquid chromatography (LC), *Anal. Chem.* 83 (2011) 7053–7060. doi:10.1021/ac201207t.
- [47] H.C. Van de Ven, A.F.G. Gargano, S.J. Van der Wal, P.J. Schoenmakers, Switching solvent and enhancing analyte concentrations in small effluent fractions using in-column focusing, *J. Chromatogr. A.* 1427 (2016) 90–95. doi:10.1016/j.chroma.2015.11.082.
- [48] S.R. Groskreutz, A.R. Horner, S.G. Weber, Development of a 1.0 mm inside diameter temperature-assisted focusing precolumn for use with 2.1 mm inside diameter columns, *J. Chromatogr. A.* 1523 (2017) 193–203. doi:10.1016/j.chroma.2017.07.015.
- [49] M.E. Creese, M.J. Creese, J.P. Foley, H.J. Cortes, E.F. Hilder, R.A. Shellie, M.C. Breadmore, Longitudinal on-column thermal modulation for comprehensive two-dimensional liquid chromatography, *Anal. Chem.* 89 (2017) 1123–1130. doi:10.1021/acs.analchem.6b03279.
- [50] L.E. Niezen, B.B.P. Staal, C. Lang, B.W.J. Pirok, P.J. Schoenmakers, Thermal modulation to enhance two-dimensional liquid chromatography separations of polymers, *J. Chromatogr. A.* 1653 (2021) 462429. doi:10.1016/j.chroma.2021.462429.
- [51] V.G. Berezkin, T.H. Dzido, The Discovery of Thin-Layer Chromatography by N.A. Izmailov and M.S. Shraiber, *JPC – J. Planar Chromatogr. – Mod. TLC.* 21 (2008) 399–403. doi:10.1556/JPC.21.2008.6.1.
- [52] G. Morlock, W. Schwack, Hyphenations in planar chromatography, *J. Chromatogr. A.* 1217 (2010) 6600–6609. doi:10.1016/j.chroma.2010.04.058.

- [53] E. Tyihák, E. Mincsovcics, H. Kalász, New planar liquid chromatographic technique: overpressured thin-layer chromatography, 174 (1979) 75–81. doi:10.1016/S0021-9673(00)87038-7.
- [54] N. Kendrick, C.C. Darie, M. Hoelter, G. Powers, J. Johansen, 2D SDS PAGE in Combination with Western Blotting and Mass Spectrometry Is a Robust Method for Protein Analysis with Many Applications, in: 2019: pp. 563–574. doi:10.1007/978-3-030-15950-4\_33.
- [55] G. Büyükköroğlu, D.D. Dora, F. Özdemir, C. Hızel, Chapter 15 - Techniques for Protein Analysis, in: D. Barh, V.B.T.-O.T. and B.-E. Azevedo (Eds.), Academic Press, 2018: pp. 317–351. doi:https://doi.org/10.1016/B978-0-12-804659-3.00015-4.
- [56] J.D. Ramsey, S.C. Jacobson, C.T. Culbertson, J.M. Ramsey, High-efficiency, two-dimensional separations of protein digests on microfluidic devices, *Anal. Chem.* 75 (2003) 3758–3764. doi:10.1021/ac0264574.
- [57] H. Becker, K. Lowack, A. Manz, Planar quartz chips with submicron channels for two-dimensional capillary electrophoresis applications, *J. Micromechanics Microengineering.* 8 (1998) 24–28. doi:10.1088/0960-1317/8/1/004.
- [58] M.A. Lerch, S.C. Jacobson, Electrokinetic fluid control in two-dimensional planar microfluidic devices, *Anal. Chem.* 79 (2007) 7485–7491. doi:10.1021/ac071003y.
- [59] R.M. McCormick, R.J. Nelson, M.G. Alonso-Amigo, D.J. Benvegna, H.H. Hooper, Microchannel Electrophoretic Separations of DNA in Injection-Molded Plastic Substrates, *Anal. Chem.* 69 (1997) 2626–2630. doi:10.1021/ac9701997.
- [60] J. Liu, C.F. Chen, S. Yang, C.C. Chang, D.L. Devoe, Mixed-mode electrokinetic and chromatographic peptide separations in a microvalve-integrated polymer chip, *Lab Chip.* 10 (2010) 2122–2129. doi:10.1039/c003505j.
- [61] B. Wouters, E. Davydova, S. Wouters, G. Vivo-Truyols, P.J. Schoenmakers, S. Eeltink, Towards ultra-high peak capacities and peak-production rates using spatial three-dimensional liquid chromatography, *Lab Chip.* 15 (2015) 4415–22. doi:10.1039/c5lc01169h.

## Chapter 2

### How two-dimensional liquid chromatography can benefit from recent technological advances

#### Contents

1.	Introduction .....	35
2.	Need for advancements in LC applicable in LC×LC .....	38
3.	Fast separations.....	42
3.1	High pressure, smaller particle diameters .....	43
3.2	High temperature .....	46
3.3	High pressure and high temperature.....	47
3.4	Core-shell particles and monoliths.....	48
3.5	Enhanced-fluidity liquid chromatography and supercritical-fluid chromatography.....	51
3.6	Alternative separation devices .....	53
4.	Conclusions .....	56
5.	References .....	57

## 1. Introduction

High-performance liquid chromatography (HPLC) is a versatile, well-established separation technique with applications in many fields [1–3]. Over time, due to a high demand for faster separations, higher efficiency, and analysis of more complex mixtures, many advancements in the instrumentation and stationary phases have been implemented in conventional (column-based) HPLC [2].

For complex samples, the most-convenient way of documenting the separation power and the limitations of current systems is by considering the peak capacity. In a one-dimensional (1D) separation, the maximum number of components that can be separated is limited by the analysis time and the peak width of the analytes [4]. The peak capacity can be seen as the maximum number of peaks that can fit next to each other (with a given resolution) in a certain period of time. In isocratic LC the peak capacity ( $n_{iso}$ ) is

$$n_{iso} = \frac{\sqrt{N}}{4R_s} \ln \left( \frac{1+k_\omega}{1+k_\alpha} \right) + 1 \quad (1)$$

where  $N$  represents the plate count,  $R_s$  corresponds to the resolution between two consecutive peaks,  $k_\omega$  is the retention factor of the last eluting peak, and  $k_\alpha$  is the retention factor of the first eluting peak [5]. In case of gradient elution

$$n_{grad} = \frac{t_G}{4R_s\sigma_{peak}} + 1 \approx \frac{t_G}{t_0} \frac{\sqrt{N}}{4R_s(1+k_e)} \quad (2)$$

where  $t_G$  is the duration of the gradient,  $\sigma_{peak}$  represents the peak dispersion (standard deviation) under gradient conditions (in time units),  $t_0$  is the dead time and  $k_e$  is the retention factor at the moment of elution [5].

In both cases the peak capacity is seen to be proportional to the square root of the number of theoretical plates available. This implies that any developments

## Chapter 2

in LC that result in higher plate counts are relevant for the separation of complex samples.

In a real separation, the analytes will not have equal peak widths and will have random elution times. The peak capacity represents an ideal case and if the retention times of the analytes are randomly distributed (*e.g.* following Poisson statistics) the number of components that can be expected to be fully resolved is much lower. Davis *et al.* proposed a theory that the peaks resolved cannot be more than 37% of the peak capacity and if single-component peaks are considered the percentage would drop to 18% [6,7]. One way to circumvent such limitations is to optimize the selectivity of the separation, so as to spread the peaks much better across the chromatogram. Many authors have designed procedures for such optimizations [8–10], but for very complex samples the peak capacity remains a limiting value. Therefore, it is still seen as the prime descriptor for the separation power of a chromatographic system.

The other main descriptor that follows from equations (1) and (2) is the analysis time. In isocratic LC very little gain can be booked by extending the maximum retention time to high values of  $k_{\infty}$ , because of the logarithm in the equation. Also, high retention factors lead to broad peaks and greatly reduced sensitivities. Therefore, gradient-elution LC is the predominant mode for separating complex samples. Equation (2) suggests that the peak capacity is proportional to the duration of the gradient. However, this is a bit deceptive, because the retention factor at the moment of elution (which is the main factor determining the peak width) increases for slower gradients. Nevertheless, gradient-elution allows a much larger number of analytes to be eluted under roughly optimal conditions.

Comprehensive two-dimensional liquid chromatography (LC×LC) has developed into a prime technique for the liquid-phase separation of highly

complex samples. This is due to practical reasons, such as the availability of high-quality (commercial) hardware and software for the purpose, but also because of fundamental advantages. To a first-order approximation, the peak capacity of an LC×LC system ( ${}^{2D}n$ ) is the product of the peak capacities in the individual dimensions ( ${}^1n$  and  ${}^2n$ ), *i.e.*

$${}^{2D}n = {}^1n \times {}^2n \quad (3)$$

whereas the total analysis time ( ${}^{2D}t$ ) is only the sum of the two analysis times

$${}^{2D}t = {}^1t + {}^2t \quad (4)$$

Equation (3) is somewhat optimistic, as it requires a sufficient number of fractions collected (“cuts”) to avoid undersampling of the first-dimension ( ${}^1D$ ) chromatogram and injection of these fractions in the second-dimension ( ${}^2D$ ) column without any additional band broadening. Moreover, the total (theoretical) peak capacity indicated by Eq. (3) can only be fully utilized if the 1D and 2D analysis times of analytes are fully independent, *i.e.* the selectivities (retention mechanisms) in the two dimensions must be completely different. Such LC systems are called “orthogonal”.

To perform LC×LC in real time (*i.e.* without stopping the  ${}^1D$  flow during the  ${}^2D$  analysis), the  ${}^2D$  separation needs to be very much faster than the  ${}^1D$  separation. For example, if 100 fractions are to be collected and separated on the  ${}^2D$  column, this latter separation should be two orders of magnitude faster than the  ${}^1D$  separation. Therefore, developments towards high-resolution LC separations in (moderately) long analysis times and developments towards very fast HPLC separation (with moderate peak capacities) are both highly relevant for eventual implementation in LC×LC systems. Therefore, developments in both directions will be discussed in detail in this review.

To avoid <sup>2</sup>D band broadening caused by the injection of relatively large-volume fractions collected from the <sup>1</sup>D separation, the inner diameter of the <sup>2</sup>D column was typically selected to be much larger than that of the <sup>1</sup>D column ( $^1d_c \ll ^2d_c$ ) [11], to the extent that <sup>2</sup>D columns could be short (50 mm) and very fat (20 mm ID) [12]. However, recent advances in the coupling between the two systems (so called active modulation, [13,14]) have largely eliminated this requirement. Therefore, high-resolution or high-speed LC columns of any diameter may be relevant for contemporary LC×LC.

The main improvements that will be discussed in this review are the use of high pressures, high temperatures, high diffusivity, different stationary phases (monoliths, core-shell particles), and non-standard separation devices (chip-based columns).

## 2. Need for advancements in LC applicable in LC×LC

The main requirement in LC×LC for the first-dimension separation is to obtain a good spread of the peaks throughout the chromatogram. The time available for the <sup>1</sup>D separation depends greatly on the <sup>2</sup>D analysis time. Several groups [5,15] have concluded that an optimal peak-production rate (peak capacity per unit time) can be achieved if two or three cuts are taken from each <sup>1</sup>D peak. In that case the <sup>2</sup>D analysis time should not exceed twice the standard deviation ( $^1\sigma_t$ ) of the 1D peak, *i.e.*  $^2t_{\text{anal}} \leq 2 \ ^1\sigma_t$ . Other authors (*e.g.* Li et al. [16]) recommend four cuts per peak to maintain the resolution obtained in the first dimension, in which case  $^2t_{\text{anal}} \leq ^1\sigma_t$ . Because LC×LC is mostly suitable for (highly) complex samples, gradient elution is the dominant mode of separation. The widths of peaks eluting during a linear gradient can be approximated by

$$^1\sigma_t \approx \frac{t_0(1+k_e)}{\sqrt{N}} \approx \frac{t_0\left(1+\frac{t_G}{S\Delta\phi t_0}\right)}{\sqrt{N}} \quad (5)$$

where  $S$  is the slope of the linear  $\ln k$  vs.  $\varphi$  line and  $\Delta\varphi$  is the span of the gradient in volume-fraction units. Eq. 5 indicates that there is a lot of flexibility to adapt the  $^1D$  separation to the  $^2D$  analysis time. Efficient  $^1D$  separations (high  $N$ ) result in relatively narrow peaks, but the gradient time and the flow rate (which determines  $t_0$ ) can be adapted. Usually, the  $^1D$  involves fairly long gradients and low flow rates.

Equation (3) is overly optimistic for real LC $\times$ LC separations. The main corrections involve undersampling of the  $^1D$  chromatogram and injection band broadening in the second dimension. Vivó Truyols *et al.* [5] have derived the following equation that corrects for these two effects, assuming gradient elution in both dimensions (with gradient durations  $^1t_G$  and  $^2t_G$ , respectively).

$${}^{2D}n_{\text{grad}\times\text{grad}} = \frac{{}^1t_G}{4R_{s,\text{req}} \sqrt{\frac{(k_e+1)^2}{1N} \cdot \frac{{}^1t_\omega^2}{\left(\frac{{}^1t_G+1}{{}^1t_0}\right)^2} + \frac{{}^2t_\omega^2}{\delta_{\text{det}}^2}}} \times \frac{{}^2t_G}{4R_{s,\text{req}} \sqrt{\frac{(k_e+1)^2}{2N} \cdot \frac{{}^2t_\omega^2}{\left(\frac{{}^2t_G+1}{{}^2t_0}\right)^2} + \left(\frac{{}^1F}{{}^2F} \frac{{}^2t_\omega}{\delta_{\text{inj}}}\right)^2}} \quad (6)$$

Here  $R_{s,\text{req}}$  is the required resolution, which is usually assumed to be equal to 1. The retention factor at the moment of elution ( $k_e$ ) depends on the analyte and the gradient conditions. For low-molecular-weight analytes under reasonable gradient conditions (*e.g.*  $t_G/t_0=10$ ) a value of  $k_e = 3$  is often assumed. For slow gradients higher values may be encountered, whereas for high-molecular-weight analytes  $k_e$  may be lower (see Eq. 5). To correct for undersampling of the first-dimension separation, the  $^2D$  separation is treated as a detector with a low sampling frequency ( $1/{}^2t_\omega$  Hz) and a value of  $\delta_{\text{det}} = \sqrt{4.76}$  was suggested by Davis *et al.* [17]. The modulation time concurs with the time it takes to perform one  $^2D$  separation and equilibrate the column for the next injection. Simultaneously, it also represents the time it takes for a fraction of the  $^1D$  effluent to be collected for further separation in the  $^2D$

## Chapter 2

column. The two actions occur in parallel, allowing for the first-dimension flow to be diverted to a modulator for sample focusing or solvent exchange.

To correct for the effect of the finite (and often relatively large) injection volume in the second dimension (without active modulation  ${}^2V_{inj} = {}^1F \times {}^2t_{\omega}$ ) a value of  $\delta_{inj}=2$  may be used [18]. The analysis time in the first dimension is  ${}^1t_{\omega}$ , which is the elution time of the last analyte. The cycle time of the second dimension, which includes the gradient and re-equilibration,  ${}^2t_{\omega}$ , which is also equal to the modulation time. The total 2D analysis time is  ${}^1t_{\omega} + {}^2t_{\omega}$ . When the effective injection volume on the second-dimension column is reduced through active modulation [13] or a prudent selection of gradient-elution conditions, the term that corrects for the injection band broadening in the second dimension may be multiplied by a factor  $(1+{}^2k_{init})/(1+{}^2k_{am})$ , where  ${}^2k_{init}$  and  ${}^2k_{am}$  are the retention factors upon injection on the  ${}^2D$  column without and with focussing or active modulation, respectively. This factor is solute dependent, but if high values of  ${}^2k_{am}$  can be realized for all relevant analytes, the  ${}^2D$  injection band broadening can effectively be neglected.

The introduction of smaller columns and smaller particles in LC $\times$ LC has a great impact on the fraction volume that can be transferred from the  ${}^1D$  to the  ${}^2D$  column. To maintain a good peak shape and efficiency, the sample volume should not exceed 10% of the column volume [19]. Three options can be employed to reduce the (effective) second-dimension injection volume, *viz.* (a) reducing the flow rate in the first dimension, (b) increasing the speed of the second dimension, so as to reduce the modulation time, or (c) implementing active modulation to concentrate the analytes from the fraction in a smaller volume [20].

The  ${}^1D$  flow rate can be reduced without increasing the analysis time by reducing the column diameter. Indeed, the  ${}^1D$  column diameter in LC $\times$ LC has

typically been much smaller than the <sup>2</sup>D column diameter ( $^1d_c < ^2d_c$ ). This was either achieved by using a narrow bore <sup>1</sup>D column (*e.g.* 1 mm i.d.) and a conventional <sup>2</sup>D column (*e.g.* 4.6 mm i.d.), or by using a conventional <sup>1</sup>D column (4.6 mm i.d.) in combination with a very wide <sup>2</sup>D column (up to 20 mm) [21]. The former approach is not attractive, because the sample loadability of the <sup>1</sup>D column will be limited and the detectability of low-concentration analytes may be impaired. The second approach is undesirable, because of the very high <sup>2</sup>D flow rate, leading to very large volumes of eluent required, and the incompatibility of detectors with such high flow rates. Therefore, active modulation is the most attractive option.

Various active-modulation strategies have been developed [22] to effectively mitigate the additional <sup>2</sup>D band-broadening. When some kind of action is taken during the modulation, instead of direct transfer between the dimensions, it is considered active modulation [23]. One way to achieve this is active solvent modulation [14], in which part of the <sup>2</sup>D eluent passes through the loop and transfers the collected fraction, while another part of the <sup>2</sup>D eluent bypasses the loop through a connector. This can alleviate the solvent mismatch between the two dimensions with incompatible eluents. Another way is stationary-phase-assisted modulation [24]. In this case the collection loops in between the two dimensions are replaced by trap columns, often of the same chemistry as the second-dimension column. The <sup>1</sup>D effluent may be diluted prior to the trap column to obtain a weaker solvent and allow strong retention of the analytes on the trap. This allows for focusing of the analytes on the trap and complete exchange of the <sup>1</sup>D eluent. Vacuum-evaporation modulation has also been applied for the transfer of fractions between dimensions, as demonstrated for NPLC×RPLC coupling [25]. The fractions from the first dimension were collected in heated loops with a vacuum applied to the outlet.

## Chapter 2

This allowed for the complete removal of the  $^1\text{D}$  solvent, followed by (re-) solvation in the  $^2\text{D}$  solvent prior to sending the analytes to the  $^2\text{D}$  column.

The undersampling of the  $^1\text{D}$  signal cannot easily be mitigated and the correction of the  $^1\text{D}$  peak capacity is often quite substantial. In the extreme case, the effective peak capacity of the LC $\times$ LC system will be the peak capacity of the second dimension multiplied by the number of fractions taken from the first dimension. In such a case the peak capacity of the first dimension was shown to have a negligible impact on the total peak capacity [16]. The impact increases when very fast second dimension cycles are used or when the  $^1\text{D}$  separations are very long and the  $^1\text{D}$  peaks relatively broad. Therefore, LC $\times$ LC performance is dramatically dependent on advancements in very fast LC ( $^2\text{D}$ ) and somewhat dependent on advances in fairly slow, efficient separations ( $^1\text{D}$ ).

The other essential factor to make full use of the separation power of LC $\times$ LC is the orthogonality of the two different separation dimensions. The selectivities in the two dimensions should be such that the separation space is used as much as possible. This will depend on the retention mechanisms (stationary and mobile phases) selected in each dimension, which will not be addressed in this review.

### **3. Fast separations**

Experimental advances made towards faster (one-dimensional) LC separations [4] that have been applied to  $^2\text{D}$  separations will be detailed in this section. These include the use of high pressures, elevated temperatures, short columns, and advances in separation media (superficially porous or non-porous particles, monoliths). Multiple second-dimension separations have also been performed in parallel by some authors [26,27], but this does not rely

on advances in (one-dimensional) LC and, therefore, will not be discussed in this review.

### 3.1 High pressure, smaller particle diameters

The use of smaller particles (sub 2  $\mu\text{m}$ ) in LC leads to faster mass transfer. This simultaneously results in reduced peak widths and increased optimum velocities [2]. A significant limitation is the maximum working pressure. Ultra-high pressure HPLC, pioneered by Jorgenson and co-workers [28], was introduced as a consequence of the desire to use smaller particle diameters. This was soon followed by the commercial availability of U(H)PLC instrumentation reaching operating pressures in excess of 1000 bar (100 MPa).

The great importance of high-pressure instrumentation when working with small particle diameters is made evident by eq. 7. The pressure drop ( $\Delta P$ ) across a column needed to achieve a mobile-phase linear velocity,  $u$ , can be correlated to the particle diameter ( $d_p$ ) by the Darcy equation [1].

$$\Delta P = \phi \eta L u / d_p^2 \quad (7)$$

where  $\phi$  is the flow-resistance factor,  $\eta$  is the viscosity of the solvent, and  $L$  is the length of the packed bed.

Moreover, it follows from the concept of reduced parameters that the optimum linear velocity ( $u_{\text{opt}}$ ) can be correlated to the particle diameter by equation 8.

$$u_{\text{opt}} \propto D_m / d_p \quad (8)$$

where  $D_m$  is the analyte's diffusion coefficient in the mobile phase [1].

Therefore, the pressure drop for a column of constant length operated at the optimal linear velocity is inversely proportional to the cube of the particle size. Because the plate height decreases in direct proportion with  $d_p$ , equal numbers

## Chapter 2

of plates can be achieved by keeping  $L/d_p$  constant. In that case the pressure drop increases with  $1/d_p^2$ . Thus, the use of smaller particles is typically combined with the use of shorter columns and increased pressures. Keeping the plate count constant, shorter columns and higher optimal flow rates result in a reduction of the analysis time by a factor  $d_p^2$ .

The highly desirable progress towards smaller particles made possible by advancements in high-pressure instrumentation came with one fundamental disadvantage, *viz.* frictional heating [29]. The energy dissipated in the column causes a radial thermal gradient that can be predicted using the following approximate equation [30].

$$\Delta T_R \approx \frac{u_s \left( \frac{dP}{dz} \right) d_c^2}{16\lambda_m} \approx \frac{F\Delta P}{4\pi L\lambda_m} \quad (9)$$

The radial thermal gradient obtained is proportional to the pressure drop per unit length ( $dP/dz$ ), the superficial velocity of the mobile-phase ( $u_s$ ), and the square of the column radius.  $\lambda_m$  is the thermal conductivity of the mobile phase. Thus, a solution for reduction of frictional heating when using smaller particles is a reduction of the column diameter. This implies that very fast contemporary separations are obtained on short, relatively narrow columns packed with very small particles.

High-pressure LC can readily lead to very fast (below 1 min) isocratic second-dimension separations. However, gradient-elution separations are more complicated. Carr et al [29] presented the challenges faced when moving to gradient separations. One of these was the need to minimize the system (dwell) volume. This was addressed by reducing the mixer volume from 1 mL to 100  $\mu$ L and by using narrow tubing. A small dwell volume (from pump heads to the column entrance) allows fast delivery of the gradient. The extra-column volume (from injector to detector) is much smaller, so as to not greatly

affect the speed of separation, but it should be minimized to limit the contribution of extra-column band broadening. In case of gradient elution, the analytes can usually be focussed at the top of the column at the starting conditions, so that only the post column volume (from column to detector) contributes to the extra-column band broadening.

High pressures have been applied in many LC×LC applications in the last years. The first application of UHPLC in LC×LC was for the separation of phenolic compounds in wine [31]. A comparison was made between HPLC×HPLC and HPLC×UHPLC. The highest peak capacity was obtained by using silica monoliths in the second dimension under HPLC conditions (inlet pressure 8 MPa or 80 bar). UHPLC conditions were not exploited to the full for any of the second-dimension columns tested (maximum pressure used 52 MPa) and the injection volume was kept the same for HPLC and UHPLC while a narrower column was used in the latter case. Kivilompolo et al. [31] made it clear that increasing the operating pressure alone was not enough to achieve higher peak capacities. Other parameters, such as the injection volume, extra-column volume, and the use of optimal conditions for the separation also play important roles.

Holčapek et al. [32] showed the first fully comprehensive LC×LC separation of complex lipidomics samples from human plasma and porcine brain with a <sup>2</sup>D separation of 1 min. The combination of lipid-species separation using RPLC (<sup>1</sup>D) and lipid-class separation with HILIC (<sup>2</sup>D), i.e. RPLC×HILIC, yielded a very fast separation. However, fewer lipids were identified as compared to offline or stop-flow LC×LC. This research drew attention to the great need to improve 2D-LC technology and to increase the sensitivity, so as to allow a fair comparison with well-optimized 1D systems.

For the separation of polymers Uliyanchenko et al. [33] used “ultra-high” pressures in both dimensions, combining UHPLC in the first dimension (pressure varying from 45 to 75 MPa during the gradient) to achieve separation based on the polymer chemical composition and ultra-high-pressure size-exclusion chromatography (UHPSEC) in the second dimension (at 85 MPa) for size-based separation. With the set-up proposed, <sup>2</sup>D separations were achieved in less than 1 min and complete separations of a complex mixture of copolymers within 22 min. The <sup>2</sup>D separations could be sped up to 30 s by overlapping SEC injections.

### **3.2 High temperature**

Use of higher temperature in LC was demonstrated to increase the speed and efficiency and improve the peak shape and the resolution of the separation [34]. Temperature may also be used to tune the selectivity. Faster separations at elevated temperatures can be achieved due to shorter gradients and decreased retention. The mobile-phase viscosity decreases with increasing temperatures, allowing increased mobile-phase velocities (or reduced pressures). Efficiency and resolution are positively impacted by a faster mass transfer between the mobile and stationary phases, thanks to an increase in analyte diffusivity with increasing temperature. Overall, elevated temperatures lead to greater efficiency per unit time. Selectivity can be impacted by temperature, especially for ionizable analytes due to the temperature dependency of the ionization equilibrium [35].

High-temperature LC (HTPLC) has been applied also in LC×LC. Stoll et al. demonstrated the possibility of reducing the <sup>2</sup>D separation time to 20 s with the use of high-temperature LC [36]. The proposed set-up used RP-HPLC separations in both dimensions, but with different column chemistries. The

first dimension was a pentafluorophenylpropyl-bonded silica column, operated at 40°C, while the second dimension contained a temperature-stable carbon-coated-zirconia stationary phase, operated at 110°C. The separation of metabolites from maize extracts showed very high peak-production rates, obtaining a peak capacity of about 900 in 25 min.

Another application of high temperature RPLC×RPLC was shown by Le Masle et al. [37] for the separation of bio-oils. Some 15 column chemistries were investigated at temperatures between 30 and 90°C. Two gradients with different slopes were run to allow the *in-silico* screening of 237 possible LC×LC combinations for the highest orthogonality and peak capacity. The combination of a non-silica-based and a silica-based column and high <sup>2</sup>D temperature was predicted to offer the best results. After experimental optimization of the LC×LC setup, the combination with the highest orthogonality and peak capacity was found to be a Hypercarb <sup>1</sup>D column operated at 60°C (maximum temperature of the <sup>1</sup>D oven) and a CSH Phenyl Hexyl <sup>2</sup>D column operated at 80°C. The calculated peak capacity was almost 2000. However, the run time was 285 min.

### 3.3 High pressure and high temperature

Heinish et al. confirmed [38] that the highest theoretical peak capacity for a second-dimension separation could be achieved by combining high-pressure and high-temperature conditions. The peak capacity was calculated for a 1 mm ID <sup>1</sup>D column at 10 µL/min and for a 2.1 mm ID <sup>2</sup>D column operated at flow rates between 0.5 and 5 mL/min, where pressure permitted. The simulated peak capacity increased in the order HPLC (20°C, 35 MPa, maximum observed peak capacity  $n_{p,max} \approx 40$ ) < HTLC (90°C, 35 MPa,  $n_{p,max} \approx 70$ ) < UHPLC (20°C, 80 MPa,  $n_{p,max} \approx 100$ ) < HT-UHPLC (90°C, 80 MPa,  $n_{p,max} \approx$

170). The HT-UHPLC <sup>2</sup>D conditions were also applied for the separation of tryptic peptides with RPLC×RPLC and RPLC×HILIC. The use of HT-UHPLC allowed for very short <sup>2</sup>D analysis times (30 s), while maintaining a high peak capacity.

### **3.4 Core-shell particles and monoliths**

Core-shell particles have emerged as an alternative to the use of very small porous particles that require UHPLC conditions [39]. The principle employed is the use of a solid core (usually silica) and a porous shell built up in layers. Salisbury et al. [40] showed that a column packed with 2.7 μm core-shell particles (1.7 μm solid silica core and 0.5 μm porous silica layer) offered 80% of the efficiency of a column packed with 1.7 μm particles, while giving half of the backpressure.

The advantages of this technology are the shorter diffusion paths, higher permeability, high homogeneity of particle dimensions, and higher thermal conductivity [41]. Faster separations can be achieved due to the shorter diffusion paths, and thus, faster mass transfer (C-term in the van Deemter equation) and higher permeability which allowed higher velocities. The efficiency is also thought to be increased due to the narrower size distribution, leading to a more homogeneously packed column (A-term in the van Deemter equation) and due to the higher thermal conductivity that improves heat dissipation. In combination with the lower pressures, this allows wider columns to be used without a radial temperature gradient causing additional band broadening.

Monoliths are integral (“one piece”) porous media that can be created in chromatographic columns instead of a packed bed [42–44]. Monoliths can be created in-situ in (capillary) columns or they may be inserted in a tight (polymeric) sleeve. In either case, convective flow between the wall of the

column and the monoliths should be avoided. Two types of monoliths are commonly used, i.e. silica monoliths and organic monolith. Also, combinations of these two types of materials have been used, yielding promising “hybrid” monoliths [45]. The main advantage of monoliths is their higher permeability. This allows longer columns to be used without an increase in pressure. However, in LC×LC the <sup>1</sup>D flow rate is usually low and pressure is rarely a limiting factor in the first dimension (see section 2). The higher permeability of monoliths also allows higher flow rates to be used, which make them an attractive option for very fast <sup>2</sup>D separations. The main limitation of organic monoliths in particular is their limited efficiency.

Core-shell particles or monoliths can be applied in LC×LC to speed up the second dimension separation. The challenge to reach very fast and efficient separations can be mitigated by the advantages of core-shell particles [46]. Monoliths also promise an increase in speed due to their higher permeability and low resistance to mass transfer. However the high eddy-diffusion contribution has led to lower efficiencies compared to packed columns [47].

Pirok et al. combined hydrodynamic chromatography (HDC) and SEC into HDC×SEC for nanoparticle analysis [48]. The nanoparticles were separated by size in the <sup>1</sup>D-HDC separation and broken down into the constituting polymers in a modulator. Thereafter, the polymers were separated according to their hydrodynamic radius in the <sup>2</sup>D-SEC separation. A faster <sup>2</sup>D separation was achieved by coupling three core-shell C18 columns in series. This yielded a similar or better resolution than a porous-particle SEC column, but in a shorter time. Thanks to overlapping injections in the <sup>2</sup>D-SEC separation, a modulation time of 36 s was achieved.

The implementation of core-shell particles for the <sup>2</sup>D column was compared to sub-2- $\mu\text{m}$  fully porous particles by Haidar Ahmad et al. [49]. The

## Chapter 2

conditions considered were fast gradients (9 - 120 s) at a high temperature (95°C), either at the same linear flow velocity or at the same back pressure. When operated at the same pressure, the core-shell column gave slightly higher peak capacities. However, the flow for the core-shell column was higher, which can be highly advantageous in the <sup>2</sup>D separation to overcome the system dwell volume and to equilibrate the column faster (within 3 s).

Core-shell particles were compared to fully porous particles for the <sup>2</sup>D stationary-phase also by Sommella et al. [50]. The separation of peptides in 90 min by RPLC×RPLC showed the highest experimental peak capacity ( $n_c = 2096$ ) when the core-shell column was used to obtain a fast <sup>2</sup>D separation (45 s), outperforming the fully-porous-particle column. The opposite was observed when the <sup>2</sup>D separation was longer (60 s). In that case, the fully-porous-particle column outperformed the core-shell column.

From the practical applications presented above, sub-2- $\mu\text{m}$  fully-porous particles and core-shell particles (approximately 3  $\mu\text{m}$ ) offer similar performance. The demonstrated advantage of the core-shell columns was the possibility to operate them at higher linear velocities without a great increase in backpressure. Also, core-shell particles allow larger internal diameters, resulting in higher volumetric flow rates and shorter dwell times.

The use of a <sup>2</sup>D monolithic column in LC×LC was shown by Hu et al. [51] for the separation of traditional Chinese medicines. A comparison was made with a packed <sup>2</sup>D column. By introducing a silica-monolithic column with C18 ligands instead of a packed column, the speed of the second-dimension separation could be greatly increased. This allowed for a shorter modulation time. Hence, a higher flow velocity was possible in the first dimension. The operation of the <sup>1</sup>D column at a more optimal linear flow velocity, led to a 50% increase in the plate count and a great reduction in total analysis time

(from 215 min down to 130 min), while obtaining an increase in the number of observed peaks by more than 50%.

Tanaka et al. [52] investigated several ways of performing 2D-LC separations for hydrocarbons and benzene derivatives, employing a silica-monolithic C18 column in the second dimension. In the case of an LC×LC setup, the monolithic column was run at a linear flow velocity of 10 mm/s with a pressure lower than 10 MPa. This allowed for a 30-s <sup>2</sup>D separation, resulting in a total peak capacity of about 1000 in 60 min.

Dugo et al. [53] showed the use of a monolithic column as a way of dealing with solvent incompatibility between the first- and second-dimension separations. They presented the use of a microcolumn for the <sup>1</sup>D separation (normal-phase LC; 1 mm ID) and an RPLC monolithic column (4.6 mm ID) in the second dimension. The use of low flow rates in the first-dimension (15.4 μL/min) combined with very high flow rates in the second-dimension (4 mL/min) allowed them to minimize the second-dimension injection volume and to achieve peak-focussing at the top of the <sup>2</sup>D column.

### **3.5 Enhanced-fluidity liquid chromatography and supercritical-fluid chromatography**

Enhanced-fluidity liquid chromatography (EFLC) [54] has emerged as a bridge between high-performance liquid chromatography (HPLC) and supercritical-fluid chromatography (SFC).

In both cases conventional HPLC mobile phases are combined with liquefied gases, such as carbon dioxide (CO<sub>2</sub>) [55]. In SFC, CO<sub>2</sub> is the main (or, occasionally, only) component of the mobile phase. In EFLC CO<sub>2</sub> is the minor component.

## Chapter 2

Mobile phases in SFC or EFLC feature enhanced diffusion and reduced viscosity in comparison with liquid solvents, while maintaining a high solvent strength. This results in increased efficiency at lower backpressures.

The first online LC×SFC coupling was shown with SEC in the first dimension coupled to capillary (open-tubular) SFC [56]. However, this type of hyphenation did not spark much interest in the following years, due to the diminishing interest in capillary SFC. Later, with the advancements in packed column SFC, LC×SFC hyphenations have re-emerged [57] in many research fields, such as bioenergy, food, lipidomics, pharmaceuticals, *etc.*

Sarrut et al. [58] showed the application of RPLC×SFC for the separation of neutral compounds in bio-oil samples. The RPLC×SFC separation was compared to an RPLC×RPLC separation in terms of orthogonality and efficiency. The authors found a slightly higher overall peak capacity for the RPLC×SFC setup, which was said to be due to the high degree of orthogonality. However, the RPLC×SFC system still showed limitations, such as large dwell and extra-column volumes, which impacted the separation efficiency and sensitivity.

Another RPLC×SFC combination was presented by Sun et al. for the separation of depolymerized lignin samples [59]. The interface between the SFC and LC was realized either with loops or with trapping columns. The latter showed a (two-fold) reduction in analysis time and better sensitivity, due to a focusing effect. One disadvantage mentioned was the undersampling of the first dimension in the case of trapping columns, which lead to a decrease in peak capacity.

SFC×LC has also been reported in literature. Donalito et al. [60] proposed SFC×RPLC hyphenation as an alternative to the highly orthogonal, but impractical NPLC×RPLC combination. By post-column addition of water and

use of trapping columns in between the two dimensions, the analytes were successfully focused before they were sent to the <sup>2</sup>D column. The SFC×RPLC analysis of carotenoids in red chili pepper was performed in half the time needed for the corresponding NPLC×RPLC separation. SFC×RPLC allowed for a larger number of identified compounds (50 vs. 33) and the column lifetime could be extended by avoiding the damaging solvents normally used in NPLC.

EFLC was shown to alleviate some of the limitations encountered when separating hydrophilic compounds in SFC, while still using mobile phases with lower viscosities than in HPLC [61]. The technique was successfully applied using an amide column for the separation of nucleotides, nucleosides [62], fructans [63], and hydrophilic proteins up to 80 kDa in size [64].

EFLC was also demonstrated in the separation of polystyrene standards by SEC [65], using tetrahydrofuran (THF) mixed with CO<sub>2</sub> as eluent. The chromatographic efficiency was enhanced when increasing the concentration of CO<sub>2</sub> (up to 50 mol %), while the optimal linear flow velocity increased. Therefore, faster and more-efficient separations were achieved. To our knowledge, comprehensive two-dimensional separations that use EFLC in either dimension have not been reported yet.

### **3.6 Alternative separation devices**

Column-based comprehensive two-dimensional LC (LC×LC) has shown great improvements over 1D-LC. However, when dealing with highly complex samples we need to strive for even greater separation power. Higher separation powers have been shown to be achievable either by addition of another separation dimension [66] or by employing spatial separations [67].

Three dimensional column-based (“temporal”) separations are difficult to implement, due to increasing time restrictions going from the first to the

## Chapter 2

second and to the third dimension. Every additional separation has to be completed in the time it takes to fractionate the previous separation. If the total separation time is not greatly extended, the <sup>3</sup>D separation will need to be completed in a matter of few seconds (or less) [68]. Only one such column-based three-dimensional liquid-phase separation has ever been reported, using SEC (hours), RPLC (minutes), and capillary electrophoresis (CE, seconds) in the three dimensions [69]. Such separations are extremely challenging, as they demand extreme robustness from the <sup>3</sup>D separation.

Alternatively, the increase in separation power may be achieved by spatial separations. Davydova et al. [67] calculated the theoretical performance of different types of separation systems. They concluded that spatial 2D separations may be advantageous in comparison with time-based LC×LC separations, even at modest pressures (5 MPa). Comprehensive three-dimensional spatial separations, if they can be realized, hold immense promise, with peak capacities of up to a million in a few hours.

Davydova et al. [70] proposed a design for a microfluidic device that uses a channel for the <sup>1</sup>D spatial separation and multiple perpendicular <sup>2</sup>D channels for a spatial or temporal <sup>2</sup>D separation. In this design all the second dimension separations would be developed simultaneously instead of sequentially. The device allows for all the <sup>1</sup>D eluent to be transferred concomitantly to the second dimension channel, resulting in a great reduction of the total separation time. Challenges still confront these microfluidic devices, such as flow confinement and introduction of orthogonal retention mechanisms (stationary phases). However, more investigations have emerged that look into solutions for implementation of microfluidic devices in separation sciences.

In a further development Wouters et al. [71] proposed a 3D microfluidic chip with 16 <sup>2</sup>D channels and 256 <sup>3</sup>D channels. Flow confinement was obtained by

implementing physical barriers. A stationary phase was synthesised in situ by forming organic monoliths using thermal UV-induced polymerization. The device was intended to have spatial separations in the first two dimensions and temporal separation in the third ( $^x\text{LC} \times ^x\text{LC} \times ^T\text{LC}$ ), to allow “stamping” of the analytes for easier detection. However, such separations were not yet reported.

Adamopoulou et al. [72] have proposed a TWo-dimensional Insertable Separation Tool (TWIST) that would provide a complete flow confinement between the first separation channel and the multiple second dimension channels. The microfluidic device was designed to have a rotatable cylinder containing the first dimension channel that is inserted in a device containing a flow distributor and multiple  $^2\text{D}$  channels. During the first-dimension separation the  $^1\text{D}$  channel outlets are offset compared to the  $^2\text{D}$  channels, allowing complete flow confinement. Followed by twisting of the cylinder containing the 1D channel to align it with the 2D channels, allowing the second dimension separation to proceed.

Passamonti et al. [73] investigated the confinement of stationary phases in microfluidic devices, by formation of monoliths in selected areas. Using titanium 3D-printed devices equipped with heating and cooling jackets, the monolith formation could be confined in the heated half of the channel, while the polymerization mixture could be flushed away from the cooled half of the channel. This advancement brings a solution to the introduction of different (orthogonal) stationary phases inside devices, with the limitation of a quite intricate design and large space needed for the implementation of the jackets around each channel or separation space.

## 4. Conclusions

The aim of this review was to provide an overview of the major advances in one-dimensional liquid chromatography that have been applied to make comprehensive two-dimensional chromatography a more-accessible and more-attractive analysis tool for many sample types.

The need for analysis of highly complex samples has driven the development of liquid-chromatographic technologies and, in particular, of multidimensional separations. The goal for faster and more-efficient separations has inspired developments in column technology, instrument capabilities and ingeniously designed separation devices. In this ever-growing field, the major progress in the past decades may be attributed to the development of UHPLC, ultra-small particles, core-shell particles, monoliths, and microfluidic devices.

The applications shown in this review, are ample proof that comprehensive two-dimensional liquid chromatography, even if it can be seen as a highly complex tool, has gained popularity in fields such as biopharmaceuticals, proteomics, food science, polymers, etc. The development of LC×LC greatly benefited from all progress in LC, especially from increases in the speed of separation.

The future holds great prospects for the development of alternative separation devices, such as those for spatial 2D and 3D separations. The need for improvement still lies in the device-manufacturing process, better connections with the instrument, introduction of stationary phases, flow confinement, and detection capabilities.

## 5. References

- [1] L.R. Snyder, J.J. Kirkland, Introduction to modern liquid chromatography, 1979. doi:10.1093/jaoac/58.1.169.
- [2] D. Guillarme, J. Ruta, S. Rudaz, J.L. Veuthey, New trends in fast and high-resolution liquid chromatography: A critical comparison of existing approaches, *Anal. Bioanal. Chem.* 397 (2010) 1069–1082. doi:10.1007/s00216-009-3305-8.
- [3] B.A. Olsen, B.C. Castle, D.P. Myers, Advances in HPLC technology for the determination of drug impurities, *TrAC - Trends Anal. Chem.* 25 (2006) 796–805. doi:10.1016/j.trac.2006.06.005.
- [4] D.R. Stoll, Recent progress in online, comprehensive two-dimensional high-performance liquid chromatography for non-proteomic applications, *Anal. Bioanal. Chem.* 397 (2010) 979–986. doi:10.1007/s00216-010-3659-y.
- [5] G. Vivó-Truyols, S. Van Der Wal, P.J. Schoenmakers, Comprehensive study on the optimization of online two-dimensional liquid chromatographic systems considering losses in theoretical peak capacity in first- and second-dimensions: A pareto-optimality approach, *Anal. Chem.* 82 (2010) 8525–8536. doi:10.1021/ac101420f.
- [6] J. Calvin Giddings, Maximum Number of Components Resolvable by Gel Filtration and Other Elution Chromatographic Methods, *Anal. Chem.* 39 (1967) 1027–1028. doi:10.1021/ac60252a025.
- [7] J.M. Davis, J.C. Giddings, Statistical Theory of Component Overlap in Multicomponent Chromatograms, *Anal. Chem.* 55 (1983) 418–424. doi:10.1021/ac00254a003.
- [8] B.W.J. Pirok, A.F.G. Gargano, P.J. Schoenmakers, Optimizing separations in online comprehensive two-dimensional liquid chromatography, *J. Sep. Sci.* 41 (2018) 68–98. doi:10.1002/jssc.201700863.
- [9] D. V. McCalley, Study of the selectivity, retention mechanisms and performance of alternative silica-based stationary phases for separation of ionised solutes in hydrophilic interaction chromatography, *J. Chromatogr. A.* (2010). doi:10.1016/j.chroma.2010.03.011.
- [10] U.D. Neue, J.E. O’Gara, A. Méndez, Selectivity in reversed-phase separations. Influence of the stationary phase, *J. Chromatogr. A.* 1127 (2006) 161–174. doi:10.1016/j.chroma.2006.06.006.
- [11] P.J.P.J. Schoenmakers, G. Vivó-Truyols, W.M.C.W.M.C. Decrop, A protocol for designing comprehensive two-dimensional liquid chromatography separation systems., *J. Chromatogr. A.* 1120 (2006) 282–90. doi:10.1016/j.chroma.2005.11.039.

## Chapter 2

- [12] H. Pasch, K. Mequanint, J. Adrian, Two-dimensional chromatography of complex polymers. 3. Full analysis of polystyrene-poly(methyl methacrylate) diblock copolymers, *E-Polymers*. 2 (2002). doi:10.1515/epoly.2002.2.1.69.
- [13] R.J. Vonk, A.F.G. Gargano, E. Davydova, H.L. Dekker, S. Eeltink, L.J. De Koning, P.J. Schoenmakers, Comprehensive two-dimensional liquid chromatography with stationary-phase-assisted modulation coupled to high-resolution mass spectrometry applied to proteome analysis of *saccharomyces cerevisiae*, *Anal. Chem.* 87 (2015) 5387–5394. doi:10.1021/acs.analchem.5b00708.
- [14] D.R. Stoll, K. Shoykhet, P. Petersson, S. Buckenmaier, Active Solvent Modulation: A Valve-Based Approach to Improve Separation Compatibility in Two-Dimensional Liquid Chromatography, *Anal. Chem.* 89 (2017) 9260–9267. doi:10.1021/acs.analchem.7b02046.
- [15] K. Horie, H. Kimura, T. Ikegami, A. Iwatsuka, N. Saad, O. Fiehn, N. Tanaka, Calculating optimal modulation periods to maximize the peak capacity in two-dimensional HPLC, *Anal. Chem.* 79 (2007) 3764–3770. doi:10.1021/ac062002t.
- [16] X. Li, D.R. Stoll, P.W. Carr, A Simple and Accurate Equation for Peak Capacity Estimation in Two Dimensional Liquid Chromatography, *Anal. Chem.* 81 (2009) 845–850. doi:10.1021/ac801772u.
- [17] J.M. Davis, D.R. Stoll, P.W. Carr, Dependence of effective peak capacity in comprehensive two-dimensional separations on the distribution of peak capacity between the two dimensions, *Anal. Chem.* 80 (2008) 8122–8134. doi:10.1021/ac800933z.
- [18] Y. Shen, R. Zhang, R.J. Moore, J. Kim, T.O. Metz, K.K. Hixson, R. Zhao, E.A. Livesay, H.R. Udseth, R.D. Smith, Automated 20 kpsi RPLC-MS and MS/MS with chromatographic peak capacities of 1000-1500 and capabilities in proteomics and metabolomics, *Anal. Chem.* 77 (2005) 3090–3100. doi:10.1021/ac0483062.
- [19] T. Werres, T.C. Schmidt, T. Teutenberg, The influence of injection volume on efficiency of microbore liquid chromatography columns for gradient and isocratic elution, *J. Chromatogr. A*. 1641 (2021) 461965. doi:10.1016/j.chroma.2021.461965.
- [20] G. Groeneveld, M.N. Dunkle, M. Pursch, E.P.C. Mes, P.J. Schoenmakers, A.F.G. Gargano, Investigation of the effects of solvent-mismatch and immiscibility in normal-phase  $\times$  aqueous reversed-phase liquid chromatography, *J. Chromatogr. A*. 1665 (2022) 462818. doi:10.1016/j.chroma.2022.462818.
- [21] Z. Viktor, C. Farcet, C. Moire, F. Brothier, H. Pfukwa, H. Pasch, Comprehensive two-dimensional liquid chromatography for the characterization of acrylate-modified hyaluronic acid, *Anal. Bioanal. Chem.* 411 (2019) 3321–3330. doi:10.1007/s00216-019-01799-x.

- [22] Y. Chen, L. Montero, O.J. Schmitz, Advance in on-line two-dimensional liquid chromatography modulation technology, *Trends Anal. Chem.* 120 (2019) 115647. doi:10.1016/j.trac.2019.115647.
- [23] B.W.J. Pirok, D.R. Stoll, P.J. Schoenmakers, Recent Developments in Two-Dimensional Liquid Chromatography: Fundamental Improvements for Practical Applications, *Anal. Chem.* 91 (2019) 240–263. doi:10.1021/acs.analchem.8b04841.
- [24] R.J. Vonk, A.F.G. Gargano, E. Davydova, H.L. Dekker, S. Eeltink, L.J. de Koning, P.J. Schoenmakers, Comprehensive Two-Dimensional Liquid Chromatography with Stationary-Phase-Assisted Modulation Coupled to High-Resolution Mass Spectrometry Applied to Proteome Analysis of *Saccharomyces cerevisiae.*, *Anal. Chem.* 87 (2015) 5387–5394. doi:10.1021/acs.analchem.5b00708.
- [25] H. Tian, J. Xu, Y. Xu, Y. Guan, Multidimensional liquid chromatography system with an innovative solvent evaporation interface, *J. Chromatogr. A.* 1137 (2006) 42–48. doi:10.1016/j.chroma.2006.10.005.
- [26] J.N. Fairchild, K. Horváth, G. Guiochon, Theoretical advantages and drawbacks of on-line, multidimensional liquid chromatography using multiple columns operated in parallel, *J. Chromatogr. A.* 1216 (2009) 6210–6217. doi:10.1016/j.chroma.2009.06.085.
- [27] S. Yang, J. Liu, D.L. DeVoe, Optimization of sample transfer in two-dimensional microfluidic separation systems, *Lab Chip.* 8 (2008) 1145–1152. doi:10.1039/b801978a.
- [28] J.E. MacNair, K.C. Lewis, J.W. Jorgenson, Ultrahigh-Pressure Reversed-Phase Liquid Chromatography in Packed Capillary Columns, *Anal. Chem.* 69 (1997) 983–989. doi:10.1021/ac961094r.
- [29] P.W. Carr, D.R. Stoll, X. Wang, Perspectives on Recent Advances in the Speed of High-Performance Liquid Chromatography, *Anal. Chem.* 83 (2011) 1890–1900. doi:10.1021/ac102570t.
- [30] A. de Villiers, H. Lauer, R. Szucs, S. Goodall, P. Sandra, Influence of frictional heating on temperature gradients in ultra-high-pressure liquid chromatography on 2.1 mm I.D. columns, *J. Chromatogr. A.* 1113 (2006) 84–91. doi:10.1016/j.chroma.2006.01.120.
- [31] M. Kivilompolo, T. Hyötyläinen, Comparison of separation power of ultra performance liquid chromatography and comprehensive two-dimensional liquid chromatography in the separation of phenolic compounds in beverages, *J. Sep. Sci.* 31 (2008) 3466–3472. doi:10.1002/jssc.200800287.
- [32] M. Holčápek, M. Ovčáčíková, M. Lísa, E. Cífková, T. Hájek, Continuous comprehensive two-dimensional liquid chromatography–electrospray ionization mass

## Chapter 2

spectrometry of complex lipidomic samples, *Anal. Bioanal. Chem.* 407 (2015). doi:10.1007/s00216-015-8528-2.

[33] E. Uliyanchenko, P.J.C.H. Cools, S. Van Der Wal, P.J. Schoenmakers, Comprehensive two-dimensional ultrahigh-pressure liquid chromatography for separations of polymers, *Anal. Chem.* 84 (2012) 7802–7809. doi:10.1021/ac3011582.

[34] G. Vanhoenacker, P. Sandra, High temperature and temperature programmed HPLC: Possibilities and limitations, *Anal. Bioanal. Chem.* 390 (2008) 245–248. doi:10.1007/s00216-007-1671-7.

[35] D. V. McCalley, Effect of temperature and flow-rate on analysis of basic compounds in high-performance liquid chromatography using a reversed-phase column, *J. Chromatogr. A.* 902 (2000) 311–321. doi:10.1016/S0021-9673(00)00924-9.

[36] D.R. Stoll, J.D. Cohen, P.W. Carr, Fast, comprehensive online two-dimensional high performance liquid chromatography through the use of high temperature ultra-fast gradient elution reversed-phase liquid chromatography, *J. Chromatogr. A.* 1122 (2006) 123–137. doi:10.1016/j.chroma.2006.04.058.

[37] A. Le Masle, D. Angot, C. Gouin, A. D'Attoma, J. Ponthus, A. Quignard, S. Heinisch, Development of on-line comprehensive two-dimensional liquid chromatography method for the separation of biomass compounds, *J. Chromatogr. A.* 1340 (2014) 90–98. doi:10.1016/j.chroma.2014.03.020.

[38] S. Heinisch, Using elevated temperature in UHPLC: Interest and limitations, 2012. doi:10.1039/9781849735490-00102.

[39] Y. Hsieh, C.J.G. Duncan, J.M. Brisson, Fused-core silica column high-performance liquid chromatography/tandem mass spectrometric determination of rimonabant in mouse plasma, *Anal. Chem.* 79 (2007) 5668–5673. doi:10.1021/ac070343g.

[40] J.J. Salisbury, Fused-core particles: A practical alternative to sub-2 micron particles, *J. Chromatogr. Sci.* 46 (2008) 883–886. doi:10.1093/chromsci/46.10.883.

[41] V. González-Ruiz, A.I. Olives, M.A. Martín, Core-shell particles lead the way to renewing high-performance liquid chromatography, *TrAC - Trends Anal. Chem.* 64 (2015) 17–28. doi:10.1016/j.trac.2014.08.008.

[42] R.D. Arrua, T.J. Causon, E.F. Hilder, Recent developments and future possibilities for polymer monoliths in separation science, *Analyst.* 137 (2012) 5179–5189. doi:10.1039/c2an35804b.

[43] F. Svec, Y. Lv, Advances and recent trends in the field of monolithic columns for chromatography, *Anal. Chem.* 87 (2015) 250–273. doi:10.1021/ac504059c.

- [44] P. Jandera, Advances in the development of organic polymer monolithic columns and their applications in food analysis - A review, *J. Chromatogr. A.* 1313 (2013) 37–53. doi:10.1016/j.chroma.2013.08.010.
- [45] T. Zhu, K.H. Row, Preparation and applications of hybrid organic-inorganic monoliths: A review, *J. Sep. Sci.* 35 (2012) 1294–1302. doi:10.1002/jssc.201200084.
- [46] P. Jandera, T. Hájek, M. Staňková, Monolithic and core-shell columns in comprehensive two-dimensional HPLC: A review, *Anal. Bioanal. Chem.* 407 (2015) 139–151. doi:10.1007/s00216-014-8147-3.
- [47] G. Guiochon, Monolithic columns in high-performance liquid chromatography, *J. Chromatogr. A.* 1168 (2007) 101–168. doi:10.1016/j.chroma.2007.05.090.
- [48] B.W.J. Pirok, N. Abdulhussain, T. Aalbers, B. Wouters, R.A.H. Peters, P.J. Schoenmakers, Nanoparticle Analysis by Online Comprehensive Two-Dimensional Liquid Chromatography combining Hydrodynamic Chromatography and Size-Exclusion Chromatography with Intermediate Sample Transformation, *Anal. Chem.* 89 (2017) 9167–9174. doi:10.1021/acs.analchem.7b01906.
- [49] I.A. Haidar Ahmad, A. Soliven, R.C. Allen, M. Filgueira, P.W. Carr, Comparison of core-shell particles and sub-2 $\mu$ m fully porous particles for use as ultrafast second dimension columns in two-dimensional liquid chromatography, *J. Chromatogr. A.* 1386 (2015) 31–38. doi:10.1016/j.chroma.2014.11.069.
- [50] E. Sommella, G. Pepe, G. Ventre, F. Pagano, M. Manfra, G. Pierri, O. Ismail, A. Ciogli, P. Campiglia, Evaluation of two sub-2 $\mu$ m stationary phases, core-shell and totally porous monodisperse, in the second dimension of on-line comprehensive two dimensional liquid chromatography, a case study: Separation of milk peptides after expiration date, *J. Chromatogr. A.* 1375 (2015) 54–61. doi:10.1016/j.chroma.2014.11.072.
- [51] L. Hu, X. Chen, L. Kong, X. Su, M. Ye, H. Zou, Improved performance of comprehensive two-dimensional HPLC separation of traditional Chinese medicines by using a silica monolithic column and normalization of peak heights, *J. Chromatogr. A.* 1092 (2005) 191–198. doi:10.1016/j.chroma.2005.06.066.
- [52] N. Tanaka, H. Kimura, D. Tokuda, K. Hosoya, T. Ikegami, N. Ishizuka, H. Minakuchi, K. Nakanishi, Y. Shintani, M. Furuno, K. Cabrera, Simple and Comprehensive Two Dimensional Reversed-Phase HPLC Using Monolithic Silica Column, *Anal. Chem.* 76 (2004) 1273–1281. doi:10.1021/ac034925j.
- [53] P. Dugo, M. del M.R. Fernández, A. Cotroneo, G. Dugo, L. Mondello, Optimization of a comprehensive two-dimensional normal-phase and reversed-phase liquid chromatography system, *J. Chromatogr. Sci.* 44 (2006) 561–565. doi:10.1093/chromsci/44.9.561.

## Chapter 2

- [54] Y. Cui, S. V. Olesik, High-Performance Liquid Chromatography Using Mobile Phases with Enhanced Fluidity, *Anal. Chem.* 63 (1991) 1812–1819. doi:10.1021/ac00017a028.
- [55] J. Bian, S. V. Olesik, Separation and characterization of KRas proteins and tryptic peptides using enhanced-fluidity liquid chromatography tandem mass spectrometry, *Analyst.* 144 (2019) 6270–6275. doi:10.1039/c9an01454c.
- [56] R. Moulder, K.D. Battle, A.A. Clifford, Coupled Microcolumn Size-exclusion Liquid Chromatography-Capillary Supercritical Fluid Chromatography, 116 (1991) 1293–1298.
- [57] M. Burlet-Parendel, K. Faure, Opportunities and challenges of liquid chromatography coupled to supercritical fluid chromatography, *TrAC - Trends Anal. Chem.* 144 (2021) 116422. doi:10.1016/j.trac.2021.116422.
- [58] M. Sarrut, A. Corgier, G. Crétier, A. Le Masle, S. Dubant, S. Heinisch, Potential and limitations of on-line comprehensive reversed phase liquid chromatography×supercritical fluid chromatography for the separation of neutral compounds: An approach to separate an aqueous extract of bio-oil, *J. Chromatogr. A.* 1402 (2015) 124–133. doi:10.1016/j.chroma.2015.05.005.
- [59] M. Sun, M. Sandahl, C. Turner, Comprehensive on-line two-dimensional liquid chromatography × supercritical fluid chromatography with trapping column-assisted modulation for depolymerised lignin analysis, *J. Chromatogr. A.* 1541 (2018) 21–30. doi:10.1016/j.chroma.2018.02.008.
- [60] P. Donato, D. Giuffrida, M. Oteri, V. Inferrera, P. Dugo, L. Mondello, Supercritical Fluid Chromatography × Ultra-High Pressure Liquid Chromatography for Red Chilli Pepper Fingerprinting by Photodiode Array, Quadrupole-Time-of-Flight and Ion Mobility Mass Spectrometry (SFC × RP-UHPLC-PDA-Q-ToF MS-IMS), *Food Anal. Methods.* 11 (2018) 3331–3341. doi:10.1007/s12161-018-1307-x.
- [61] R. Bennett, M. Biba, J. Liu, I.A. Haidar Ahmad, M.B. Hicks, E.L. Regalado, Enhanced fluidity liquid chromatography: A guide to scaling up from analytical to preparative separations, *J. Chromatogr. A.* 1595 (2019) 190–198. doi:10.1016/j.chroma.2019.02.017.
- [62] M.C. Beilke, M.J. Beres, S. V. Olesik, Gradient enhanced-fluidity liquid hydrophilic interaction chromatography of ribonucleic acid nucleosides and nucleotides: A “green” technique, *J. Chromatogr. A.* 1436 (2016) 84–90. doi:10.1016/j.chroma.2016.01.060.
- [63] R. Bennett, S. V. Olesik, Enhanced fluidity liquid chromatography of inulin fructans using ternary solvent strength and selectivity gradients, *Anal. Chim. Acta.* 999 (2018) 161–168. doi:10.1016/j.aca.2017.10.036.
- [64] R. Bennett, S. V. Olesik, Protein separations using enhanced-fluidity liquid chromatography, *J. Chromatogr. A.* 1523 (2017) 257–264. doi:10.1016/j.chroma.2017.07.060.

- [65] H. Yuan, I. Souvignet, S. V. Olesik, High-Performance Size Exclusion Chromatography Using Enhanced-Fluidity Liquid Mobile Phases, *J. Chromatogr. Sci.* 35 (1997) 409–416. doi:10.1093/chromsci/35.9.409.
- [66] B. Wouters, E. Davydova, S. Wouters, G. Vivo-Truyols, P.J. Schoenmakers, S. Eeltink, Towards ultra-high peak capacities and peak-production rates using spatial three-dimensional liquid chromatography, *Lab Chip*. 15 (2015) 4415–4422. doi:10.1039/c5lc01169h.
- [67] E. Davydova, P.J. Schoenmakers, G. Vivó-Truyols, Study on the performance of different types of three-dimensional chromatographic systems, *J. Chromatogr. A*. 1271 (2013) 137–143. doi:10.1016/j.chroma.2012.11.043.
- [68] N. Abdulhussain, S. Nawada, P. Schoenmakers, Latest Trends on the Future of Three-Dimensional Separations in Chromatography, *Chem. Rev.* 121 (2021) 12016–12034. doi:10.1021/acs.chemrev.0c01244.
- [69] A.W. Moore, J.W. Jorgenson, Comprehensive Three-Dimensional Separation of Peptides Using Size Exclusion Chromatography/Reversed Phase Liquid Chromatography/Optically Gated Capillary Zone Electrophoresis, *Anal. Chem.* 67 (1995) 3456–3463. doi:10.1021/ac00115a014.
- [70] E. Davydova, S. Wouters, S. Deridder, G. Desmet, S. Eeltink, P.J. Schoenmakers, Design and evaluation of microfluidic devices for two-dimensional spatial separations, *J. Chromatogr. A*. 1434 (2016) 127–135. doi:10.1016/j.chroma.2016.01.003.
- [71] B. Wouters, E. Davydova, S. Wouters, G. Vivo-Truyols, P.J. Schoenmakers, S. Eeltink, Towards ultra-high peak capacities and peak-production rates using spatial three-dimensional liquid chromatography, *Lab Chip*. 15 (2015) 4415–22. doi:10.1039/c5lc01169h.
- [72] T. Adamopoulou, S. Deridder, G. Desmet, P.J. Schoenmakers, Two-dimensional insertable separation tool (TWIST) for flow confinement in spatial separations, *J. Chromatogr. A*. 1577 (2018) 120–123. doi:10.1016/j.chroma.2018.09.054.
- [73] M. Passamonti, I.L. Bremer, S.H. Nawada, S.A. Currivan, A.F.G. Gargano, P.J. Schoenmakers, Confinement of monolithic stationary phases in targeted regions of 3d-printed titanium devices using thermal polymerization, *Anal. Chem.* 92 (2020) 2589–2596. doi:10.1021/acs.analchem.9b04298.

## Chapter 3

# Accurate modelling of the retention behaviour of peptides in gradient-elution hydrophilic interaction liquid chromatography

Liana S. Roca, Suzan E. Schoemaker, Bob W. J. Pirok, Andrea F. G. Gargano,  
Peter J. Schoenmakers

DOI: 10.1016/j.chroma.2019.460650

## Contents

1.	Introduction .....	66
2.	Experimental.....	69
2.1	Materials .....	69
2.2	Sample preparation .....	70
2.3	Instrumentation .....	70
2.4	Methods .....	71
2.5	Data processing and retention modelling .....	73
3.	Results and discussion .....	74
3.1	Effect of additives in HILIC separation of peptides.....	74
3.2	Retention modelling.....	77
3.3	RPLC retention modelling .....	80
3.4	HILIC-goodness of fit.....	82
3.5	HILIC - Retention-time prediction.....	83
4.	Conclusion.....	86
5.	Acknowledgements.....	88
6.	References .....	88

## **Abstract**

The applicability of models to describe peptide retention in hydrophilic interaction liquid chromatography (HILIC) was investigated. A tryptic digest of bovine-serum-albumin (BSA) was used as a test sample. Several different models were considered, including adsorption, mixed-mode, exponential, quadratic and Neue-Kuss models. Gradient separations were performed on three different HILIC stationary-phases under three different mobile-phase conditions to obtain model parameters. Methods to track peaks for specific peptides across different chromatograms are shown to be essential. The optimal mobile-phase additive for the separation of BSA digest on each of the three columns was selected by considering the retention window, peak width and peak intensity with mass-spectrometric detection. The performance of the models was investigated using the Akaike information criterion (AIC) to measure the goodness-of-fit and evaluated using prediction errors. The F-test for regression was applied to support model selection. RPLC separations of the same sample were used to test the models. The adsorption model showed the best performance for all the HILIC columns investigated and the lowest prediction errors for the amide and W-silica columns. In most cases prediction errors were within 1%.

## **Keywords**

HILIC, retention modelling, bottom-up proteomics, mass spectrometry

## 1. Introduction

Proteomics is a field comprising of different techniques used to identify and quantify the proteins present in cells, tissues and organisms [1]. A distinction can be made between top-down proteomics [2], where intact proteins are analysed, and bottom-up proteomics [3], where proteins are first digested to yield peptides, prior to analysis and interpretation. The identification and quantification is challenging, due to the high complexity of the sample, especially in bottom-up proteomics, and the great differences in relative abundance of proteins in a cell proteome [4]. An indispensable analytical technique in this field is mass spectrometry (MS). However, data quality can be detrimentally impacted if many species are infused at the same time. Therefore, MS alone cannot be used to analyse complex samples, such as whole-cell lysates. For this reason, separation techniques are typically coupled to MS analysis, providing the much needed simplification of the sample prior to its introduction into the MS.

Liquid chromatography (LC) is one of the most frequently employed separation techniques, since it can be directly coupled to MS. Moreover, for common LC modes employed, little or no additional sample preparation is needed. The most commonly used LC separation mode for bottom-up proteomics is reversed-phase liquid chromatography (RPLC). In RPLC, analytes are separated based on differences in partitioning between the hydrophilic (aqueous) mobile phase and the hydrophobic stationary phase. To facilitate timely elution of strongly retained analytes from the stationary phase, the fraction of organic modifier can be gradually increased using a gradient program. However, one limitation of RPLC is the lack of separation based on the polar functional groups which are abundantly present in peptides. Therefore, a complementary technique that would be able to retain polar compounds is needed to extend the analysis of a proteomic sample. This is

especially relevant for multi-dimensional separations, in which two (or three) vastly different (“orthogonal”) retention mechanisms are employed to greatly improve the separation of complex mixtures [5,6].

One method with a retention mechanism and selectivity that is very different from that of RPLC is hydrophilic-interaction liquid chromatography (HILIC). HILIC was introduced as a separation mode for polar compounds [7], but it is also used as a fractionation technique for bottom-up proteomics prior to a RPLC separation to decrease sample complexity [8]. Whereas hydrophobic alkyl-based stationary-phase chemistries are used in RPLC, HILIC employs a polar stationary phases, such as bare silica, or silica modified with amide, amino or diol groups [9]. Charged stationary-phases can also be used such as silica modified with cationic groups (*e.g.* poly aspartamide) or zwitterionic groups (*e.g.* ZIC HILIC). The mobile phases in HILIC mainly comprise of non-polar organic solvents, with small percentages (*e.g.* 3%) of water or aqueous buffer. The exact retention mechanism is still being investigated. However, there is a general consensus that retention is based on partitioning between an aqueous layer formed on the surface of the stationary phase and the mostly organic bulk mobile phase, with electrostatic interactions (ionic interactions and hydrogen bonding) also influencing the retention [7,10,11]. The exact magnitude of the different interactions highly depends on the employed stationary and mobile phases, but also on the properties of the analyte.

The large influence on retention of the selected stationary phase, mobile-phase solvent and additives, dramatically complicates method development for HILIC separations. In order to improve the adoption of HILIC, computational tools for method development are needed. Such tools generally rely on prediction of retention times with respect to the combination of stationary phase and mobile phase. Several models have been proposed for predicting

## Chapter 3

the retention times of peptides, based on their amino-acid composition, sequence and conformation [12–15], assessing the chemical structure of the analyte to predict retention. However, the development of such models depends heavily on large numbers of experiments using various mobile and stationary phases.

An alternative approach is based on establishing retention parameters of (unknown) analytes using the concept of so-called gradient-scanning techniques [16]. Here, the retention times are recorded for each analyte in a few experiments under pre-set conditions and the resulting data are fed into the underlying retention model. Entirely theoretical models require a thorough understanding of the underlying retention mechanism, which is challenging for HILIC. Alternatively, (semi-) empirical models can be used to describe the data.

Computer-aided method development for HILIC has been extensively studied by several groups [17,18]. Recently, the feasibility of accurate prediction of retention times of peaks eluting before, during or after a gradient was demonstrated, using only a small number of scouting measurements [19]. Several retention models were investigated and the prediction performance was shown to depend on the type of stationary-phase chemistry and the mobile-phase components. In addition, while the method was found to have great potential for smaller molecules, such as metabolites, dyes and tea components, its application for predicting retention times of peptides proved fruitless. However, in the above study only a small number of peptide standards were included, which were not representative of the peptides typically encountered in bottom-up proteomics.

In this study, we investigate the prediction of retention times of peptides for a larger number of combinations of stationary-phase chemistries and mobile-

phase additives. A more-complex sample (BSA digest), rather than standard peptides, is used that is much-more representative of a bottom-up-proteomics sample. Bovine serum albumin is attractive as bench mark sample because it is easily available and it includes a sufficient number of diverse peptides. Moreover, we rigorously evaluate the contemporary tools used to assess prediction performance. Computer aided method development for HILIC has been massively restricted by shortcomings in retention modelling on certain types of columns (particularly amide) and for certain types of analytes, especially peptides. The results of the present work remove these restrictions. In addition, the results help understand the retention behaviour in HILIC and they provide means to reduce the uncertainty in peptide identification. Finally, a number of general recommendations for HILIC separations of peptides are proposed.

## 2. Experimental

### 2.1 Materials

Milli-Q water (18.2 m $\Omega$ ) was obtained from a purification system (Millipore, Bedford, MA, USA). Acetonitrile (ACN, MS grade), 2-propanol (IPA, HPLC grade) and toluene were purchased from Biosolve Chimie (Dieuze, France). Ammonium formate (AF, BioUltra;  $\geq 99\%$ ) and ammonium bicarbonate (Bioultra;  $\geq 99.5\%$ ) were purchased from Fluka Analytical (Buchs, Switzerland). Acetic acid (glacial) was obtained from ACROS organics (Geel, Belgium).

The following chemicals were purchased from Sigma-Aldrich (Darmstadt, Germany), bovine serum albumin (BSA,  $\geq 96\%$ ), urea (bioreagent,  $\geq 98\%$ ), dithiothreitol (DTT,  $\geq 99\%$ ), iodoacetamide (IAA,  $\geq 99\%$ ), trypsin (BRP), uracyl ( $\geq 99\%$ ), ammonium acetate (AA, for molecular biology,  $\geq 98\%$ ), trifluoroacetic acid (TFA,  $\geq 99\%$ ), Formic acid (FA, Analytical grade; 98%),

SPE cartridges (3 mL, C18), thiourea (GR for analysis ACS) and sodium hydroxide (for analysis).

### 2.2 Sample preparation

The peptide samples were obtained by trypsin digestion. Denatured protein (100  $\mu$ L, 1  $\mu$ g/ $\mu$ L) in urea (6M) was reduced with DTT (5  $\mu$ L, 30 mg/mL in 25 mM ammonium bicarbonate) for an hour at 37°C. The protein was alkylated with IAA (20  $\mu$ L, 36 mg/mL in 25 mM ammonium bicarbonate) for one hour in the dark at room temperature. Then 20  $\mu$ L of DTT and 900  $\mu$ L of 25-mM ammonium-bicarbonate solution and finally trypsin (1:30 weight ratio trypsin:protein) were added. The protein was digested overnight at 37°C. The next day TFA (10%, 40  $\mu$ L) was added to acidify the sample to pH 2-3 before desalting the peptides using SPE cartridges (C18). The peptide solution was freeze-dried and reconstituted in 80% ACN, 20% buffer (1 mg/mL) before use.

### 2.3 Instrumentation

The LC-MS measurements were performed on an Agilent 1100 Series LC system with a quaternary pump (G1311A), an auto-sampler (G1313A) (Agilent, Waldbronn, Germany) in combination with a Micro-QTOF from Bruker (Bremen, Germany). The electrospray ionization (ESI) parameters used were end-plate offset -500 V, capillary voltage 4.4 kV, nebuliser 1 bar, dry gas 8 L/min, dry temperature 220°C. Compass Data analysis from Bruker was used to extract the  $m/z$  and retention time information. The dwell volume of the LC system was experimentally determined to be 0.81 mL and the dead time for the HILIC columns was 0.33 mL, measured using toluene and an Agilent DAD detector (1- $\mu$ L flow cell, 1290 Infinity diode-array detector (G4212A)).

A system comprised of an Eksigent Ekspert nanoLC 425 (Sciex, Singapore) coupled to a TripleTOF 5600+ mass spectrometer (Sciex, Singapore) was used for MS/MS measurements for sample identification. The columns used during this investigation are listed in table 1.

*Table 1: Columns used for the separation of BSA digest.*

Column	Brand and type of stationary phase	Selectivity	Designation	Dimensions (mm)	Particle size ( $\mu\text{m}$ )	Pore size ( $\text{\AA}$ )
1	Waters, Acquity, BEH	Amide	Amide	2.1×150	1.7	130
2	Waters, Atlantis	Silica	W-silica	2.1×150	3	100
3	Agilent, Zorbax, HILIC Plus	Silica	Z-silica	2.1×150	1.8	95
4	Phenomenex*, Kinetex	RP	XB-C18	4.6×150	3.5	100
5	In house packed, Magic C18**	RP	M-C18	0.075×100	5	100

\* Phenomenex (Torrance, CA, USA)

\*\* NanoLCMS Solutions (Oroville, CA, USA)

## 2.4 Methods

### 2.4.1 HILIC separation of peptides

Three different columns were chosen for the HILIC separations, W-silica (Waters), Z-silica (Zorbax) and amide. The effect of mobile phase additives on the retention and selectivity of the HILIC column was investigated using formic acid or two buffers, 10 mM ammonium formate, pH 3, and 10 mM ammonium acetate, pH 6. These conditions were selected based on the MS compatibility of the volatile additives and the pH range (in the working pH range of the columns), and to observe the effect of using a buffer compared to only an acidic environment. At acidic pH the silanol groups present in the stationary phase will be protonated, thus minimizing electrostatic interactions. All the HILIC columns were chosen to have the same dimensions, but the particle size varied (see Table 1). Bovine serum albumin (BSA) digested with

## Chapter 3

trypsin was used to provide a good range of peptides with varying properties and concentrations.

For each combination of mobile and stationary phase, six gradients were measured. Mobile-phase A was always 97% ACN with 3% water or buffer and B was 100% water or buffer. In the case of formic acid 0.3% (volume) was added to both A and B. The initial condition, isocratic 100% A was held for 0.25 min. This was followed by a linear gradient from 0% B to 40% B (amide and Z-silica column) or 50% (W-silica) in 10, 17, 30, 52, 70 or 80 min. The final condition was maintained for 1 min (amide and Z-silica) or 5 min (W-silica), after which the system was switched back to the initial conditions in 1 min. The equilibration time was set to 30 minutes (amide) or 50 min (Z-silica and W-silica). The flow rate was 0.2 mL/min. The sample was dissolved in 80% ACN 20% buffer with a concentration of 1 mg/mL. The injection volume was 5  $\mu$ L for the three shortest gradients and 10  $\mu$ L for the three longest gradients to overcome the problem of dilution.

In order to identify the peptides in the gradient runs, the same sample was measured on C18 column 75  $\mu$ m ID 10 cm length (M-C18) coupled to a high resolution mass spectrometer. The peptides identified using MS/MS were compared to peptides measured on the microQTOF and were considered a match if the m/z value was within 0.02 of the MS/MS identified peptides. A list of 15 peptides was constructed by comparing measurements with all stationary-phases and seven of these were selected to show the influence of mobile-phase additives due to their similar intensity.

The initial separation method was developed initially for the amide column and then for the silica columns. A scouting gradient from 97% ACN to 40% ACN was used and the final solvent composition was adjusted to have a better peak spreading. The length of the equilibration time was set initially to 20 min

and then increased to 30 min. Triplicate measurements were overlaid and no significant variations were observed in the retention times therefore the column was considered to be well equilibrated. Changes had to be made during measurements for the other columns. In the case of the Z-silica column, a peak shift was noticed between triplicate measurements. Therefore, the equilibration time after each run was increased. For the W-silica column, carry-over and peak shifting were observed, and therefore the final percentage of aqueous eluent was increased and the equilibration time was chosen the same as for the Z-silica column. The equilibration time has previously [20] been correlated to the water uptake capability of the stationary phase, with faster equilibration corresponding to higher water uptake. The amide stationary phases were reported to have the highest water uptake followed by bare silica, which was in line with our observations.

#### **2.4.2 RPLC separation of peptides**

BSA digest was separated on an RPLC column using the same linear gradient lengths as for HILIC, with 0.1% FA in water and with 10 mM ammonium formate pH 3 buffer as mobile phase A and 80% ACN mobile-phase B. The flow-rate used was 0.4 mL/min since the internal diameter was larger than that of the HILIC columns (4.6 mm). The gradient ran from 5% to 60% B, followed by a 10 min equilibration. We observed a slight decrease in retention when using buffer. However, the resolution between some peptides was increased.

#### **2.5 Data processing and retention modelling**

The data were processed using Compass Data Analysis from Bruker and PIOTR [21]. A longer gradient (52 min or 70 min) was chosen from each data set and the dissect option was used to obtain the  $m/z$  and retention-time list. The  $m/z$  values were assigned to a peptide sequence using MS/MS measurements with the same sample on the Sciex TripleTOF 5600+ MS. The

MS confidence of identification was chosen to be 95% or above and no modifications were considered. The observed ions in the HILIC measurements were matched to a peptide sequence if the value was within 0.02  $m/z$ . Once the longer gradient was assigned, the same peptide list was searched in the other gradients using extracted-ion chromatograms (EIC). A unique list for all the columns of 15 peptides was obtained after processing all the data sets. Peak lists consisting of the retention time of each peptide for each gradient experiment were prepared for each column. These data were supplied to the PIOTR program to fit the different retention models. The computational approach has been explained previously [19,21]. Briefly, the retention models were used to calculate the model coefficients and the goodness-of-fit values, to compute the F-test of regression, and to predict retention. For the Z-silica and W-silica columns the 10-min gradient gave rise to a high degree of co-elution, which hindered peak detection and diminished the accuracy of the extracted retention times. Therefore, only five gradients were used in the analysis for these columns.

### **3. Results and discussion**

#### **3.1 Effect of additives in HILIC separation of peptides**

Among the conditions explored – three different columns (amide and A and B type silica stationary phases) and three mobile-phase additives (0.3% formic acid, 10 mM ammonium acetate pH 6, 10 mM ammonium formate pH3) – not all chromatograms showed good chromatography, in terms of retention and peak shape. Therefore, we first set out to establish the optimal combinations of columns and additives (figure 1). For this purpose, we compared the peak width, peak intensity and elution window for each of the conditions (see table 2). The performance of the amide column was good with all three mobile-phase additives. When using a buffer (ammonium acetate and formate), slightly sharper peaks were obtained. However, the intensity decreased by one

order of magnitude. Retention was also affected by the use of buffers. Formic acid gave rise to the lowest retention, followed by ammonium acetate and then ammonium formate (figure S1). This could be explained by an expansion of the water layer when using buffers. Dinh et al. [20] showed that when ammonium acetate (5 to 50 mM) was added to the ACN/water mobile phase, the ions were adsorbed on the surface of the stationary phase. The authors observed an increase in the water layer of up to 50% for bare silica phases. The elution order also varies with different conditions. Due to the higher signal intensity and adequate resolution, formic acid was chosen as the optimal additive for the amide stationary phase.

*Table 2: Seven peptides that were used to assess the optimal mobile-phase additive for the HILIC separation. The 30 min gradient duration measurements were used. FA=formic acid, AF= ammonium formate, AA= ammonium acetate.*

Column/ additive	Max $t_R$ (min)	Min $t_R$ (min)	Retention window (min)	Average peak height (counts) $\times 10^3$	Average peak width (min)
Amide FA	29.70	21.71	7.99	56.3	0.133
Amide AF	31.54	24.49	7.04	6.74	0.114
Amide AA	32.60	15.86	16.74	20.2	0.124
W-silica FA	23.18	17.27	5.90	83.7	0.185
W-silica AF	28.89	21.64	7.25	24.2	0.157
W-silica AA	39.64	21.60	18.04	49.5	0.201
Z-silica FA	28.41	19.86	8.55	9.91	0.225
Z-silica AF	34.97	25.03	9.93	39.2	0.125
Z-silica AA	37.21	24.33	12.88	27.9	0.223

The Z-silica column required a buffer for the elution and separation of the peptides (figure S2). Therefore, the separations using the formic acid as additive were not considered for modelling. The elution order was the same with the two buffers. However, with ammonium acetate the peaks were tailing and the resolution was decreased. At pH=6 a large fraction of the silanol groups will be dissociated, whereas some groups (arginines, lysines and

histidines) on the peptides may still be positively charged. This creates a strong ion-exchange contribution to a mixed retention mechanism, which may explain the tailing. Therefore, ammonium formate was chosen as the optimal additive for the Z-silica column.

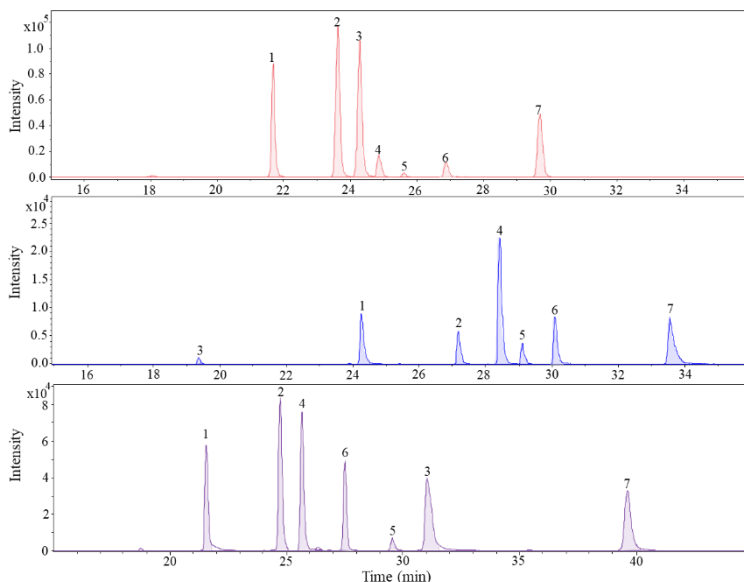


Figure 1: Optimal conditions for the separation of BSA digest on the amide column (red, top), Z-silica column (blue, middle), W-silica column (purple, bottom). For details see text. Analyte peptides: 1.  $m/z = 1002.5830$ , 2.  $m/z = 740.4014$ , 3.  $m/z = 509.2956$ , 4.  $m/z = 789.4716$ , 5.  $m/z = 689.3729$ , 6.  $m/z = 922.4880$ , 7.  $m/z = 571.8608$

Finally, also the separations using the W-silica column required a buffer (figure S3) [22]. Good peak shapes were obtained with both buffers. The elution order was also the same, with the exception of two peptides (3 and 5), which showed a decreased retention with ammonium formate. Both peptides had a theoretical pI of about 9.7 (basic). McCalley showed previously that for this silica column the retention of basic solutes increased when increasing the pH from 3 to 6 [23]. The number of negatively charged silanol groups at the surface increases at higher pH, providing stronger interaction with the

positively charged solutes. Ammonium acetate (pH 6) gave higher retention and a better resolution. Hence, it was chosen as the optimal buffer.

### 3.2 Retention modelling

The models used to fit the data were the exponential, mixed-mode, adsorption, quadratic and Neue-Kuss models.

The exponential model has been shown to fit RPLC data [24] and has the following form

$$\ln k = \ln k_0 - S \phi \quad (1)$$

Where  $k_0$  represents the extrapolated retention of an analyte at  $\phi = 0$  (100% water in case of RPLC) and  $S$  the so-called “solvent-strength parameter”, describing the change in retention with increasing concentration (volume fraction) of strong solvent ( $\phi$ ).

The adsorption model is typically used to describe normal-phase separations.[25]

$$\ln k = \ln k_0 - n \ln \phi \quad (2)$$

Here,  $n$  is meant to represent the ratio between the surface occupied by the analyte molecules and the molecules of strong solvent.

The mixed-mode model is a combination of the previous two models and is thought to take into account both partitioning and adsorption [26].

$$\ln k = \ln k_0 + S_1 \phi + S_2 \ln \phi \quad (3)$$

The quadratic model was developed to characterize retention over a larger range of mobile-phase compositions [27].

$$\ln k = \ln k_0 + S_1 \phi + S_2 \phi^2 \quad (4)$$

## Chapter 3

The Neue-Kuss model is an empirical model that can easily be integrated to predict retention under gradient conditions [28].

$$\ln k = \ln k_0 + 2\ln(1 + S_2\phi) - \frac{S_1\phi}{1+S_2\phi} \quad (5)$$

This study was conducted using retention times obtained using gradient-elution programs. Thus, the retention models were applied for gradient separations as described previously [19]. For the mixed-mode and quadratic model the gradient equation cannot be solved. Therefore, a numerical approach by use of the Simpsons' approximation was applied when needed.

The PIOTR program was used to fit these different retention models to the experimental data for each analyte. We have previously described this approach to establish the retention parameters [19,21]. Briefly, PIOTR utilizes a non-linear programming solver which searches for the minimum residuals. In essence, the constants (e.g.  $\ln k_0$  and  $S$  for the exponential model) are varied until the simulated result matches the experimental retention times with a minimum of residual error. This is carried out within the constraints of the applied gradient to record the experimental data.

The goodness of fit of the five models was determined using the Akaike information criterion (AIC) [29]. The minimum number of scouting gradients needed was three to fit all the models since the quadratic, mixed-mode and Neue-Kuss contain three parameter model coefficients. The retention time of the peptides under different gradient conditions were used as the input data. The data sets contained 15 peptides, analysed with the three HILIC columns run at optimal conditions as described in the previous section and one RPLC column. The 15 peptides featured different properties with regard to length, amino-acid composition, net charge, pI, and the grand average of hydrophobicity index (GRAVY). The properties of the peptides can be found in table 3. Peptides KVPQVSTPTLVEVSR and KQTALVELLK were

removed from the final results due to large variations in the AIC values and prediction errors. The AIC values were calculated and predictions were performed using the in-house-developed Matlab program PIOTR [21].

*Table 3: Peptides used for the retention modelling; Properties were obtained from [32].*

<b>Sequence</b>	<b>m/z</b>	<b>Measured charge</b>	<b>MW</b>	<b>pI</b>	<b>GRAVY index</b>
LGEYGFQ	407.193	2+	812.369	4.00	-0.35
GFQNALIVR	509.296	2+	1016.575	9.75	0.57
FWGK	537.282	1+	536.274	8.75	-
KQTALVELLK	571.861	2+	1141.705	8.59	0.19
TDLTK	577.319	1+	576.310	5.50	-1
LVNELTEFAK	582.319	2+	1162.621	4.53	0.13
AWSVAR	689.373	1+	688.364	9.79	0.26
STVFDK	696.356	1+	695.347	5.55	-0.31
GLVLIAF	732.465	1+	731.456	5.52	2.92
LGEYGFQNALIVR	740.401	2+	1478.786	6.00	0.29
LVTDLTK	789.472	1+	788.462	5.84	0.42
KVPQVSTPTLVEVSR	820.473	2+	1638.928	8.75	-0.06
AEFVEVTK	922.488	1+	921.479	4.53	0.17
LVVSTQTALA	1002.583	1+	1001.574	5.52	1.39
QTALVELLK	1014.619	1+	1013.61	6.00	0.64

The AIC parameter is calculated as follows.

$$AIC = 2p_m + n \left( \ln \left( \frac{2\pi * SSQ}{n} \right) + 1 \right) \quad (6)$$

Where  $n$  is the number of input data points,  $p$  is the number of parameters of the model and  $SSQ$  is the sum of squared errors. By using this value, we can compare models that have different numbers of parameters. A good fit is indicated by a small, often negative, AIC value. Each peptide considered gives an AIC value for each model. Therefore, we considered the average values and the standard deviations across all peptides. Indeed, the AIC value itself does not provide any qualitative information about the fit. AIC values can only be used to relatively compare a series of values. Even then, as can also be seen in Figure 3, the AIC values are not always conclusive, especially not when a large standard deviation is observed. Therefore, we also considered the average error of prediction and the F-test of regression to draw clear conclusions.

### 3.3 RPLC retention modelling

Separation of BSA digest with reversed-phase liquid chromatography was performed to facilitate identification of the peptides using existing libraries on the Triple TOF instrument. RPLC data were also used to verify the functionality of the models and to compare the selectivity with the HILIC separations. RPLC has been extensively characterized [30] and the retention of the analyses can be accurately described by an exponential model (equation 1).

Using the same procedures for the data treatment as outlined in section 2.6 we calculated the goodness of fit and prediction errors with the five models. We observed that only the exponential, mixed-mode and quadratic models performed well, showing low prediction errors ( $\leq 0.5\%$ ) and negative AIC values (figure 2). The adsorption and Neue-Kuss models did not perform well.

When inspecting the models (section 3.2), we observed that the three equations that provided a good fit shared the terms of the exponential model, with one extra parameter in the case of the mixed-mode and quadratic models. The mixed-mode and the quadratic models can be viewed as the exponential model when considering only the first two parameters. This could be an indication that the third parameter does not contribute significantly to the performance of the model. To test this hypothesis, we looked into the influence of the third parameter by using the statistical F-test for regression [31]. In contrast to the AIC value, this statistical F-test does not assess the fit in general. Instead, it allows comparison of a model with a reduced version. For example, the exponential model (Eq. 1) can be seen as a reduced version of the quadratic model (Eq. 4), differing by one term. The F-test can be used to compare the residual sum-of-squares of the full model ( $SS_{res,full}$ ) with that of the reduced model ( $SS_{res,red}$ ) and consequently determine the significance of the additional parameter. This is shown in Eq. 7

$$F = \frac{MS_{res,diff}}{MS_{res,full}} = \frac{(SS_{res,full} - SS_{res,red}) / (df_{red} - df_{full})}{SS_{res,full} / df_{full}} \quad (7)$$

where  $MS$  denotes the mean squares and  $df_{red}$  and  $df_{full}$  are the degrees of freedom of the reduced and full model, respectively. Using PIOTR, the cumulative distribution function of the F-distribution is assessed to yield a  $p$  value. If the  $p$  value is statistically significant ( $<0.05$ ), then this indicates that the additional term (and thus the full model) is statistically significant. It is good to emphasize that this specific F-test provides no information on the goodness-of-fit.

All the values obtained were added in the supplementary information (table S1). The minimum  $p$  values obtained were 0.26 for the mixed-mode and 0.51 for the quadratic model. From this it can be concluded that the added

contribution of the third parameter in the mixed-mode and quadratic models was not statistically significant.

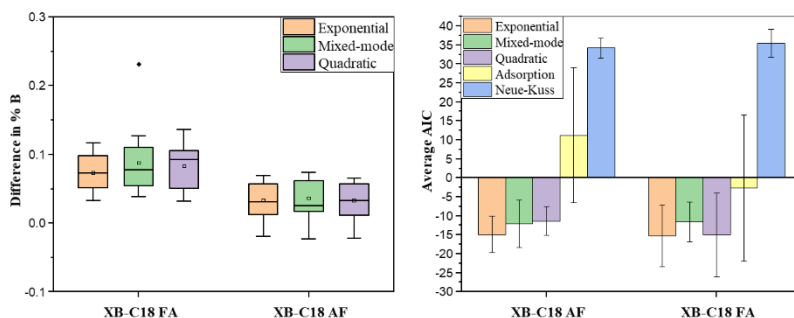


Figure 2: BSA digest separation of XB-C18; left: average AIC values and right: errors in prediction expressed in % of mobile-phase B; 3 input gradients were used 17, 52 and 80 min duration and 30 min gradient was predicted.

### 3.4 HILIC-goodness of fit

Firstly, we investigated how the number of input gradients affect the AIC values. We observed that the standard deviation decreased significantly when four gradients were used as input instead of three (figure S5), whereas only a slight additional decrease was observed when five input gradients were used (figure S6). The differences were more noticeable for the quadratic and Neue-Kuss models. Based on these observations, we used four input gradients to decide on the best model(s) to describe our data (figure 3).

Secondly, we investigated which model yielded the lowest AIC average for each column. For the amide and Z-silica columns, the lowest AIC values were obtained with the adsorption model with relatively low standard deviations (2.15 and 1.18 respectively). For the W-silica the lowest values were for the quadratic model. However, it showed a large standard deviation (11.04). The second lowest AIC average value was obtained with the adsorption model,

with a much lower standard deviation (3.88). Therefore, we concluded that for all columns the adsorption model could best be used to accurately fit the data.

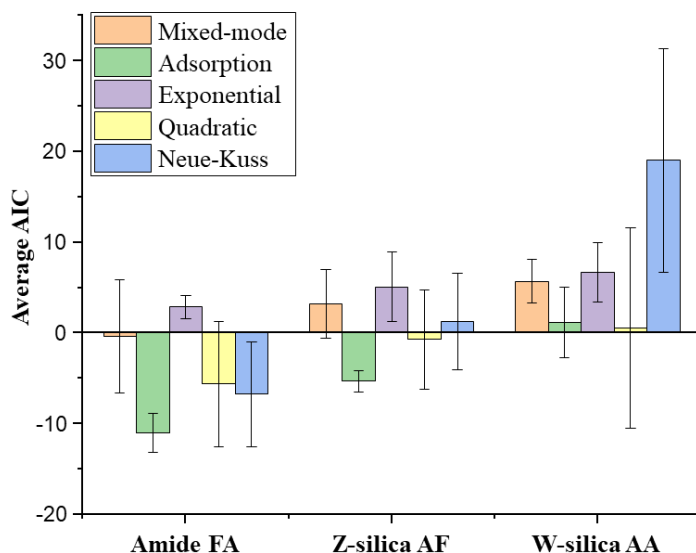


Figure 3: AIC values and standard deviations for five models on three different columns, obtained using gradients of 17, 52, 70 and 80 min duration

### 3.5 HILIC - Retention-time prediction

Prediction of retention times is an important tool in method development. An accurate model and a small number of scouting gradients may suffice to optimize a separation. We used prediction of retention times for the three HILIC columns to validate the results obtained from the goodness-of-fit for the five tested models. As previously, when investigating AIC values, we explored three or four gradients as inputs and we attempted to predict one of the measured gradients that were not used as an input. In figure 4 the results for the three-gradient-input are shown. The results obtained with four-

## Chapter 3

gradient-input data are shown in supplementary material (figure S7). We observed that there is no significant gain in accuracy from adding a fourth input gradient for prediction. Therefore, only three measurements suffice for prediction. The column with the lowest error of prediction was the amide column, followed by W-silica and then Z-silica.

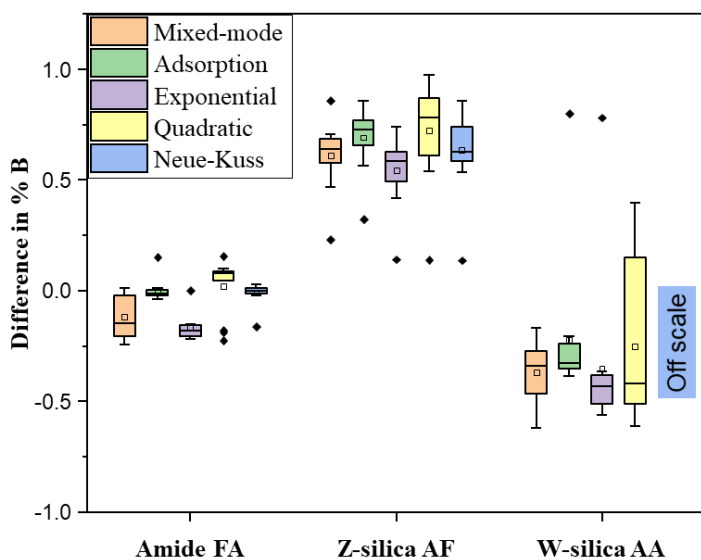


Figure 4: The error in prediction of a 30 min gradient for the separation of BSA digest expressed in mobile-phase B composition in the three HILIC columns. The input gradients for were 17, 52, 80 min duration.

The amide column showed average prediction errors close to 0 for the adsorption (0.08%), quadratic (0.35%) and Neue-Kuss (0.2%) models. However, the standard deviations for the latter two models were larger. The exponential model showed standard deviations similar to the adsorption model. However, the average error was larger (0.36%). The mixed-mode model showed errors in prediction up to 0.8%. The significance of the third parameter to the model performance was calculated for the quadratic

84

compared to exponential model and mixed-mode compared to adsorption model. There was no significant gain from adding a third parameter for the adsorption model (lowest  $p$  value was 0.31). However, for six of the thirteen peptides the third factor in the quadratic model did prove to be significant ( $p$  values  $\leq 0.01$ ). Ultimately, the adsorption model was found to be the most suitable for retention-time prediction of peptides on the amide column. This model was previously also found suitable for predicting the retention of small molecules [19].

The Z-silica column was found to give rise to a systematic error, with all models showing an average prediction error close to 0.5 min. The exponential model showed an average prediction error closer to zero (1.36%). We evaluated the significance of the third parameter in the quadratic model compared to the log-linear model. The  $p$  values for all the peptides were above 0.05, with 0.1 being the minimal value, thus indicating no significant contribution. When comparing the adsorption model with the mixed-mode model, no significance of the third parameter was observed either (lowest  $p$  value was 0.44). The exponential model performed reasonably well. However, the adsorption model may still be preferred since the difference in prediction error was just 0.5%.

The W-silica column showed a very high error of prediction for the Neue-Kuss model and a large standard deviation for the quadratic model. Therefore, these models were not further considered. When inspecting the other three models, the mixed-mode model showed a larger standard deviation, whereas the exponential and adsorption models exhibited a relatively narrow range of errors. The contribution of the third parameter in the mixed-mode compared to the adsorption model was found to be insignificant, with a lowest  $p$  value of 0.3. Among the exponential and adsorption models, the latter showed lower

prediction errors (i.e.  $\leq 0.36\%$ ). Hence, it was considered the best model for prediction.

## 4. Conclusion

In this work, we have investigated the retention of peptides in HILIC and we have explored five models to fit the data. The performance of the models was characterized by the Akaike information criterion (AIC) to determine the goodness of fit and evaluated using prediction errors. Optimal separation for a BSA digest was obtained using formic acid as additive for an amide column, ammonium formate (pH 3) for a Z-silica (Zorbax) column, and ammonium acetate (pH 6) for W-silica column (Waters-Atlantis). Equilibration times were also different for the different stationary phases, with the shortest time needed for the amide column.

RPLC experiments were performed as a benchmark to test the modelling procedures, as well as to aid in identifying the peptides in a digest sample. The best fit to the data was obtained with the exponential model, as expected, but the mixed-mode and quadratic models also performed adequately. By computing the F-statistic for regression we noted that the third parameter of these latter two models did not have a significant influence on the model performance. Therefore, these models behave like the exponential model and the added complexity has no significant benefits.

The goodness of fit values indicated that the adsorption model was the most suitable to describe retention of peptides using the three HILIC columns. At least four input gradients were needed to obtain reliable model coefficients for the quadratic and Neue-Kuss models, whereas three input gradients were sufficient for the mixed-mode, adsorption and exponential models. The

adsorption model gave the lowest AIC values with the smallest standard deviations.

We were able to predict the retention times of peptides on all three stationary-phases with errors below 2%. The amide column had the smallest average errors in prediction with the adsorption model (0.08%), followed by the W-silica column with average prediction errors of 0.78%. The Z-silica column showed higher prediction errors for all the models, exhibiting a systematic error. On this latter column the prediction error for the adsorption model was 1.76%, while the lowest errors were observed for the exponential model with 1.36%.

There have been previous studies for retention models applied in HILIC separations. Česla et al. [18] have concluded that for the isocratic separation of malto-oligosaccharides in HILIC the mixed-model provided the best fit of the data, yielding the lowest AIC values and prediction errors. Tyteca et al. [17] proposed the same model for isocratic separations of acidic, basic and neutral small molecules. However, for gradient separations they found the Neue-Kuss model to be more suitable, because it allowed analytical integration to obtain gradient retention times. The use of a large number of measurements used in the above mentioned experiments could possibly explain the better functioning of the Neue-Kuss empirical model. However, for a limited number of scouting gradients Pirok et al. [19] showed a poor performance of the Neue-Kuss model, with the adsorption model providing a better fit and yielding lower prediction errors for a variety of small molecules.

Based on the results reported previously in a study involving small-molecule analytes [19] and the results reported in this paper, we recommend that the adsorption model be used to describe retention in HILIC, unless specific information is available to support the suitability of other models.

## 5. Acknowledgements

The STAMP project is funded under Horizon 2020 – Excellent Science – European Research Council (ERC), Project 694151. The sole responsibility of this publication lies with the authors. The European Union is not responsible for any use that may be made of the information contained therein.

We acknowledge Stef R. A. Molenaar for his assistance with computations.

## 6. References

Supplementary material:



- [1] A.A. Lobas, L.I. Levitsky, A. Fichtenbaum, A.K. Surin, M.L. Pridatchenko, G. Mitulovic, A. V. Gorshkov, M. V. Gorshkov, Predictive Liquid Chromatography of Peptides Based on Hydrophilic Interactions for Mass Spectrometry-Based Proteomics, *J. Anal. Chem.* 72 (2017) 1375–1382. doi:10.1134/S1061934817140076.
- [2] T.K. Toby, L. Fornelli, N.L. Kelleher, Progress in Top-Down Proteomics and the Analysis of Proteoforms, *Annu Rev Anal Chem (Palo Alto Calif)*. 9 (2017) 499–519. doi:10.1146/annurev-anchem-071015-041550.
- [3] B. Zhan, J.R. Yates, M.-C. Baek, Y. Zhang, B.R. Fonslow, Protein Analysis by Shotgun/Bottom-up Proteomics, *Chem. Rev.* 113 (2013) 2343–2394. doi:10.1021/cr3003533.
- [4] R. Aebersold, M. Mann, *Nature* 422 (2003). doi:10.1007/978-1-4939-7804-5\_9.
- [5] M. Gilar, P. Olivova, A.E. Daly, J.C. Gebler, Orthogonality of separation in two-dimensional liquid chromatography, *Anal. Chem.* 77 (2005) 6426–6434. doi:10.1021/ac050923i.
- [6] T. Kislinger, A.O. Gramolini, D.H. MacLennan, A. Emili, Multidimensional protein identification technology (MudPIT): Technical overview of a profiling method optimized for the comprehensive proteomic investigation of normal and diseased heart tissue, *J. Am. Soc. Mass Spectrom.* (2005). doi:10.1016/j.jasms.2005.02.015.

- [7] A.J. Alpert, Hydrophilic-interaction chromatography for the separation of peptides, nucleic acids and other polar compounds, *J. Chromatogr. A.* (1990). doi:10.1016/S0021-9673(00)96972-3.
- [8] P.J. Boersema, N. Divecha, A.J.R. Heck, S. Mohammed, Evaluation and optimization of ZIC-HILIC-RP as an alternative MudPIT strategy, *J. Proteome Res.* 6 (2007) 937–946. doi:10.1021/pr060589m.
- [9] P. Hemström, K. Irgum, Hydrophilic interaction chromatography, *J. Sep. Sci.* 29 (2006) 1784–1821. doi:10.1002/jssc.200600199.
- [10] D. V. McCalley, Study of the selectivity, retention mechanisms and performance of alternative silica-based stationary phases for separation of ionised solutes in hydrophilic interaction chromatography, *J. Chromatogr. A.* (2010). doi:10.1016/j.chroma.2010.03.011.
- [11] P. Jandera, Stationary and mobile phases in hydrophilic interaction chromatography: A review, *Anal. Chim. Acta.* 692 (2011) 1–25. doi:10.1016/j.aca.2011.02.047.
- [12] T. Baczek, P. Wiczling, M. Marszał, Y. Vander Heyden, R. Kaliszan, Prediction of peptide retention at different HPLC conditions from multiple linear regression models, *J. Proteome Res.* 4 (2005) 555–563. doi:10.1021/pr049780r.
- [13] M. Gilar, A. Jaworski, Retention behavior of peptides in hydrophilic-interaction chromatography, *J. Chromatogr. A.* 1218 (2011) 8890–8896. doi:10.1016/j.chroma.2011.04.005.
- [14] O. V. Krokhin, P. Ezzati, V. Spicer, Peptide Retention Time Prediction in Hydrophilic Interaction Liquid Chromatography: Data Collection Methods and Features of Additive and Sequence-Specific Models, *Anal. Chem.* 89 (2017) 5526–5533. doi:10.1021/acs.analchem.7b00537.
- [15] M. Taraji, P.R. Haddad, R.I.J. Amos, M. Talebi, R. Szucs, J.W. Dolan, C.A. Pohl, Prediction of retention in hydrophilic interaction liquid chromatography using solute molecular descriptors based on chemical structures, *J. Chromatogr. A.* 1486 (2017) 59–67. doi:10.1016/j.chroma.2016.12.025.
- [16] P.J. Schoenmakers, Á. Bartha, H.A.H. Billiet, Gradient elution methods for predicting isocratic conditions, *J. Chromatogr. A.* 550 (1991) 425–447. doi:10.1016/S0021-9673(01)88554-X.
- [17] E. Tyteca, A. Périat, S. Rudaz, G. Desmet, D. Guillarme, Retention modeling and method development in hydrophilic interaction chromatography, *J. Chromatogr. A.* 1337 (2014) 116–127. doi:10.1016/j.chroma.2014.02.032.
- [18] P. Česla, N. Vaňková, J. Křenková, J. Fischer, Comparison of isocratic retention models for hydrophilic interaction liquid chromatographic separation of native and fluorescently

## Chapter 3

labeled oligosaccharides, *J. Chromatogr. A.* 1438 (2016) 179–188. doi:10.1016/j.chroma.2016.02.032.

[19] B.W.J. Pirok, S.R.A. Molenaar, R.E. van Outersterp, P.J. Schoenmakers, Applicability of retention modelling in hydrophilic-interaction liquid chromatography for algorithmic optimization programs with gradient-scanning techniques, *J. Chromatogr. A.* 1530 (2017) 104–111. doi:10.1016/j.chroma.2017.11.017.

[20] N.P. Dinh, T. Jonsson, K. Irgum, Water uptake on polar stationary phases under conditions for hydrophilic interaction chromatography and its relation to solute retention, *J. Chromatogr. A.* 1320 (2013) 33–47. doi:10.1016/j.chroma.2013.09.061.

[21] B.W.J. Pirok, S. Pous-Torres, C. Ortiz-Bolsico, G. Vivó-Truyols, P.J. Schoenmakers, Program for the interpretive optimization of two-dimensional resolution, *J. Chromatogr. A.* 1450 (2016) 29–37. doi:10.1016/j.chroma.2016.04.061.

[22] J.C. Heaton, J.J. Russell, T. Underwood, R. Boughtflower, D. V. McCalley, Comparison of peak shape in hydrophilic interaction chromatography using acidic salt buffers and simple acid solutions, *J. Chromatogr. A.* 1347 (2014) 39–48. doi:10.1016/j.chroma.2014.04.026.

[23] D. V. McCalley, Study of retention and peak shape in hydrophilic interaction chromatography over a wide pH range, *J. Chromatogr. A.* 1411 (2015) 41–49. doi:10.1016/j.chroma.2015.07.092.

[24] L.R. Snyder, J.W. Dolan, J.R. Gant, Gradient elution in high-performance liquid chromatography, *J. Chromatogr. A.* 165 (1979) 3–30. doi:10.1016/s0021-9673(00)85726-x.

[25] L.R. Snyder, H. Poppe, Mechanism of solute retention in liquid—solid chromatography and the role of the mobile phase in affecting separation: Competition versus “sorption,” *J. Chromatogr. A.* 184 (1980) 363–413. doi:10.1016/S0021-9673(00)93872-X.

[26] G. Jin, Z. Guo, F. Zhang, X. Xue, Y. Jin, X. Liang, Study on the retention equation in hydrophilic interaction liquid chromatography, *Talanta.* 76 (2008) 522–527. doi:10.1016/j.talanta.2008.03.042.

[27] P.J. Schoenmakers, H.A.H. Billiet, R. Tijssen, L. De Galan, Gradient selection in reversed-phase liquid chromatography, *J. Chromatogr. A.* 149 (1978) 519–537. doi:10.1016/S0021-9673(00)81008-0.

[28] U.D. Neue, H.J. Kuss, Improved reversed-phase gradient retention modeling, *J. Chromatogr. A.* 1217 (2010) 3794–3803. doi:10.1016/j.chroma.2010.04.023.

[29] H. Akaike, A New Look at the Statistical Model Identification, *IEEE Trans. Automat. Contr.* 19 (1974) 716–723. doi:10.1109/TAC.1974.1100705.

[30] D. Carr, "The handbook of analysis and purification of peptides and proteins by reversed-phase HPLC," GraceVydac. 3 (2002). doi:10.1109/MAP.1972.27137.

[31] G.E.P. Box, J.S. Hunter, W.G. Hunter, *Statistics for Experimenters*, Wiley. 2nd editio (2005).

## Chapter 4

# Development of comprehensive two-dimensional low-flow liquid-chromatography setup coupled to high-resolution mass spectrometry for shotgun proteomics

Liana S. Roca, Andrea F. G. Gargano, Peter J. Schoenmakers

DOI: 10.1016/j.aca.2021.338349

## Contents

1.	Introduction .....	94
2.	Materials and methods .....	97
2.1	Chemicals .....	97
2.2	Instrumentation .....	98
2.3	Sample preparation .....	98
2.4	Column packing .....	99
2.5	Chromatographic conditions .....	100
2.6	Mass-spectrometry conditions .....	105
2.7	Data processing .....	105
3.	Results and discussion .....	107
3.1	First-dimension HILIC - orthogonality with respect to RPLC .....	108
3.2	Optimization of second-dimension LC conditions: influence of column dimensions on peak capacity and detection .....	110
3.3	2D platform – optimization and application .....	112
4.	Conclusion .....	120
5.	Acknowledgements .....	122
6.	References .....	122

## Abstract

Bottom-up proteomics provides often small amounts of highly complex samples that cannot be analysed by direct mass spectrometry (MS). To gain a better insight in the sample composition, liquid chromatography (LC) and (comprehensive) two-dimensional liquid chromatography (2D-LC or LC×LC) can be coupled to the MS. Low-flow separations are attractive for HRMS analysis, but they tend to be lengthy. In this work, a low-flow, online, actively modulated LC×LC system, based on hydrophilic-interaction liquid chromatography (HILIC) in the first dimension and reversed-phase liquid chromatography (RPLC) in the second dimension, was developed to separate complex mixtures of peptides. Miniaturization permitted the analysis of small sample amounts (1-5 µg) and direct coupling with micro-ESI MS (1 µL/ min). All components focused and automatically transferred from HILIC to RPLC using stationary-phase-assisted active modulation (C18 traps) to deal with solvent-incompatibility or dilution issues. Optimization of the setup was performed for the HILIC columns and the RPLC columns to provide a more efficient separation and higher identification rates than obtained using one-dimensional (1D) LC. A 60% increase in peak capacity was obtained with the 2D setup compared to a 1D-RPLC separation and a 17 to 34% increase in the number of proteins identified was achieved for the samples analysed (2D-yeast-8280 peptides and 2D-kidney tissue-8843 peptides), without increasing the analysis time (2 h).

## Keywords

nano two-dimensional liquid chromatography; hydrophilic interaction liquid chromatography; active modulation; peptide separation

## 1. Introduction

Liquid chromatography (LC) coupled to high-resolution mass spectrometry (HRMS) is commonly used to study protein expression and its modification in biological samples (e.g. cell cultures, tissues) [1]. Due to the difficulties associated with the liquid separation, ionization and fragmentation of proteins in the gas phase and the detection of ions with high mass-to-charge ( $m/z$ ) ratios in MS [2], proteins are typically digested using enzymes (e.g. trypsin) and the resulting peptides are subsequently analysed using reversed-phase liquid chromatography (RPLC) coupled to tandem MS (MS/MS). To allow for the analysis of samples that are limited in quantity (and concentration), low-flow separations (e.g. 300 nL min<sup>-1</sup>) with nano-electrospray ionization (nESI) sources are used. [3,4] The MS and MS/MS data are processed using software (e.g. MaxQuant [5], Mascot [6], PeptideShaker[7]) to identify peptides and to infer the presence of proteins in the sample based on characteristic peptides (unique proteotypic peptides). This analytical approach is usually described as bottom-up proteomics [8,9].

Tens of thousands of proteins are present in biological samples of complex organisms in a wide range of different concentrations (estimated at 10 orders of magnitude [10]). Furthermore, biological processes can induce several types of post-translational modifications (PTMs, e.g. phosphorylation, acetylation, glycosylation) [11,12]. The digestion process increases the complexity of the sample by generating up to a hundred peptides per protein. Therefore, achieving high-coverage proteome analysis of a complex cell system is a challenging endeavour, crucially relying on fast and high-resolution-separation and mass-spectrometry methods. Multidimensional separations can provide a large increase in the peak capacity in comparison with one-dimensional LC methods, provided that the separation dimensions are very different (“orthogonal”)[13]. This will help reduce the coelution of

analyte components and makes multidimensional methods attractive for proteomics analysis [14–17]. Orthogonality metrics assess the fraction of the separation space that is utilized for the separation of the components in a sample. The orthogonality can be assessed in several ways, for example focusing on the coverage of the separation space (global orthogonality) or on the uniformity of the space coverage (local orthogonality)[18].

An online multidimensional LC method often employed in proteomics analysis is the multidimensional protein identification technology (MudPIT) [19–21]. A column containing ion-exchange (IEC) particles in the first part and RPLC particles in the remainder is used in a MudPIT setup. Proteins or peptides are eluted using salt pulses from a strong-cation-exchange (SCX) resin or a mixture of weak-anion-exchange and SCX resins [22], focused on the RPLC column and separated using water to ACN gradients (typically containing 0.1% formic acid). Using a single column approach avoids dead volumes between separation dimensions and does not necessitate a valve system to couple the two columns. Separation methods are used that are mutually compatible and the eluting solvent in one dimension does not (significantly) influence the migration of analytes in the other dimension.

From a chromatographic perspective, this setup presents limitations in terms of separation capacity and implementation, as it can be used only to couple IEC and RPLC separations (resulting in limited orthogonality) and employs pulsed elution in the first separation, leading to “undersampling” [23] and reducing the separation efficiency of the first separation dimension.

Other approaches have been investigated, which use online and offline comprehensive two-dimensional liquid chromatography (LC×LC) [e.g.[16,24–26]. The advantage of an online setup is the automated sample transfer. It has been shown that RPLC (at a different pH), IEC and HILIC are

good choices in combination with RPLC in a two-dimensional separation system.

In terms of selectivity, hydrophilic-interaction LC (HILIC) has emerged as a favourable alternative to IEC. The mechanism proposed for HILIC is based on partitioning between a water layer formed on the surface of the stationary phase and the bulk mobile-phase, with additional effects of electrostatic interactions and hydrogen bonding. Analytes are separated mainly based on their hydrophilicity, whereas in IEC separation is based on charge (peptides of interest generally carry two to four positive charges). HILIC provides a higher degree of orthogonality with RPLC [25,27] and can be easily coupled to MS when volatile additives are used. However, in HILIC, high concentrations of acetonitrile (ACN) are used, which creates a solvent mismatch with RPLC [28]. To overcome the solvent incompatibility, two-dimensional (2D) separations have been performed off-line, with the solvent being evaporated in between the two separations and replaced by a favourable solvent for the second-dimension (<sup>2</sup>D) separation. If a 2D-LC separation is performed on-line, very small amounts can be transferred with the aid of loops. However, this may lead to sensitivity issues.

With the implementation of stationary-phase-assisted modulation (SPAM), the solvent mismatch can be overcome and narrower columns can be used in the second dimension [29]. In this case the simple loops between the two dimensions are replaced by small columns (traps) that allows concentration of the analytes in a smaller volume. The <sup>1</sup>D effluent is not transferred directly and, thus, the flow rate is not a limiting factor. The <sup>1</sup>D effluent can be diluted with a make-up flow, which will aid in solving the solvent incompatibilities. A similar type of set-up is already implemented for large volume injections in nano-HPLC (trap-and elute setup) [30]. To avoid volume overload on an analytical column, the sample can be loaded onto a pre-column (trap) at higher

flowrates, using a loading pump and then a valve is switched to send the sample to the column using a solvent gradient.

The objectives of the present study were to develop a high-resolution LC×LC method to increase the number of analytes identified in bottom-up-proteomics studies and to enhance the coverage of the proteome. We aimed to combine HILIC with RPLC in capillary column format, using active modulation with dilution during sample transfer to circumvent solvent-incompatibility issues, all without increasing the required analysis time compared to a 1D separation.

## 2. Materials and methods

### 2.1 Chemicals

Acetonitrile (ACN, MS grade), 2-propanol (IPA, HPLC grade) and water (MS grade) for all MS measurements were purchased from Biosolve Chimie (Dieuze, France). Milli-Q water (18.2 mΩ) was obtained from a purification system (Millipore, Bedford, MA, USA). Bovine serum albumin (BSA, ≥96%) and formic acid (FA, analytical grade; 98%), were purchased from Sigma-Aldrich (Darmstadt, Germany). Yeast cell lysate was obtained from Promega (Madison, WI, USA).

Fused-silica capillaries (20, 50, 75, 100, 150 μm internal diameter (ID); all 360 μm outer diameter (OD)) (CM scientific, Silsden, United Kingdom), PEEK tubing (IDEX, Lake Forest, IL, USA), Next-advance frit kit (kasil 1624 and formamide ;Troy, NY, USA), ferules, nuts and unions (Vici-Valco, Houston, TX, USA) were used to prepare the columns and connections.

C18 particles (3 μm diameter, 100 Å pore size) for the reversed-phase columns were obtained from NanoLCMS Solutions (Magic C18, Oroville, CA, USA). HILIC columns were packed in our laboratory with hydroxyethyl A particles

(5  $\mu\text{m}$ , 300  $\text{\AA}$ ) from PolyLC (Columbia, MD, USA), Acquity UPLC BEH Amide (1.7  $\mu\text{m}$ , 130  $\text{\AA}$ ) from Waters (Milford, MA, USA), and ZIC-HILIC (3.5  $\mu\text{m}$ , 100  $\text{\AA}$ ) from Merck (Darmstadt, Germany).

### **2.2 Instrumentation**

For the 1D and 2D experiments an Ultimate 3000 (ThermoFisher Scientific, Breda, The Netherlands) system was used, equipped with nano-pump (0.1 to 1.5  $\mu\text{L}/\text{min}$ , NCP 3200RS) and nano-pump / loading-pump (0.1 to 1.5  $\mu\text{L}/\text{min}$  nano pump, 1-100  $\mu\text{L}/\text{min}$  loading pump, NCS 3500RS) modules and an auto-sampler (WPS-3000TPL RS). ProFlow nano selectors (ThermoFisher Scientific) were used as flow selectors for the nano pump. For the MS measurements an Orbitrap Q Exactive plus (QE) from ThermoFisher Scientific was used with a nanospray Flex source. The sampler was equipped with a 20- $\mu\text{L}$  loop for the RPLC measurements, a 1- $\mu\text{L}$  loop for HILIC measurements, or a 5- $\mu\text{L}$  loop for the 2D measurements.

### **2.3 Sample preparation**

The protein digestion was performed as described previously [31]. The peptide samples were dissolved either in 98% water, 2% ACN, 0.1% FA for RPLC measurements or 80% ACN, 20% 10 mM ammonium formate in water, pH 3 for HILIC and 2D measurements.

Human kidney tissue was obtained in homogenized fresh frozen form (Jasper Kers, Amsterdam UMC, Amsterdam, The Netherlands). The tissue aliquot (5 mg, 0.2 g  $\text{mL}^{-1}$  in 100-mM ammonium bicarbonate solution) was assumed to contain 1 mg of protein. The tissue was sonicated with 100  $\mu\text{L}$  of 6 M urea solution, after which the same in-solution digestion procedure was followed.

Human IMR90 lung fibroblast cells (ATCC CCL-186) were grown in Dulbecco's modified Eagle media (DMEM) supplemented with 10% heat-inactivated, sterile-filtered fetal bovine serum (Life Technologies) and

prepared according to what was described in [32]. The extracted proteins were precipitated with cold acetone ( $-20^{\circ}\text{C}$ ). The acetone was then removed and the palette was suspended in 100  $\mu\text{L}$  of 6 M urea solution. The same in-solution digestion was performed as described above.

## 2.4 Column packing

Firstly, frits were created in the fused silica capillaries. Kasil 1624 (60  $\mu\text{L}$ ) was mixed gently with formamide (20  $\mu\text{L}$ ). The capillaries cut to the desired column length plus 30 mm were dipped in the solution for 1 to 2 s [33]. Then the capillaries were placed in an oven at  $100^{\circ}\text{C}$  overnight. Before packing, the frit was cut to 1 to 2 mm and the capillary to the desired column length plus 5 mm.

The RPLC columns were packed by preparing a slurry of  $0.1\text{ g mL}^{-1}$  particles in the packing solvent (methanol:isopropanol 50:50). The slurry was inserted in an empty column (4.6 mm  $\times$  50 mm) with one end drilled to be able to connect the capillary. The capillary was inserted 5 mm inside the packing column. A flow of  $0.1\text{ mL min}^{-1}$  of the packing solvent was set. The column was kept under flow for 30 min after the packing was complete. The slurry left was collected and the packed column was removed. The top 5 mm were cut and the capillary was placed at the same level as the sleeve before making the final connection.

The same procedure was followed with the HILIC stationary phases, but the packing solvent was changed to 97% ACN, 3% 10-mM ammonium formate in water, due to the nature of the particles.

## **2.5 Chromatographic conditions**

### **2.5.1 HILIC-MS separation conditions**

Three different HILIC stationary phases were tested for the <sup>1</sup>D separation (ZIC HILIC, amide and hydroxyethyl). All were packed in-house and all columns were made to the same length (200 mm) and internal diameter (200 μm).

In this setup only one pump is used. The column is connected to the auto-sampler valve and no traps are used. The flow rate was set to 1 μL min<sup>-1</sup> and 1 μg of yeast digest was loaded on the column. Mobile phase A was 10-mM ammonium formate in water, adjusted to pH 3, and mobile phase B was 97% ACN and 3% 10-mM ammonium formate, pH 3. A multi-segment gradient was used as follows: 95% B for 1 min, 95-85% B in 2 min, 85-75% B in 59 min, 75-65% B in 39 min, 65-50% B in 1 min and then back to 95% B in 1 min. The column was equilibrated with 95% B for 30 min.

### **2.5.2 RPLC-MS conditions**

More attention was paid to the second dimension, since this has a greater impact on the final separation. The aspects considered were the efficiency of the separation (section 2.5.2.1 and 2.5.2.2 and the detection sensitivity (section 2.5.2.3). The mobile phases used were water with 2% ACN and 0.1% formic acid for channel A and the loading pump, and 80% ACN, 20% water, 0.1% formic acid for channel B.

For the RPLC optimization, all measurements were carried out in trap-and-elute mode using a 5 mm length, 300 μm ID trap column (C18, ThermoFisher Scientific). The loading pump (20 μL min<sup>-1</sup>) was used to transfer the sample from the injector to the trap in 3 min. The column was kept in a column oven at 45°C. A gradient from 5% B to 35% B was used for all measurements. For the peak integration and the determination of the peak width at half height MZmine (version 2.40.1) was used. The processing method will be detailed in

section 2.7. Bovine-serum-albumin digest was chosen to represent a real proteomics sample and was used to characterize the 2D columns. The sample was dissolved in water containing 2% ACN and 0.1% FA in concentrations of  $0.2 \mu\text{g } \mu\text{L}^{-1}$  and  $0.05 \mu\text{g } \mu\text{L}^{-1}$ .

### 2.5.2.1 RPLC-MS experiments to determine the optimal linear flow velocity

BSA digest  $0.25 \mu\text{L}$  ( $50 \text{ ng}$ ,  $0.2 \mu\text{g } \mu\text{L}^{-1}$ , quantified at protein level) was loaded on an RPLC column (C18, 10 mm length,  $100 \mu\text{m}$  ID,) to determine the effect of linear flow velocity on the peak capacity. The flow rates employed were 0.3, 0.5, 0.7, 0.9, 1.2, and  $1.5 \mu\text{L min}^{-1}$ . The gradient time was varied in order to keep the same volumetric gradient ( $t_g/t_0$ ) (see *Table S1.1*). The identified peptides from all the measurements were compared. From the common list of peptides, the most intense 35 peaks were chosen to perform the peak capacity calculations (supplementary material *Table S1.2*). Equation 1 was used to calculate peak capacity [34] (derived in supplementary material *Equations S1.1, S1.2, S1.3*) and equation 2 and 3 were used to convert from volumetric flow rate to linear flow velocity.

$$n_c = \frac{t_g}{1.7 \times w_{\frac{1}{2}h}} + 1 \quad (1)$$

Where  $n_c$  is the peak capacity,  $t_g$  the gradient time (min) and  $w_{\frac{1}{2}h}$  is the peak width at half height (min).

$$\mu_s = \frac{F}{\pi \times r^2} \quad (2)$$

Where  $\mu_s$  is the linear flow velocity in an empty cylinder (“superficial velocity”) ( $\text{mm s}^{-1}$ ),  $F$  is the volumetric flow rate ( $\text{mm}^3 \text{ s}^{-1}$ ) and  $r$  is the column radius (mm)

$$\mu_t = \mu_s / \varepsilon_t \quad (3)$$

Where  $\mu_t$  is the mobile-phase velocity and  $\varepsilon_t$  is the total porosity of the column. We assumed a medium porosity column which would give a value of about 0.6 for  $\varepsilon_t$  [35].

The optimal mobile phase velocity was determined to be approximately 1.8 mm s<sup>-1</sup>. (*Figure S1.1* supplementary material)

### **2.5.2.2 RPLC-MS effect of gradient steepness on peak capacity**

BSA digest (50 ng injected on column for all experiments) was used as the peptide sample. Three RPLC column dimensions were tested (100 mm length; 75, 100 and 150  $\mu\text{m}$  ID) at an optimal linear flow velocity of 1.8 mm s<sup>-1</sup> (see section 2.5.2.1), which corresponded to 300, 533 and 1200 nL min<sup>-1</sup>, respectively. The gradient times used were 3, 4, 5, 7, 10 and 15 min. The widths of 15 peptide peaks were used to calculate the peak capacity of each separation (for a list see supplementary material, *Table S2.1*).

### **2.5.2.3 RPLC-MS effect of flow rate on sensitivity**

RPLC columns with the same dimensions as those described in section 2.5.2.2 were used at their optimal linear flow velocity. The gradient time was kept constant (10 min) and the quantity of BSA digest loaded was varied (5, 10, 20 and 50 ng). The areas of extracted ion currents (EIC) for selected peptides (same list as in 2.5.2.2) were considered to compare the MS sensitivity at different flow rates.

### **2.5.3 HILIC×RPLC-MS optimization**

A schematic of the HILIC×RPLC-MS setup is shown in *Figure 1*. A HILIC <sup>1</sup>D column was run at 1  $\mu\text{L min}^{-1}$ . The <sup>2</sup>D RPLC column was run at 1.2  $\mu\text{L min}^{-1}$ , either with the 100- $\mu\text{m}$  ID column or with the 150- $\mu\text{m}$  ID column. A dilution flow of water containing 0.1% FA (9  $\mu\text{L min}^{-1}$ ) was provided by a

loading pump, which was connected to the outlet of the HILIC column using a VHP MicroTee Assembly for 360 $\mu$ m OD (P/N UH-750, Idex, Lake Forest, IL, USA). The tenfold diluted flow <sup>1</sup>D effluent containing the sample was retained on C18 traps (5 mm  $\times$  300  $\mu$ m ID). This allows for the entire sample (peptides) to be transferred from the first to the second dimension in a solvent favourable for RPLC separation. The traps were attached to the valve using two Viper connections (10 mm  $\times$  30  $\mu$ m ID; ThermoFisher Scientific). The other connections were made with fused-silica capillaries (250 mm  $\times$  20  $\mu$ m ID, except 300 mm  $\times$  50  $\mu$ m ID for the connection from the T-split to the valve, figure 1).

The gradient and valve switches were programmed using Xcalibur. A long step gradient was programmed for the first dimension and repeated short gradients for the second dimension. The <sup>2</sup>D gradient duration was set equal to the modulation time minus one minute. This latter minute was used to wash the RPLC column increasing the % B to 80% in 0.1 min. Thereafter, the composition was programmed to return to the initial conditions in 0.4 min and the column was then equilibrated for 0.5 min. The first <sup>2</sup>D gradient ran from 5% B to 60% B. The gradient was then changed gradually, with the initial %B increasing linearly to 15% and the final %B decreasing linearly to 35%. This was because the more-hydrophobic components eluted in the first modulations from the HILIC 1D column required a higher % of ACN to be eluted from the <sup>2</sup>D RPLC column than the more-hydrophobic components eluting in the later modulations.

Multiple modulation times were considered (5, 10, 15 and 30 min) to determine a compromise between the sampling of the <sup>1</sup>D chromatogram and the resolution of the <sup>2</sup>D separation. A complication factor is that increasing the number of modulations implies that the fraction of the time lost due to sample loading and column equilibration is increased.

## Chapter 4

In our setup, the volume of the trap and the valve ports used were calculated to be about 640 nL. At a flow rate of 300 nL min<sup>-1</sup> this will result in a delay in excess of 2 min. This may be quite significant. For example, in case of a 10 min modulation a 2 min delay represents a 20% reduction of the 2D separation time. By increasing the flow rate to 1200 nL min<sup>-1</sup> we can reduce the effect of the system volume to 0.5 min. However, we must still consider the dead volume of the 2D column. A 100 mm × 75 μm ID column (RP75) run at 300 nL min<sup>-1</sup> will have a dead time of about 1 min. If we increase the column ID, while keeping the length and linear flow velocity constant, the column dead time will stay the same. Running the separation at a higher than optimal linear flow velocity would reduce the dead time and the system dwell time simultaneously. The 2D setup was therefore operated with the 150-μm or 100-μm ID columns (RP 150, RP100) at 1.2 μL min<sup>-1</sup>.

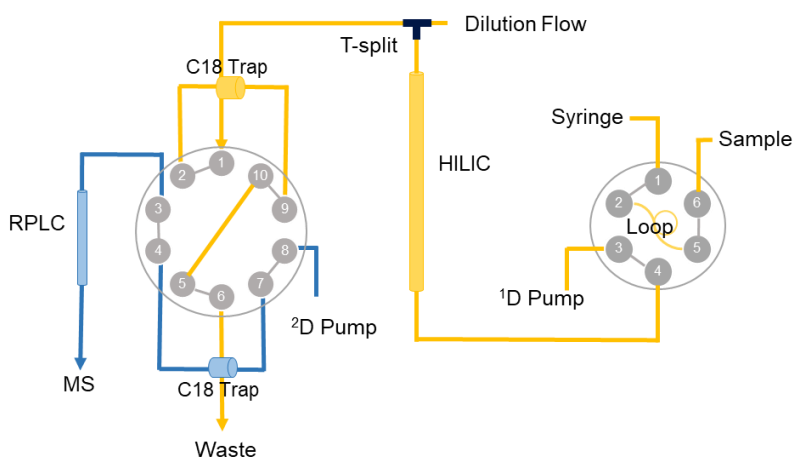


*Figure 1: Schematic of the 2D-LC setup used. The 6-port valve represents the injector valve and the 10-port valve is the modulation unit allowing to collect fractions of the sample from the first dimension and inject these in the second dimension. The 10-port valve and the RPLC column were kept in an oven at 45°C.*

## 2.6 Mass-spectrometry conditions

All separations were performed with direct injection into the nano-LC setup coupled using a nanospray Flex source to a Q-Exactive Plus (Thermo Fisher, Bremen, DE).

The tune method was set with the following parameters: capillary temperature 275°C, S-lens RF level 55, and spray voltage between 1.85 and 2.1 kV, depending on the status of the emitter. The MS1 conditions were set to a resolution of 70,000, automatic gain control (AGC) target  $3 \cdot 10^6$ , maximum IT 60 ms, and a scan range from  $m/z = 375$  to 1575. The MS2 parameters were: resolution 17,500, AGC target  $10^5$ , maximum IT 100 ms, isolation window ( $\Delta m/z$ ) 1.8, fixed first mass  $m/z = 110$ , normalized collision energy (NCE) 27, number of MS/MS (loop count) 10. The data-dependent settings were a minimum AGC target of  $2 \cdot 10^3$ , intensity threshold  $2 \cdot 10^4$ , and charge exclusion of unassigned species, charge of 1, 7, 8 and larger than 8. The dynamic exclusion was set to 20 s and the chromatographic peak width was set to 15 s for the 1D experiments and 10 s for the 2D experiments.

## 2.7 Data processing

### 2.7.1 Bottom-up MS/MS database searches

MaxQuant (open-source computational platform, version 1.6.5.0) and Proteome Discoverer (Thermo Scientific, version 2.4.1.15) were used to identify the peptides in all samples. Carbamidomethyl (C) was used as a fixed modification and the variable modifications were set to oxidation (M) and acetylation (protein N-Terminal). Trypsin was specified as the enzyme, with a maximum of two missed cleavages. The false discovery rate (FDR) for the peptide identification was set to 1% [36].

FASTA files [37] with reviewed peptide sequences were downloaded from uniprot.org[38]. For the yeast measurements, baker's yeast was selected and

only the reviewed sequences were downloaded in uncompressed form (created on 05.07.2019). For the kidney-tissue samples and the IMR90 cell-line sample, reviewed sequences of the complete human proteome were downloaded (created on 12.02.2019). To speed up the identification, for BSA only the reviewed sequences for the protein were downloaded (created on 13.06.2019) and not the bovine proteome. Information on the peptides, proteins, peptide-to-spectrum matches (PSMs), and retention times was gathered from both MaxQuant and Proteome Discoverer.

The mass spectrometry proteomics data have been deposited to the ProteomeXchange Consortium via the PRIDE [39] partner repository with the dataset identifier PXD022330 and 10.6019/PXD022330.

### **2.7.2 Extraction of chromatographic characteristics**

Identified sequences from MaxQuant or Proteome Discoverer were used to create csv files for targeted peak detection in MZmine (the peptide lists can be found in supporting materials S1 and S2). For each type of experiment an intermediate gradient duration was chosen for creating the csv file containing  $m/z$  values, retention times and sequences identified. The assignment was performed using the targeted-peak-detection function with the correct peak list, intensity tolerance 50%, noise level  $6.0 \cdot 10^3$ ,  $m/z$  tolerance 0.02 Da or 10 ppm. The retention time tolerance was set to an arbitrary high value of 15 min due to the very different conditions between some of the measurements. The deconvolution function was used on the obtained peak lists to determine the charge state of the species. The peak integration was assessed visually and all peptides with poor integration were removed from further consideration. The retention time, peak width at half height and charge state were extracted for each peptide analyzed.

### 2.7.3 Orthogonality calculations

Scatter plots between the HILIC and RPLC data were created (see *Figure 2*), using the retention times of common peptides. If one sequence was identified multiple times the sequence with the highest identification score was chosen. The retention times of the peptides were normalized using equation 3.

$$t_{i \text{ (normalised)}} = \frac{t_i - t_{\min}}{t_{\max} - t_{\min}} \quad (3)$$

Where  $t_{\min}$  and  $t_{\max}$  represent the first and the latest eluting peak in the chosen series, respectively, and  $t_i$  is the retention time of the chosen peak. The orthogonality scores were calculated with a modified Matlab script (courtesy of John Mommers, DSM Material Science Centre, Geleen, The Netherlands) [40], in which the bin-counting method [27] and the equations for the Asterisk approach [41] were implemented. The results from the bin-counting method is dependent of the number of analytes in the sample. It determines the space coverage as the percentage of occupied bins in the 2D separation space. Ideally, each analyte will occupy one bin. Thus, the number of bins should match the number of analytes to be able to make a fair conclusion. Therefore, the bin-counting method was modified so as to have a number of bins similar to the number of analytes included in the scatter plots. For the Asterisk method the same equations were applied, independent of the number of analytes included in the calculations. The Asterisk metric calculates the orthogonality from the distances of each peak to four axes, the vertical axes, the horizontal axes and the two diagonals. The final orthogonality is given as a percentage.

## 3. Results and discussion

Online coupling of HILIC×RPLC for the separation of peptides shows great promise in increasing the peak capacity without a great increase in analysis time. This is expected to lead to a better analysis of complex proteomics

samples. In this project a 2D setup was built with micro flow rates in both dimensions. The effects of an increase in flow rate in the second dimension on peak capacity and MS sensitivity were investigated. Three samples with different levels of complexity were used, *i.e.* bovine serum albumin digest (one protein), yeast-proteome digest (about 6,700 proteins) and human tissue (about 20,000 proteins).

### **3.1 First-dimension HILIC - orthogonality with respect to RPLC**

We tested three types of HILIC stationary-phase chemistries, *viz.* two neutral phases (hydroxyethyl and amide) and one charged type (sulfobetaine, ZIC-HILIC). The method was developed on the basis of previously described research [31]. HILIC-MS methods were optimized in order to spread the yeast peptides across the chromatogram. A total of 8908 unique peptides were identified from the three HILIC columns and the RPLC column. The highest number was obtained with the RPLC separation (7904 peptides, 1497 proteins) followed by ZIC HILIC (3098 peptides, 695 proteins), amide HILIC (2432 peptides, 584 proteins) and hydroxyethyl HILIC (2389 peptides, 556 proteins). The larger number of identified peptides can be explained by a more-efficient separation in RPLC compared with HILIC, augmented by the lower internal diameter and flow rate used for RPLC, while keeping the amount injected constant. The calculated peak capacity for the RPLC separation was 398. For the HILIC columns the calculated peak capacity was 158 for ZIC HILIC, 84 for the amide column and 141 for the hydroxyethyl column.

The identified peptides from the separations on the three HILIC columns and the RPLC column were compared and a common list was obtained (1064 peptides). To select the HILIC column with the highest separation power and orthogonality with RPLC, the retention times were normalized and scatter

plots were created (*Figure 2*). To assess the orthogonality both the asterisk equation [41] and the bin-counting method [27] were adopted.

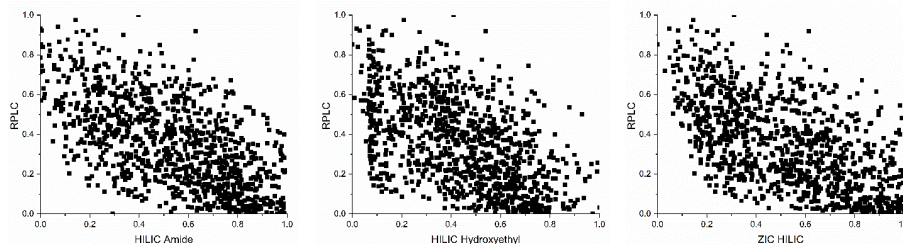


*Figure 2: Scatter plots of retention data obtained from one-dimensional separations using RPLC and three different HILIC columns. A common list of peptides between the four measurements was considered. Axes show normalized retention times.*

The column showing the least correlation and the highest orthogonality based on the Asterisk metric was the ZIC HILIC column, followed by amide and then the hydroxyethyl. When considering the bin-counting method, the amide columns was found to outperform the ZIC HILIC column by 2% (see *Table 1*). Another observation was a clustering of peaks at the beginning of the separation on the hydroxyethyl column. If this were to be improved the orthogonality would be increased. It can be concluded that any of the three column chemistries would provide a largely orthogonal separation when coupled with RPLC. Irrespective of the column chemistry, the peptide retention order on the HILIC columns is quite similar (*Figure S3.1*, supporting information). Due to its higher peak capacity, higher number of proteins identified and higher orthogonality to RPLC, the ZIC HILIC column was selected for use in the 2D setup.

*Table 1 Orthogonality considerations of the three HILIC column compared to RPLC separation. 1064 common peaks were considered and the number of bins was 1024 (32×32).*

<b>Column</b>	<b>Bin %</b>	<b>Asterisk</b>
HILIC Amide	48	59
HILIC Hydroxyethyl	42	51
HILIC ZIC	46	60

### **3.2 Optimization of second-dimension LC conditions: influence of column dimensions on peak capacity and detection**

The second dimension was developed to provide a fast, efficient separation, while maintaining the sensitivity of low-flow LC-MS analysis. The parameters investigated were column internal diameter, flow rate and gradient duration, to establish a balance between speed of analysis and efficiency.

Potential loss in peak capacity, when using fast <sup>2</sup>D gradients to improve the first-dimension sampling rate, was investigated. Theoretically the peak capacity of the 2D-system will be the product of the peak capacities of the two dimensions used. However, since in a low-flow setup adequate sampling of each <sup>1</sup>D peak is not possible, the total peak capacity will be better approximated as the peak capacity of the second dimension multiplied by the number of modulations.

In all of the three columns (with different dimensions) investigated an increase of the peak capacity approximately with the square root of the gradient duration was observed. As seen in figure 3A, the 75- $\mu$ m ID column presented peak capacities between 26 and 59 for the tested gradient lengths. The 100- $\mu$ m ID column showed peak capacities from 32 to 89 and the 150- $\mu$ m ID column exhibited a peak capacity of 43 to 117. Larger columns, running at higher flow rates, resulted in more-efficient separations.

Another consideration was the influence on the MS response, due to changes in sample dilution. Introduction of miniaturized ESI sources have shown great

promise for increasing the sensitivity of detection and for allowing smaller sample quantities to be used. The standard setup for contemporary proteomics features a 75- $\mu\text{m}$  ID column packed with C18 particles, run at 300 nL  $\text{min}^{-1}$  [42]. This has been a compromise between sensitivity, enhanced by lower flow rates, and robustness of the setup. Lately, the advantages of micro-flow liquid chromatography (columns of around 1 mm ID) for proteomics have been discussed [43]. The separation efficiency improves by having sharper peaks and avoiding column overloading, but the MS sensitivity suffers due to sample dilution, hence an ion-suppression effect.

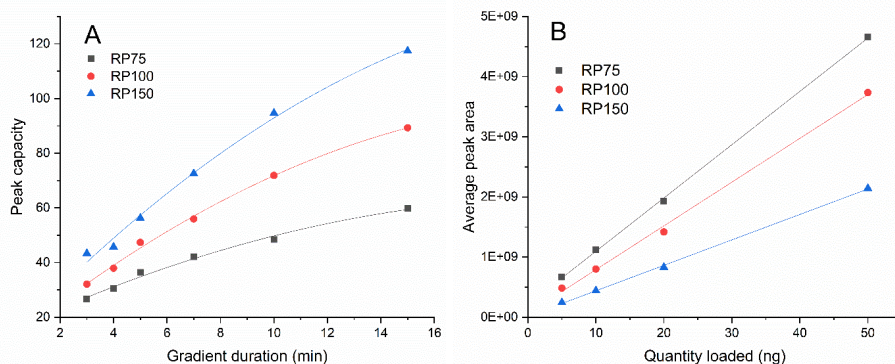


Figure 3 (A) Peak capacity of three RPLC column with different dimensions as a function of gradient duration. Linear flow velocity was kept at 1.13  $\text{mm s}^{-1}$ . (B) MS sensitivity of three RPLC columns with different dimensions determined from the average peak area of 14 peptides. Black ( $\square$ ) 75  $\mu\text{m}$  ID, red ( $\bullet$ ) 100  $\mu\text{m}$  ID, blue ( $\Delta$ ) 150  $\mu\text{m}$  ID columns.

In this work, we explored the use of second-dimension columns with slightly larger diameters than the standard 75- $\mu\text{m}$  ID column, to improve the sample loading and to obtain sharper peaks (higher peak capacity). In figure 3-B a 1.3-fold decrease in sensitivity is observed when going to the 100- $\mu\text{m}$  ID column and a 2.3-fold decrease when using a 150- $\mu\text{m}$  ID column.

Clearly, we must compromise the MS sensitivity to have a faster and more efficient separation. However, by increasing the quantity of peptides loaded

we could overcome the decreased sensitivity, while maintaining an increased peak capacity.

### **3.3 2D platform – optimization and application**

The low flow 2D-LC setup was used to analyze yeast-proteome digest as a standard test sample and finally was applied for the separation of fresh-frozen human-kidney-tissue homogenate and an IMR90 cell-line lysate. The protein digestion was performed in-house as described previously [31]. Stationary-phase-assisted modulation was used to transfer the fractions from the first dimension to the second dimension. In this way, the solvent incompatibility issues between HILIC and RPLC were solved and all sample could be transferred automatically. The RPLC was coupled to ESI-MS for the analysis of the sample.

#### **3.3.1 Modulation time**

When developing a miniaturized LC×LC setup some of the critical aspects to consider are the (column) dead volume and the (system) dwell volume and their influence on the second-dimension separation. In analytical-scale setups, system dwell volumes are small with respect to the flow rates used (*e.g.* 100  $\mu\text{L}$  of dwell volumes at flow rates of  $1 \text{ mL min}^{-1}$  result in a 6-s dwell time), allowing fast second dimension-separations (*e.g.* below 1 min) and frequent sampling of the first-dimension separation, significantly increasing the peak capacity of the 2DLC separation system [44]. However, in nano-LC the dwell volumes tend to be relatively large with respect to the operative flow rates, introducing significant time gaps between second-dimension runs. This can be clearly observed in a series of modulations as analysis gaps in which no peptide is observed by the mass spectrometer.

We investigated the effect of the modulation time and the number of modulations per run. The duration of the HILIC gradient was kept constant at

two hours, independent of the modulation time tested. The total run time was expanded by up to 20 min to accommodate the final modulation. We expected more-efficient <sup>2</sup>D separations for longer modulation times. However, the <sup>1</sup>D separation will be jeopardized by undersampling. The modulation times tested were 5, 10, 15, and 30 min. The resulting numbers of modulations were 24, 12, 8, 4 respectively. A table documenting the peptide and protein identification in each case is included in supplementary material (*Table S4.1*).

When considering the 150- $\mu$ m ID <sup>2</sup>D column run at the optimal linear flow velocity (1.2  $\mu$ L min<sup>-1</sup>; see Supplementary Material *S1*), the dwell volume of 0.64  $\mu$ L of our system will result in a dwell time (<sup>2</sup> $t_D$ ) of 0.5 min, while the column dead (<sup>2</sup> $t_0$ ) time is 1 min, resulting in a total time loss per modulation (<sup>2</sup> $t_D + ^2t_0$ ) of 1.5 min. This implies that 30% of the time will be lost in case of 5-min modulations, 15% for 10-min modulations, 10% for the 15 min modulations, and only 5% for the 30-min modulations. If we replace the second-dimension column with a 100- $\mu$ m ID one and we keep the flow rate the same, the <sup>2</sup> $t_0$  is reduced to 0.5 min, and <sup>2</sup> $t_D + ^2t_0$  becomes 1 min. This implies that we regain 10% of the separation space for the 5-min modulations and 5%, 3.3% and 1.7% for the 10-min, 15-min and 30-min modulations, respectively (see supplementary material *Figure S4.1*).

However, the separation efficiency should be lower when using a smaller column run at a much higher linear flow velocity. The peak capacities for the two setups were calculated for one of the modulations, assuming that for all modulations in one run the second-dimension peak capacity (<sup>2</sup> $n$ ) should be similar. One 10 min modulation run was selected for both the RP100 and RP150 columns. 15 peptide peaks were selected from modulation #7, 15 values for peak capacity were estimated based on the band widths of each of the peptides, and these 15 values were then averaged (for a list of peptides see supplementary material, *Table S4.2*). The RP150 showed a peak capacity of

83 and the RP100 setup one of 81. Assuming that the total peak capacity of the system equals the peak capacity of the second dimension multiplied by the number of modulations ( $n_{\text{mod}}=12$ ). Therefore, the total peak capacity of the system will be about 1000. This is a great improvement when considering the peak capacity of the 1D RP75 separation of the same 2-h duration (about 400).

Due to the very small difference in the obtained peak capacities of the two setups the 100  $\mu\text{m}$  ID column was thought to provide a better option due to the lower dead time ( $^2t_D + ^2t_0$ ). The longer modulations were determined to be more suitable for our setup, providing enough fractionation of the sample in the first dimension and a more limited time lost due to the dead time system.

### **3.3.2 Method optimization and repeatability**

Triplicate measurements were performed to check the repeatability of the 2D-setup. The RPLC column was kept in a column oven at 45°C to minimize the effects of fluctuations in the room temperature and to decrease the backpressure.

The identified species (about 4800 peptides per run) were not considered a good indication of the repeatability, due to the variability of the sample, ionization efficiency and precursor selection for MS/MS. Therefore, the retention times of a selection of the identified peptides were considered to determine the degree of variation between the triplicate measurements. We considered the common peptides without post-translational modifications from the three measurements (2742 peptides). We found an average variability of 1.7% (rsd) in the retention times between the triplicate measurements. Of the common peptides 192 showed a variability above 1%. If these were to be removed the average variability for the remaining 2550 peptides would drop to 0.01%. The observed variability may also be influenced by an incorrect assignment of an  $m/z$  value to a peptide sequence. We observed that multiple

retention times (peaks) were assigned to some of the peptides. We used the identification score in Proteome Discoverer (xcorr) to filter out the duplicate assignments. During this filtering the wrong retention time may be removed, leading to an increased variability in the retention time for the triplicate measurements. Due to the large number of common peptides manual verification was not feasible. For an example of three overlaid extracted-ion-current chromatograms see supplementary material (*Figure S4.2*).

After the system was deemed repeatable, further considerations were made to optimize the method. The optimization of a 2D-LC system can be difficult and time consuming, due to the many parameters that can influence the efficiency of both the <sup>1</sup>D and <sup>2</sup>D separations, such as the linear flow velocity, the column temperature, the mobile-phase composition and the gradient program [44]. In this work, the parameters investigated were the linear flow velocity using two different column diameters in <sup>2</sup>D, the mobile-phase composition and the gradient duration. The latter factor is closely related to the modulation time. The optimization was performed by visual assessment of the obtained chromatograms.

Initially, it was observed that the first <sup>2</sup>D RPLC modulations needed a higher concentration of ACN to elute the peptides as compared to later modulations. This was expected, since more-hydrophobic peptides will elute first in HILIC (<sup>1</sup>D) and will require higher concentrations of ACN for elution in RPLC (<sup>2</sup>D). A variable (“shifting”) gradient was programmed, where the initial concentration of B (80% ACN, 20% water, 0.1% formic acid) was decreased linearly from 15% to 5% and the final concentration of B from 60% to 35% from the first to last modulation. A visual representation of the effect of the variable gradient compared to an identical repeated gradient can be found in supplementary materials (*Figure S4.4*).

The HILIC gradient was also modified to improve the spreading of the peaks. Initially the gradient was started at 95% B and held for 5 min, followed by a first step from 95% to 80% B in 40 min, then to 55% B in 72 min. The column was washed by going to 40% B in 1 min, to 70% B in 2 min, to 40% B in 1 min and back to 95% B in 1 min. The column was equilibrated for 28 min. With this gradient program it was observed that the middle fractions contained larger numbers of peaks. The elution of peptides earlier in the HILIC gradient was promoted by starting the gradient at 90% B and adding a step to 85% B in 5 min. The next step was from 85% to 70% B in 60 min, followed by a decrease to 50% B in 52 min. The washing steps were the same as in the previous gradient program. The column was equilibrated at 90% B for 28 min.

After the optimization of the HILIC gradient, the RPLC gradient for the 15 min modulation was optimized for each modulation individually (see *Figure 4*). In supplementary materials *Figure S4.5* a clear improvement in the separation can be observed for the manually adjusted gradient for each modulation versus the shifting linear gradient described above (see supplementary material figure *S4.6 and S4.7*). The improvement was also noticed in the number of peaks that could be subjected to MS/MS analysis (“sequenced peaks”) and the number of peptides identified. For a generic shifting gradient, the number of peaks was 39,107 and 4,529 peptides were identified, while for the manually optimized variable gradients the number of peaks increased to 49,194 and the number of peptides identified was 6,606.

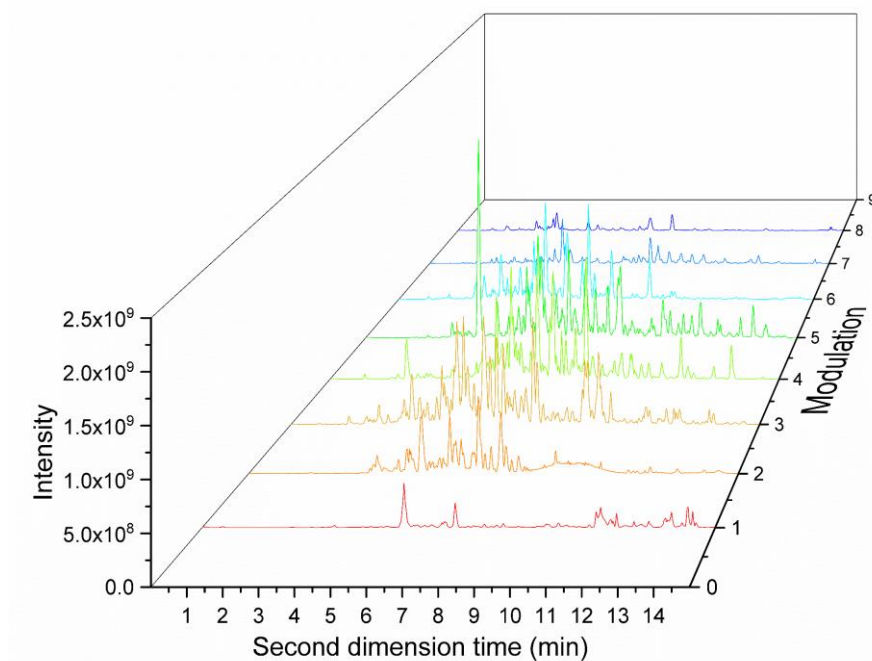


Figure 4 2D separation of yeast-proteome digest using 15-min modulations (120 min separation). ZIC HILIC as first dimension and C18 (100  $\mu\text{m}$  ID) as second dimension. For conditions see Section 3.5.2 and supplementary materials figure S4.6.

### 3.3.3 Application of the 2D setup and comparison with 1D RPLC

The same yeast sample was also run with 1D-RPLC with two column dimensions, *i.e.* 75  $\mu\text{m}$  ID (300  $\text{nL min}^{-1}$ ) and 150  $\mu\text{m}$  ID (1.2  $\mu\text{L min}^{-1}$ ). The gradient duration was equal to that of the 1D HILIC gradient in the 2D measurements (120 min). Dilution in the column is proportional to the square of the column diameter [42]. Therefore, a 4-fold greater dilution was expected when increasing the column diameter from 75 to 150  $\mu\text{m}$ . This was also observed experimentally. The narrower column performed better when the same sample quantity was loaded (1  $\mu\text{g}$ ). However, a five-time increase in the sample quantity injected on the larger-diameter column led to more peptides being identified than with the 75- $\mu\text{m}$  ID column. This beneficial effect is

## Chapter 4

expected also for the 2D setup, since larger column diameters were used. Both 1  $\mu\text{g}$  and 5  $\mu\text{g}$  sample amounts were loaded during the 2D experiments to determine the effect of the sample concentration and to allow a comparison with the 1D runs.

The numbers of peptides and proteins identified are listed in table 2. When 1  $\mu\text{g}$  of sample was separated the RP75 column (1D) yielded the highest number of peptides identified, followed by the RP150 column and then the 2D separation (15 min modulation). However, for the number of proteins identified, the RP75 and 2D separations yielded similar values (nearly 1500), while about 300 fewer proteins were found with the RP150 column. When 5  $\mu\text{g}$  were loaded, slightly more peptides were identified with the 2D and RP150 separations compared to the RP75 column (with 1  $\mu\text{g}$  injected). The number of proteins found was comparable between RP150 (5  $\mu\text{g}$ ) and RP75 (1  $\mu\text{g}$ ). The 2D separation of 5  $\mu\text{g}$  yeast-proteome digest yielded the highest number of proteins identified, with between 400 and 500 more proteins identified than on either 1D system (RP75, 1  $\mu\text{g}$  or RP150, 5  $\mu\text{g}$ ). It can be concluded that dilution has a large effect on the identification of peptides in a sample as it decreases the intensity of the peaks present and consequentially increase MS1 and MS/MS ion injection time, reducing the number of MS/MS scans that can be performed per analysis.

Finally, the setup was used for the characterization of proteomics samples from complex organisms: human-kidney-tissue proteome and IMR90 cells proteome. The same trends as with yeast were observed, but a larger number of proteins were identified, likely due to the more complex proteome.

For the IMR90 cells proteome we observed the highest number of identifications. We observed similar numbers of identified peptides and a slightly (5%) higher number of identified proteins using the 2D setup (15 min

modulation) in comparison with the 1D separation on the RP75 column, when loading the same amount of sample (1  $\mu\text{g}$ ) on the two systems.

For the kidney-tissue-proteome, loading 1  $\mu\text{g}$  of sample yielded similar results in terms of protein identification for the 1D (RP75) and 2D (15 min modulation) systems. When 5  $\mu\text{g}$  of sample were loaded on the 2D system, the number of proteins identified increased by about 1000. This represents a 34% increase in the number of proteins identified using the 2D platform, without any increase in measurement time. The higher protein coverage available from the 2DLC-MS setup in the analysis of kidney samples suggest that 2D approaches could significantly help in the analysis samples from complex matrices.

Moreover, when comparing the chromatographic performance of the 1DLC analysis respect to the 2DLC analysis the average peak width of the peptides identified was 2.5 times higher. It is likely that the cycle time for the MS experiments in the MS system used in this study (between 0.9 and 1.3 s) does not allow to fully exploit the gain in chromatographic performance from the 2DLC-MS. We suggest that 2DLC methods in combination with the latest generation of orbitrap and or ion mobility -time of flight mass spectrometry instruments would allow to capture to a greater extent the chromatographic gains in terms of peak width reduction (and hence peak capacity) that 2DLC analysis allows for.

## Chapter 4

Table 2: Comparison of results obtained with 1D-RPLC compared to 2D HILIC-RPLC separations of the yeast proteome, kidney- tissue proteome and IMR90 cells proteome.

File	Quantity loaded	Sample	Peptides	Proteins
1D RP75	1 µg	Yeast	7904	1497
1D RP150	1 µg	Yeast	6240	1130
1D RP150	5 µg	Yeast	8436	1457
2D (15 min modulation)	1 µg	Yeast	5905	1469
2D (15 min modulation)	5 µg	Yeast	8280	1931
1D RP75	1 µg	Kidney tissue	6629	1803
1D RP150	1 µg	Kidney tissue	5574	1351
2D (15 min modulation)	1 µg	Kidney tissue	5944	1764
2D (15 min modulation)	5 µg	Kidney tissue	8843	2750
2D (30 min modulation)	1 µg	Kidney tissue	5935	1868
1D RP75	1 µg	IMR90	10005	2495
2D (15 min modulation)	1 µg	IMR90	9993	2624

## 4. Conclusion

In this work we developed an online low-flow 2DLC setup for the separation of complex protein digest. The two separation dimensions were developed separately, keeping in mind their final application in the 2D-LC setup. The first dimension was chosen to be HILIC, due to its high orthogonality with RPLC. This was demonstrated with three types of column chemistries tested, which all showed a surface coverage in excess of 42% and asterisk orthogonality indices above 51%. The best performing column under the conditions tested was a ZIC HILIC column, which yielded a surface coverage of 46% and an asterisk orthogonality index of 60%. Therefore, this column was used in the 2D setup.

For the second-dimension separation a short run time, high peak capacity and good MS sensitivity are needed. For this purpose, three columns were

investigated with different internal diameters (75, 100, and 150  $\mu\text{m}$  ID) containing the same C18 particles (3  $\mu\text{m}$  diameter) and having the same length (100 mm). The optimal linear flow velocity was determined to be about 1.8  $\text{mm s}^{-1}$ , corresponding to volumetric flow rates of 300, 533 and 1200  $\text{nL min}^{-1}$  in the three columns. The peak capacity increased, but the MS sensitivity decreased with increasing column diameter. The reduction in sensitivity was overcome by loading larger quantities of peptides.

Considering the implementation of the two-dimensional system, higher flow rates were needed to minimize the detrimental effects of the dwell volume and the column dead volume. Therefore, the 100- $\mu\text{m}$  and 150- $\mu\text{m}$  ID columns were used in the second dimension at a flow rate of 1.2  $\mu\text{L min}^{-1}$ . The repeatability of the 2D setup was determined by considering the retention time variation. An average relative standard deviation of 1.7% was found. Manual, sample-dependent optimization of both dimensions (including variable gradients for each modulation) was needed to achieve the best result. In the future, computer-aided optimization would be highly attractive for an easier implementation of such a setup.

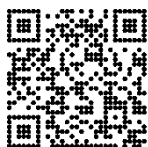
The 2D setup performed better than a one-dimensional separation with the 150- $\mu\text{m}$  ID RPLC column. When the quantity of peptides was adapted the 2D setup also performed better than the 75- $\mu\text{m}$  ID RPLC column. With the 2D setup we could obtain a much higher peak capacity in the same separation time (about 1000, as compared to 400 in 1D), which explains the better separation and higher identification capacity. A 17% increase in the number of proteins identified was obtained for the yeast proteome and a 34% for the human kidney-tissue-proteome with the 2D-LC setup compared to 1D RPLC (75  $\mu\text{m}$  ID) when loading a five-fold higher quantity in the 2D setup.

## 5. Acknowledgements

The STAMP project is funded under Horizon 2020 –Excellent Science – European Research Council (ERC), Project 694151. The sole responsibility of this publication lies with the authors. The European Union is not responsible for any use that may be made of the information contained therein. AG acknowledges financial support by the Netherlands Organization for Scientific Research, NWO Veni grant IPA (722.015.009). The authors would like to acknowledge Andrew Alpert (PolyLC) for providing the hydroxyethyl-A stationary phase, John Mommers (DSM) for providing the Matlab script for orthogonality calculations, Anniek Verstegen for initial tests, Stef R. A. Molenaar and Theodora Adamopoulou from the University of Amsterdam for their assistance with computations, Garry Corthals (University of Amsterdam) and Jasper Kers (Amsterdam UMC) for providing the kidney-tissue sample.

## 6. References

Supplementary material:



- [1] M. Larance, A.I. Lamond, Multidimensional proteomics for cell biology, *Nat. Rev. Mol. Cell Biol.* 16 (2015) 269–280. doi:10.1038/nrm3970.
- [2] Y. Zhang, B.R. Fonslow, B. Shan, M.-C. Baek, J.R. Yates III, J.R. Yates, Protein Analysis by Shotgun/Bottom-up Proteomics, *Chem. Rev.* 113 (2014) 2343–2394. doi:10.1021/cr3003533.Protein.
- [3] M. Wilm, M. Mann, Analytical properties of the nanoelectrospray ion source, *Anal. Chem.* 68 (1996) 1–8. doi:10.1021/ac9509519.
- [4] M.R. Emmett, R.M. Caprioli, Micro-Electrospray Mass Spectrometry: Ultra-High-Sensitivity Analysis of Peptides and Proteins, *J. Am. Soc. Mass Spectrom.* 5 (1994) 605–613.

- [5] J. Cox, M. Mann, MaxQuant enables high peptide identification rates, individualized p.p.b.-range mass accuracies and proteome-wide protein quantification, *Nat. Biotechnol.* 26 (2008) 1367–1372. doi:10.1038/nbt.1511.
- [6] D.J.C. Pappin, D.M. Creasy, J.S. Cottrell, Probability-based protein identification by searching sequence databases using mass spectrometry data *Proteomics and 2-DE*, (1999).
- [7] M. Vaudel, J.M. Burkhardt, R.P. Zahedi, E. Oveland, F.S. Berven, A. Sickmann, L. Martens, H. Barsnes, PeptideShaker enables reanalysis of MS-derived proteomics data sets: To the editor, *Nat. Biotechnol.* 33 (2015) 22–24. doi:10.1038/nbt.3109.
- [8] B. Zhan, J.R. Yates, M.-C. Baek, Y. Zhang, B.R. Fonslow, Protein Analysis by Shotgun/Bottom-up Proteomics, *Chem. Rev.* 113 (2013) 2343–2394. doi:10.1021/cr3003533.
- [9] S.S. Thakur, T. Geiger, B. Chatterjee, P. Bandilla, F. Frohlich, J. Cox, M. Mann, Deep and highly sensitive proteome coverage by LC-MS/MS without prefractionation, *Mol. Cell. Proteomics.* 10 (2011) 1–9. doi:10.1074/mcp.M110.003699.
- [10] S. Eeltink, S. Dolman, R. Swart, M. Ursem, P.J. Schoenmakers, Optimizing the peak capacity per unit time in one-dimensional and off-line two-dimensional liquid chromatography for the separation of complex peptide samples, *J. Chromatogr. A.* 1216 (2009) 7368–7374. doi:10.1016/j.chroma.2009.02.075.
- [11] M. den Ridder, P. Daran-Lapujade, M. Pabst, Shot-gun proteomics: Why thousands of unidentified signals matter, *FEMS Yeast Res.* 20 (2020) 1–9. doi:10.1093/femsyr/foz088.
- [12] M. Ke, H. Shen, L. Wang, S. Luo, L. Lin, J. Yang, R. Tian, Identification, Quantification, and Site Localization of Protein Posttranslational Modifications via Mass Spectrometry-Based Proteomics., *Adv. Exp. Med. Biol.* 919 (2016) 345–382. doi:10.1007/978-3-319-41448-5\_17.
- [13] P. Dugo, F. Cacciola, T. Kumm, G. Dugo, L. Mondello, Comprehensive multidimensional liquid chromatography: Theory and applications, *J. Chromatogr. A.* 1184 (2008) 353–368. doi:10.1016/j.chroma.2007.06.074.
- [14] M. Gilar, P. Olivova, A.E. Daly, J.C. Gebler, Two-dimensional separation of peptides using RP-RP-HPLC system with different pH in first and second separation dimensions, *J. Sep. Sci.* 28 (2005) 1694–1703. doi:10.1002/jssc.200500116.
- [15] V.-A. Duong, J.-M. Park, H. Lee, Review of Three-Dimensional Liquid Chromatography Platforms for Bottom-Up Proteomics, *Int. J. Mol. Sci.* 21 (2020) 1524. doi:10.3390/ijms21041524.
- [16] G. Vanhoenacker, I. Vandenneede, F. David, P. Sandra, K. Sandra, Comprehensive two-dimensional liquid chromatography of therapeutic monoclonal antibody digests, *Anal. Bioanal. Chem.* 407 (2015) 355–366. doi:10.1007/s00216-014-8299-1.

## Chapter 4

- [17] M. Kwiatkowski, D. Krösser, M. Wurlitzer, P. Steffen, A. Barcaru, C. Krisp, P. Horvatovich, R. Bischoff, H. Schlüter, Application of Displacement Chromatography to Online Two-Dimensional Liquid Chromatography Coupled to Tandem Mass Spectrometry Improves Peptide Separation Efficiency and Detectability for the Analysis of Complex Proteomes, *Anal. Chem.* 90 (2018) 9951–9958. doi:10.1021/acs.analchem.8b02189.
- [18] J. Jáčová, A. Gardlo, J.M.D. Dimandja, T. Adam, D. Friedecký, Impact of sample dimensionality on orthogonality metrics in comprehensive two-dimensional separations, *Anal. Chim. Acta.* 1064 (2019) 138–149. doi:10.1016/j.aca.2019.03.018.
- [19] A.J. Link, J. Eng, D.M. Schieltz, E. Carmack, G.J. Mize, D.R. Morris, B.M. Garvik, J.R.I. Yates, Direct analysis of protein complexes using mass spectrometry, *Nat. Biotechnol.* 17 (1999) 676–82. doi:10.1038/10890.
- [20] M.P. Washburn, D. Wolters, J.R. Yates, Large-scale analysis of the yeast proteome by multidimensional protein identification technology, *Nat. Biotechnol.* 19 (2001) 242–247. doi:10.1038/85686.
- [21] D.A. Wolters, M.P. Washburn, J.R. Yates, An automated multidimensional protein identification technology for shotgun proteomics, *Anal. Chem.* 73 (2001) 5683–5690. doi:10.1021/ac010617e.
- [22] K.J. Webb, T. Xu, S.K. Park, J.R. Yates, Modified MudPIT separation identified 4488 proteins in a system-wide analysis of quiescence in yeast, *J. Proteome Res.* 12 (2013) 2177–2184. doi:10.1021/pr400027m.
- [23] G. Vivó-Truyols, S. Van Der Wal, P.J. Schoenmakers, Comprehensive study on the optimization of online two-dimensional liquid chromatographic systems considering losses in theoretical peak capacity in first- and second-dimensions: A pareto-optimality approach, *Anal. Chem.* 82 (2010) 8525–8536. doi:10.1021/ac101420f.
- [24] E. Nägele, M. Vollmer, P. Hörth, C. Vad, 2D-LC/MS techniques for the identification of proteins in highly complex mixtures, *Expert Rev. Proteomics.* 1 (2004) 37–46. doi:10.1586/14789450.1.1.37.
- [25] P.J. Boersema, N. Divecha, A.J.R. Heck, S. Mohammed, Evaluation and optimization of ZIC-HILIC-RP as an alternative MudPIT strategy, *J. Proteome Res.* 6 (2007) 937–946. doi:10.1021/pr060589m.
- [26] Y. Zhao, R.P.W. Kong, G. Li, M.P.Y. Lam, C.H. Law, S.M.Y. Lee, H.C. Lam, I.K. Chu, Fully automatable two-dimensional hydrophilic interaction liquid chromatography-reversed phase liquid chromatography with online tandem mass spectrometry for shotgun proteomics, *J. Sep. Sci.* 35 (2012) 1755–1763. doi:10.1002/jssc.201200054.

- [27] M. Gilar, P. Olivova, A.E. Daly, J.C. Gebler, Orthogonality of separation in two-dimensional liquid chromatography, *Anal. Chem.* 77 (2005) 6426–6434. doi:10.1021/ac050923i.
- [28] G. Groeneveld, M.N. Dunkle, M. Rinken, A.F.G. Gargano, A. de Niet, M. Pursch, E.P.C. Mes, P.J. Schoenmakers, Characterization of complex polyether polyols using comprehensive two-dimensional liquid chromatography hyphenated to high-resolution mass spectrometry, *J. Chromatogr. A* 1569 (2018) 128–138. doi:10.1016/j.chroma.2018.07.054.
- [29] R.J. Vonk, A.F.G. Gargano, E. Davydova, H.L. Dekker, S. Eeltink, L.J. de Koning, P.J. Schoenmakers, Comprehensive Two-Dimensional Liquid Chromatography with Stationary-Phase-Assisted Modulation Coupled to High-Resolution Mass Spectrometry Applied to Proteome Analysis of *Saccharomyces cerevisiae*, *Anal. Chem.* (2015). doi:10.1021/acs.analchem.5b00708.
- [30] G. Mitulović, M. Smoluch, J.P. Chervet, I. Steinmacher, A. Kungl, K. Mechtler, An improved method for tracking and reducing the void volume in nano HPLC-MS with micro trapping columns, *Anal. Bioanal. Chem.* 376 (2003) 946–951. doi:10.1007/s00216-003-2047-2.
- [31] L.S. Roca, S.E. Schoemaker, B.W.J. Pirok, A.F.G. Gargano, P.J. Schoenmakers, Accurate modelling of the retention behaviour of peptides in gradient-elution hydrophilic interaction liquid chromatography, *J. Chromatogr. A* (2019) 460650. doi:10.1016/j.chroma.2019.460650.
- [32] P.F. Doubleday, L. Fornelli, N.L. Kelleher, Elucidating Proteoform Dynamics Underlying the Senescence Associated Secretory Phenotype, *J. Proteome Res.* 19 (2020) 938–948. doi:10.1021/acs.jproteome.9b00739.
- [33] M.F. Wahab, D.C. Patel, R.M. Wimalasinghe, D.W. Armstrong, Fundamental and Practical Insights on the Packing of Modern High-Efficiency Analytical and Capillary Columns, *Anal. Chem.* (2017). doi:10.1021/acs.analchem.7b00931.
- [34] X. Li, D.R. Stoll, P.W. Carr, A Simple and Accurate Equation for Peak Capacity Estimation in Two Dimensional Liquid Chromatography, *Anal. Chem.* 81 (2009) 845–850. doi:10.1021/ac801772u.
- [35] H.M. Quinn, A Reconciliation of Packed Column Permeability Data: Column Permeability as a Function of Particle Porosity, *J. Mater.* 2014 (2014) 1–22. doi:10.1155/2014/636507.
- [36] D. Wang, B. Eraslan, T. Wieland, B. Hallström, T. Hopf, D.P. Zolg, J. Zecha, A. Asplund, L. Li, C. Meng, M. Frejno, T. Schmidt, K. Schnatbaum, M. Wilhelm, F. Ponten, M.

## Chapter 4

Uhlen, J. Gagneur, H. Hahne, B. Kuster, A deep proteome and transcriptome abundance atlas of 29 healthy human tissues, *Mol. Syst. Biol.* 15 (2019) 1–16. doi:10.15252/msb.20188503.

[37] W.R. Pearson, D.J. Lipman, Improved tools for biological sequence comparison., *Proc. Natl. Acad. Sci. U. S. A.* 85 (1988) 2444–2448. doi:10.1073/pnas.85.8.2444.

[38] The UniProt Consortium, UniProt: A worldwide hub of protein knowledge, *Nucleic Acids Res.* 47 (2019) D506–D515. doi:10.1093/nar/gky1049.

[39] Y. Perez-Riverol, A. Csordas, J. Bai, M. Bernal-Llinares, S. Hewapathirana, D.J. Kundu, A. Inuganti, J. Griss, G. Mayer, M. Eisenacher, E. Pérez, J. Uszkoreit, J. Pfeuffer, T. Sachsenberg, Ş. Yilmaz, S. Tiwary, J. Cox, E. Audain, M. Walzer, A.F. Jarnuczak, T. Ternent, A. Brazma, J.A. Vizcaíno, The PRIDE database and related tools and resources in 2019: Improving support for quantification data, *Nucleic Acids Res.* 47 (2019) D442–D450. doi:10.1093/nar/gky1106.

[40] J. Mommers, S. van der Wal, Two metrics for measuring orthogonality for two-dimensional chromatography, *J. Chromatogr. A.* 1586 (2019) 101–105. doi:10.1016/j.chroma.2018.11.081.

[41] M. Camenzuli, P.J. Schoenmakers, A new measure of orthogonality for multi-dimensional chromatography, *Anal. Chim. Acta.* 838 (2014) 93–101. doi:10.1016/j.aca.2014.05.048.

[42] S.R. Wilson, T. Vehus, H.S. Berg, E. Lundanes, Nano-LC in proteomics: Recent advances and approaches, *Bioanalysis.* 7 (2015) 1799–1815. doi:10.4155/bio.15.92.

[43] Y. Bian, R. Zheng, F.P. Bayer, C. Wong, Y.C. Chang, C. Meng, D.P. Zolg, M. Reinecke, J. Zecha, S. Wiechmann, S. Heinzlmeir, J. Scherr, B. Hemmer, M. Baynham, A.C. Gingras, O. Boychenko, B. Kuster, Robust, reproducible and quantitative analysis of thousands of proteomes by micro-flow LC–MS/MS, *Nat. Commun.* 11 (2020) 1–12. doi:10.1038/s41467-019-13973-x.

[44] D.R. Stoll, X. Li, X. Wang, P.W. Carr, S.E.G. Porter, S.C. Rutan, Fast, comprehensive two-dimensional liquid chromatography, *J. Chromatogr. A.* 1168 (2007) 3–43. doi:10.1016/j.chroma.2007.08.054.



## Chapter 5

### Introduction of octadecyl-bonded porous particles in 3D-printed transparent housings with multiple outlets

Liana S. Roca, Theodora Adamopoulou, Suhas H. Nawada, Peter J. Schoenmakers

DOI: 10.1007/s10337-022-04156-w

#### Contents

1.	Introduction .....	130
2.	Materials and methods .....	132
2.1	Chemicals .....	132
2.2	Instrumentation .....	133
2.3	Design of device and printing .....	133
2.4	Connections (frit) .....	135
2.5	Packing procedure.....	135
2.6	Characterization of the packed devices .....	136
2.7	Separation and MS detection .....	136
3.	Results and discussion .....	137
3.1	Design of the 3D printed device.....	137
3.2	Packing considerations for 3D-printed devices .....	138
3.3	Characterization of packed devices .....	142
4.	Conclusions .....	148
5.	Acknowledgments .....	150
6.	Compliance with Ethical Standards .....	150
7.	Statements and Declarations .....	150
8.	References .....	150

## **Abstract**

Microfluidic devices for comprehensive three-dimensional spatial liquid chromatography will ultimately require a body of stationary-phase with multiple in- and outlets. In the present work 3D-printing with a transparent polymer resin was used to create a simplified device that can be seen as a unit cell for an eventual three-dimensional separation system. Complete packing of the device with 5- $\mu\text{m}$  C18 particles was achieved, with reasonable permeability. The packing process could be elegantly monitored from the pressure profile, which implies that optical transparency may not be required for future devices. The effluent flow was different for each of the four outlets of the device, but all flows were highly repeatable, suggesting that correction for flow-rate variations is possible. The investigation into flow patterns through the device was supported by computational-fluid-dynamics simulations. A proof-of-principle separation of four standard peptides is described, with mass-spectrometric detection for each of the four channels separately.

## **Keywords**

Additive manufacturing, microfluidics, packing, flow distribution, flow control, separation devices

## 1. Introduction

Liquid chromatography is a versatile technique that is used to analyse samples from many fields, such as proteomics, metabolomics, lipidomics, *etc.* [1–3]. One of the common characteristics of life-science samples is the high degree of complexity, which necessitates a high peak capacity to fully resolve all components [4]. The introduction of ultra-high performance liquid chromatography (UHPLC) allows the use of higher pressures, *viz.* longer columns and/or smaller particle diameters. In combination with shallow gradients such systems have shown great promise in increasing resolving power [5]. However, a maximum peak capacity of 1400 to 1600 is predicted for one-dimensional (1D) LC [6] and a random distribution of peaks implies that only about 37% of the full peak capacity of a system can be realized [7]. To fully resolve life-science samples, higher peak capacities are needed. These can be achieved with multidimensional separations.

Multidimensional LC, employing orthogonal separation mechanisms in the different dimensions, promises much greater separation power. Ideally, the total peak capacity of the system will be the product of the peak capacities in each dimension [8]. In this way a higher peak capacity can be obtained without a great increase in measurement time [9]. Multidimensional LC can be achieved in time-based separations by coupling different columns or in spatial separations [10]. The latter provides parallel, simultaneous separation in all but the first dimensions, which keeps the total analysis time much shorter and results in a much higher peak-production rate (peak capacity per unit time).

A design for a microfluidic device has been proposed previously [11]. The first-dimension (<sup>1</sup>D) separation takes place in a channel, the second-dimension (<sup>2</sup>D) separation in a perpendicular direction in a rectangular planar space (“flat bed”), and the third dimension (<sup>3</sup>D) separation, again in a perpendicular direction, in a block. The analytes will be separated spatially in the <sup>1</sup>D channel

and <sup>2</sup>D bed and eluted from the <sup>3</sup>D block in the final separation. (“temporal” separation). Flow distributors are needed to transfer the analytes to the next dimensions and to create homogeneous flow in the <sup>2</sup>D and <sup>3</sup>D directions. To create such a device 3D-printing techniques have been proposed and flow-control [12], implementation of stationary phases [13,14] and detection methods all need to be considered for its operation. Given the current state of the art of 3D printing we envisage devices slightly larger than that described before [11] to accommodate channels of between 1 and 2 mm internal diameter. Smaller devices are feasible with high resolution 3D-printing, such as two-photon polymerization [15] or hybrid stereolithography [16].

The stationary phase can be a packed bed (polymer or silica-based particles) or a monolith, with various surface functionalities. Monoliths are formed from a liquid mixture of monomers, cross-linkers, porogens and initiator, which has the advantage that it can easily be introduced in any structure. The formation of the organic monolith can be performed by UV irradiation or thermal initiation. However, the polymerization process is highly exothermic[17]. This causes temperature differences in large spaces, with the centre getting warmer than the edges, leading to a heterogeneous bed. Particle-packed columns yield higher separation efficiencies and better reproducibility than organic monolithic column and the former are used much-more widely.

However, the introduction of particles in a device can present its own set of challenges. Procedures for the packing and consolidation of cylindrical columns are well established, and sources of packing heterogeneities have been the subject of several studies [18–21]. There are few published examples of packing channels in microfluidic devices [22,23]. The demands of a spatial 2D or 3D device introduce their own set of considerations, compared to packing a cylindrical column with a single inlet and outlet, or a single channel in a microfluidic device. A cuboidal or block-shaped region, necessary for all

dimensions, creates dead-zones, where packing densities may be lower. The proposed devices also require flow distributors and/or collectors to distribute fluid flow homogeneously within the <sup>2</sup>D and <sup>3</sup>D spaces. The design of these flow distributors will also influence the homogeneity of the packed regions. An additional consideration is the 3D-printing method used to create the device, which can introduce surface features [24] not present in mechanically polished cylindrical columns. Nonetheless, it is highly relevant to attempt creating particle-based stationary phases, because of their suitability to larger aspect ratios needed for <sup>2</sup>D and <sup>3</sup>D regions

In this project we aimed to study the introduction of particles in a block-shaped region, akin to a possible third-dimension block in a 3D spatial-LC device. We sought a transparent material for 3D printing suitable for Reversed-Phase Liquid Chromatography (RPLC) separations that would allow the visualization of the packing and withstand the pressure needed for introducing the particles. Moreover, we aimed to develop a packing procedure, to test the properties of the packed device, and to produce a proof-of-principle separation.

## 2. Materials and methods

### 2.1 Chemicals

Acetonitrile (ACN, MS grade) and 2-propanol (IPA, HPLC grade) were purchased from Biosolve Chimie (Dieuze, France). Milli-Q water (18.2 mΩ) was obtained from a purification system (Millipore, Bedford, MA, USA). C18 particles (5 μm diameter, 100 Å pre size) were purchased from Fuji Silica Chemical (Lausanne, Switzerland). An HPLC peptide-standard mixture was purchased from Sigma Aldrich (Darmstadt, Germany). The methacrylate-

based resin Formlabs Durable was purchased from Formlabs (Somerville, MA, USA).

A Next-Advance frit kit (Troy, NY, USA), fused silica-capillaries (200  $\mu\text{m}$  ID, 360  $\mu\text{m}$  OD) (CM scientific, Silsden, UK), PEEK tubing (IDEX, Lake Forest, IL, USA), and ferules, nuts and unions (Vici-Valco, Houston, TX, USA) were used to prepare the connections.

## **2.2 Instrumentation**

For constructing the devices, the Form-2 3D-printer (Formlabs) and Form Cure chamber (405 nm wavelength; Formlabs) were used. Packing of the devices was performed using a Shimadzu LC-10AD VP pump (Shimadzu, 's Hertogenbosch, The Netherlands). The flow measurements were performed with an Agilent 1100 Series Pump (Agilent, Waldbronn, Germany). The LC-MS measurements were performed with Waters ACQUITY UPLC and Waters Synapt G2 (Waters Corporation, Milford, US).

## **2.3 Design of device and printing**

To study the efficacy of particle packing and the performance of the bed for a potential third dimension, devices with a flow distributor (FD) starting from one inlet, a  $7\times 10\times 10$  mm <sup>3</sup>D space and four outlets were studied. The initial device, shown in Figure 1, comprised an FD with 1.4-mm ID channels and a wall thickness of 1 mm. In following iterations, the wall-thickness was increased to 2.5 mm in order to enhance the pressure resistance of the devices. Additionally, the ID of the flow-distributor channels was adjusted from 1.4 mm to 2 mm to enhance the ease of packing. All devices were designed via Autodesk Inventor (Autodesk, San Rafael, CA, USA).

In order to visualize the anticipated influence of packing heterogeneities, computational-fluid-dynamics (CFD) simulations were performed. ANSYS Workbench Fluids and Structures Academic package (version 17.1) was used

## Chapter 5

(ANSYS, Canonsburg, PA, USA). The examined case was discretized with ANSYS Meshing. The geometry was meshed with tetrahedral cells and inflation layers were used on the flow distributor. The total number of cells in this setup was 12,956,270. All simulations were conducted using the Fluent solver (ANSYS), solving for flow and species transport [25]. In order to simulate the effect of packing heterogeneities on the flow profile, a mixture of dye and water (1% dye) was injected from the <sup>3</sup>D inlet and flushed with one device volume of water towards the <sup>3</sup>D space. Two cases were examined, *viz.* one with perfect packing of the whole device and one where a part of the FD was not fully packed. In both cases the permeability was set at  $10^{-15}$  m<sup>2</sup>. The value of the velocity at the device inlet was adjusted so as to obtain a velocity of 1 mm/s in the block-shaped region.

The device was fabricated through 3D-printing, more specifically stereolithography. First, the design was converted to STL format and then loaded to PreForm (FormLabs software). Printing orientation and settings were optimized for high resolution and fabrication time, after which the form file was loaded to the Form-2 printer. After printing, post-processing of the parts was necessary (figure S6, supplementary information). This included sonication and flushing of channels with 2-propanol and compressed air to remove any uncured resin. Thereafter, the parts were placed in a Form Cure chamber (405 nm; Formlabs) for UV and thermal curing for 60 min at 60°C.

For fluidic connections, straight threads (#10-32 UNC, major diameter 4.83 mm, thread pitch 0.794 mm or #6-32 UNC, major diameter 3.5 mm, thread pitch 0.794 mm) were created using a hand tap. Conical ferrule seats were included in the designs of the devices to prevent leakage.

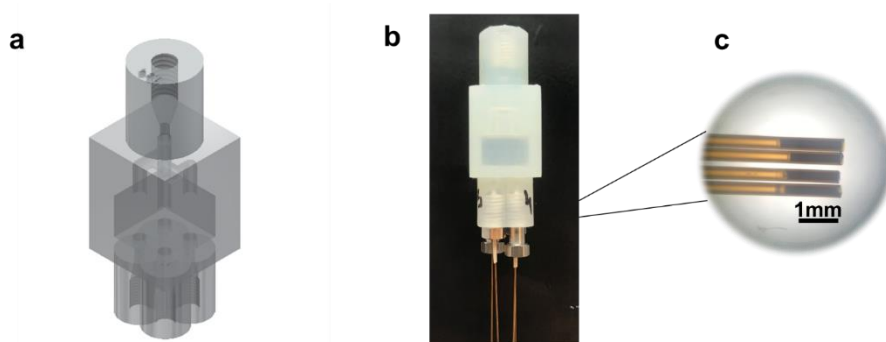


Figure 1: Design of the 3D printed device (a- CAD picture; b- Printed device). Fused-silica capillaries (200  $\mu\text{m}$  ID) containing frits (Kasil) were used to contain the particles (c).

## 2.4 Connections (frit)

Confinement of the particles inside the device needs a barrier permeable for the solvent, but not for the stationary-phase particles. In this project the confinement was achieved by the use of silica frits. These were created inside fused-silica capillaries (200- $\mu\text{m}$  internal diameter). A solution of Kasil 1624 (60  $\mu\text{L}$ ) and formamide (20  $\mu\text{L}$ ) was prepared and vortexed gently. The capillaries were dipped (1-2 s) in this mixture and then placed in an oven at 100°C overnight. After the formation of the frit with 10 to 20 mm length, the capillary was cut so as to retain only 1 or 2 mm of monolith (Figure 1C). On the frit side of the capillary, a sleeve and ferrule were added and the connection was made. Two sizes of nuts were used to allow for more space to tighten them (see Figure 1B).

## 2.5 Packing procedure

A slurry of 0.8 g of particles in 4 mL of IPA/water 50/50 by volume (0.2 g/mL) was prepared and sonicated for 15 min. The slurry chamber was an empty cylinder (250  $\times$  4.1 mm ID, 3.3 mL internal volume) with a piece of metal tubing (specified as 0.04" ID, 100 mm length) connected at the end to make the connection with the device. The setup was aligned vertically with the slurry chamber on top, followed by the metal tubing connected to the inlet of

the 3D printed device. The components were held in place using metal clamps. The slurry was introduced in the cylinder and the top was connected to a pump (Shimadzu LC-10AD VP pump). Packing was performed under constant flow (100  $\mu\text{L}/\text{min}$ ) and the pump was stopped when a sharp increase in pressure was observed and the pump pressure reached 40 bar (4 MPa). Higher pressures were not possible, due to the limited pressure resistance of the device (see supplementary information, figure S8).

### 2.6 Characterization of the packed devices

The permeability of the devices was determined by measuring the pressure drop across the empty device and across the device after packing when being flushed with water at various flow rates. Equation 1 was used to calculate the permeability [26]:

$$k = \frac{\mu \times L \times Q}{A \times \Delta P} \quad (1)$$

Where  $k$  is the permeability ( $\text{m}^2$ ),  $\mu$  is the viscosity of the solvent ( $\text{Pa}\times\text{s}$ ),  $L$  is the length of the column ( $m$ ),  $Q$  is the flow rate ( $\text{m}^3/\text{s}$ ),  $A$  is the surface area ( $\text{m}^2$ ) and  $\Delta P$  is the difference in pressure drops between the empty device and the packed device (Pa).

The uniformity of the effluent flow was determined by flushing the packed device with water at 0.2 mL/min for 15 min. The effluent from each outlet was collected and weighted in triplicate. The total weight collected was expected to be 3 g and the weight collected from each outlet 0.75 g (25%). The average percentage collected from each outlet and the standard deviations were determined.

### 2.7 Separation and MS detection

Since the device contained four outlets, the backpressure caused by a connecting one of the outlet tubings to a detector would influence the flow

through the device. Therefore, an MS detector was used that did not add any backpressure. The effluent flow from all each of the outlets was measured. The connection was made using a PEEK nut added to the outlet capillary, which was then connected to the inlet of the MS (Figure S12, supplementary information). After that the device was connected to the MS (Waters Synapt G2) and detection was performed individually after each of the four outlets, with the effluent flow measured for each of the three remaining outlets to verify that the MS did not affect the flow rates through the different channels.

The device was used under reversed-phase conditions to perform separation of four peptides (Gly-Tyr, Val-Tyr-Val, Met-Enkephalin, Leu-Enkephalin). A gradient from 15% ACN to 50% ACN (with a constant 0.1% of formic acid, FA, as additive) in 10 min was performed at 0.3 mL/min. The peptides were dissolved in water containing 2% ACN and 0.1% FA by volume (0.02 mg/mL of each peptide) and 5  $\mu$ L were loaded on the device (0.1  $\mu$ g of each peptide).

The MS method was set to negative mode, capillary voltage 1.8 kV, sampling cone 20 V, extraction cone 2 V, source temperature 110°C, desolvation temperature 350°C, cone gas 10 L/h and desolvation gas 800 L/h. The mass range was 100 to 1200 Da, and only MS<sup>1</sup> was acquired.

### 3. Results and discussion

#### 3.1 Design of the 3D printed device

The 3D-spatial separation devices that we are aiming for consist of a first-dimension channel, a second-dimension planar separation space in a perpendicular direction, and a third-dimension separation block underneath the second dimension (figure S1 in supplementary information). The design of the present device is a simplification of the third dimension space, intended to study possible packing techniques. Multiple aspects need to be considered when building a 3D separation block, so as to ensure flow confinement and

added selectivity. The aspects of flow confinement have been investigated using simulations [12] and it was concluded that a permeability difference of two orders of magnitude is needed for a good flow confinement between the second and third dimensions. One possibility to achieve this may be a highly permeable monolith in the second-dimension separation space and a particle-packed bed for the third-dimension separation. Our simplified device, shown in *Figure 1*, contains a flow distributor on top, a separation block and four outlets at the bottom, which may be seen as an elementary unit of the ultimate separation device.

### **3.2 Packing considerations for 3D-printed devices**

#### **3.2.1 Solvent used for packing**

When packing devices, a very important consideration is the suspension of the particles in the packing solvent. For C18 particles, due to their hydrophobic nature, organic solvents, such as methanol, iso-propanol (IPA), chloroform, acetone, *etc.*, may provide good, stable suspensions. In contrast, particles agglomerate and float on top when submerged in water (figure S5, supplementary information). The stability of suspensions is also enhanced by a higher solvent viscosity and a small density difference between solvent and particles. However, we also had to consider the solvent compatibility of the device. The material used for printing the devices (Formlabs durable) was not stable in methanol, acetone or chloroform and showed swelling when exposed for a long duration to pure IPA or acetonitrile (ACN) (see figure S4 in supplementary information).

IPA is the recommended solvent for post-processing of the 3D-printed devices (see section 2.3). Also, it has a relatively high viscosity and is miscible with water. Therefore, a mixture of IPA and water was thought to be a good solvent for packing. The C18 particles were suspended 50% IPA in water (by volume), which allowed for solvation of the particles and a yielded a homogeneous

slurry. Sonication of the slurry for 15 min was used to prevent any possible agglomeration of the particles. Thereafter, the slurry was added to the packing cylinder and a constant flow of 50% IPA was used for packing.

### **3.2.2 Pressure resistance**

Initially, the device was designed to have a wall thickness of 1 mm around the separation space. The device was connected to the LC pump with 150- $\mu$ m ID connection tubing. The pressure of the system was measured at different flowrates (0.1 – 1.5 mL/min), without the device installed. After installing the device, we ramped up the flowrate (starting at 0.1 mL/min) and thus the pressure. The devices typically functioned well until about 35 bar (3.5 MPa). At that point the wall around the separation space would break and start to leak (see figure S3 in supplementary information). This was performed to see at what pressure the empty device would break or start leaking and which were the weak points.

The wall thickness was increased to 2.5 mm to improve the pressure resistance of the device. This still allowed for a good visualization of the separation space. The highest pressure achieved with this device was 80 bar for a for a short period of time (packed device). The vulnerable points in the device were the walls surrounding the empty block and the fittings. A further increase in wall thickness was deemed undesirable, as this would reduce the transparency of the device. At a flowrate of 1.1 mL/min the pressure drop was dominated by the system and connections. The empty device proved stable at this flowrate and showed a fairly constant pressure of 30 to 40 bar. Only after prolonged operation at a higher pressure cracks around the separation space or leaks from the connections were observed. Therefore, pressures should not exceed 40 bar if at all possible. While the increased wall thickness increased the pressure resistance of the device, swelling of the packing chamber was not completely eliminated.

Another cause of failure of the printed devices after repeated use was erosion of the printed substrate in the threaded ports. PEEK fittings (UNF 10-32) at the inlet of the device were found to be less damaging when attached and removed repeatedly, compared to metal fittings. PEEK fittings (UNF 6-32) were also tried at the outlets, but the nut did not tighten enough to hold the capillaries in place. Metal fittings were used at the outlets instead. When the fittings started leaking the device could not be used anymore.

### **3.2.3 Packing procedure**

The packing procedure was monitored visually (Figure 2A) and by monitoring the backpressure (Figure 2B). Initially (region 1), the outlet zones were packed, resulting in a steep rise of the pressure. This was followed by a gradual increase while the main region was being packed (zones 2 and 3). The flowrate was chosen so as to have a reasonable backpressure while packing. Most devices had a pressure around 20 bar for the main part of the packing procedure at a constant flowrate (0.2 mL/min; see Figure 2B). When the flow distributor and the metal tubing connecting the device to the packing cylinder also started to be filled with particles, the pressure increased rapidly and the device was considered to be fully packed (region 4 in figure 2B). At this point the flow was stopped.

For six devices that were packed without any interruption, the average packing pressure was 21.5 bar and the average time it took until the devices were fully packed was 13.7 min. By using this procedure to monitor the packing, transparency of the device is not a prerequisite. Packing of non-transparent devices (e.g. metal printed devices) may also be performed by monitoring the pressure during packing. This would remove the limitation on compatible solvents currently encountered and increase the maximum pressure during packing and operation. However, the design of the connections should be adapted and the effects of the surface roughness should be investigated.

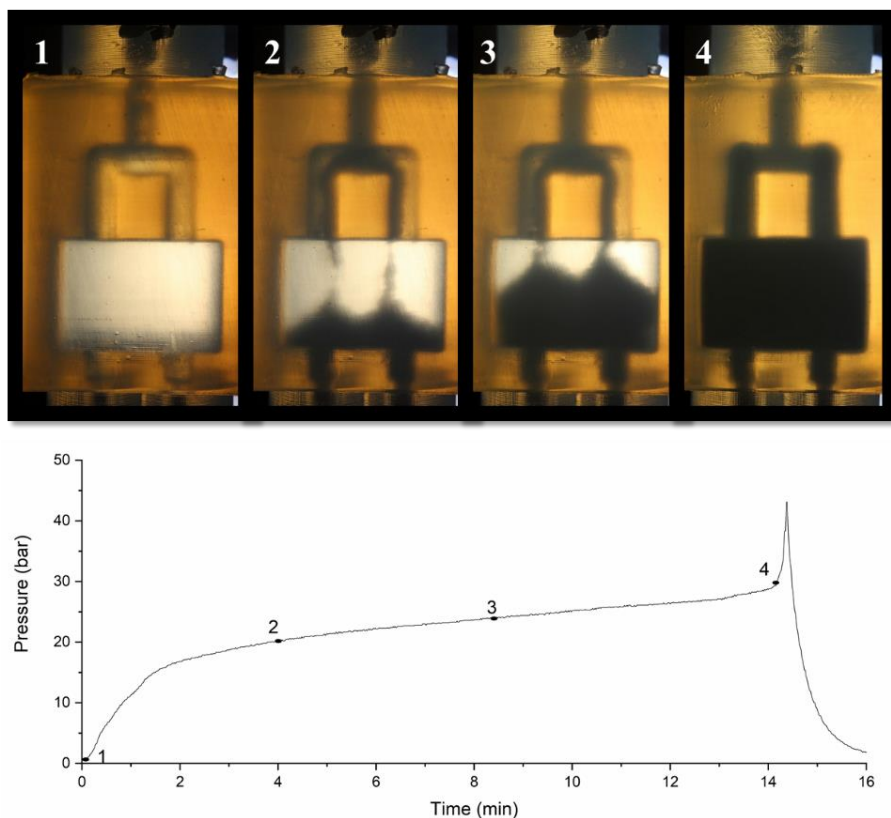


Figure 2: Illustration of the process of packing a device. a, visual observation at various stages of the process; b, pressure profile during packing with the numbers corresponding to the pictures of Fig. 2a. C18 particles  $5\ \mu\text{m}$  introduced as a slurry in 50% IPA.

Sonication during packing was also attempted. It has been shown for capillary columns that using sonication can prevent particle aggregation, hence column clogging, and can make the packing process faster, ensuring stability of the slurry suspension [27]. We observed that the packing pressure was lower during sonication, probably because the bed was not consolidating until the end of the process. However, the observed permeability was comparable to that observed without sonication, while the uniformity of flow output was slightly worse (see figures S9 and S10 in supplementary information).

Moreover, due to the sonication, the outlet nuts moved, loosening the connections and allowing particles to escape around the ferrule and into the threads. Therefore, sonication was not considered a valuable addition to packing of the devices.

### **3.3 Characterization of packed devices**

The devices packed with C18 particles were characterized by measuring the effluent flow from each outlet, the permeability and by the separation of peptides under gradient conditions.

#### **3.3.1 Flow uniformity**

During experimental testing measurements were performed in triplicate to determine the variability in effluent flow from each outlet and the variability between the outlets. In figure 3 the average relative flow collected is illustrated for three devices. The lowest flow recorded from any outlet was 15% (instead of the expected 25%), which indicates a large variability. However, the variability of individual outlets for the triplicate measurements were very low. This would suggest that a packed device with multiple channels may eventually be used in practice, provided that a flow marker is used to correct for the residence time in each channel. The added value for the separation power of the device can still be realized, even with deviations at the flow distribution, as long as the measurements are repeatable.

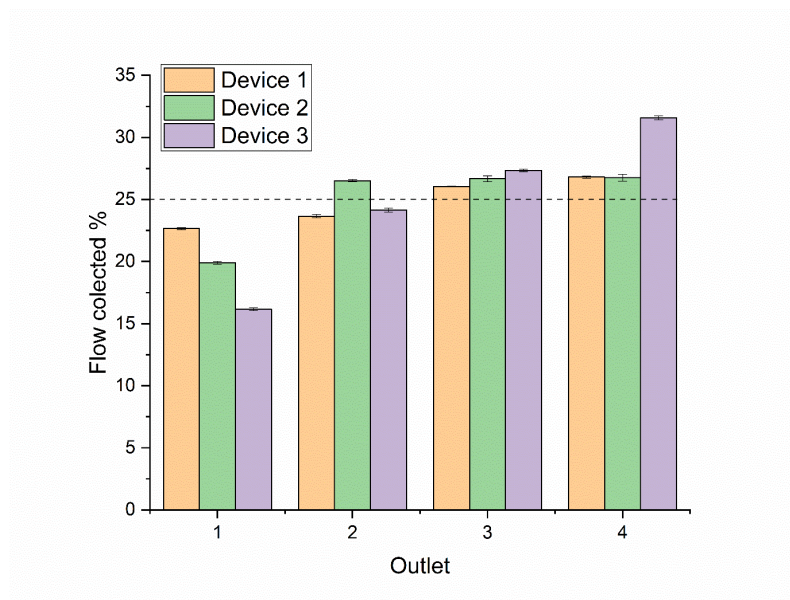


Figure 3: Relative effluent flow rates from all outlets of three different devices, measured by collecting and weighing. Measurements were performed in triplicate and the average value was plotted with the standard deviation. 25% from each outlet would represent an ideal situation.

### 3.3.2 Permeability

The permeability of the devices was also considered as a measure of packing uniformity. The permeability was calculated by measuring the pressure drop across the packed device corrected for that across the empty device at a given flow rate. The permeability of three devices can be seen in figure 4. The average permeability was calculated using water at three different flow rates (0.1, 0.2 and 0.4 mL/min). Higher flow rates were not used to avoid high backpressures. The contribution of the flow distributor was not considered in the calculation of the permeability. Only the area and length of the separation space were used in the equation 1 (see section 2.6). Permeability values in the order of  $10^{-16}$  were obtained. For a column packed with 5  $\mu\text{m}$  particles a permeability of  $10^{-14}$  would be expected [28,29]. From our results it seems that the packed bed obtained was denser or that the flow distributor had a large impact on the permeability calculation. Considering the presence of particles

in the channels of the flow distributor, the latter is considered more likely. This assumption can also be supported by a theoretical calculation on the influence of the packed flow distributor on the device pressure. We found that 94% of the backpressure is due to the flow distributor and only 2% due to the separation space (Supplementary information Table S1).

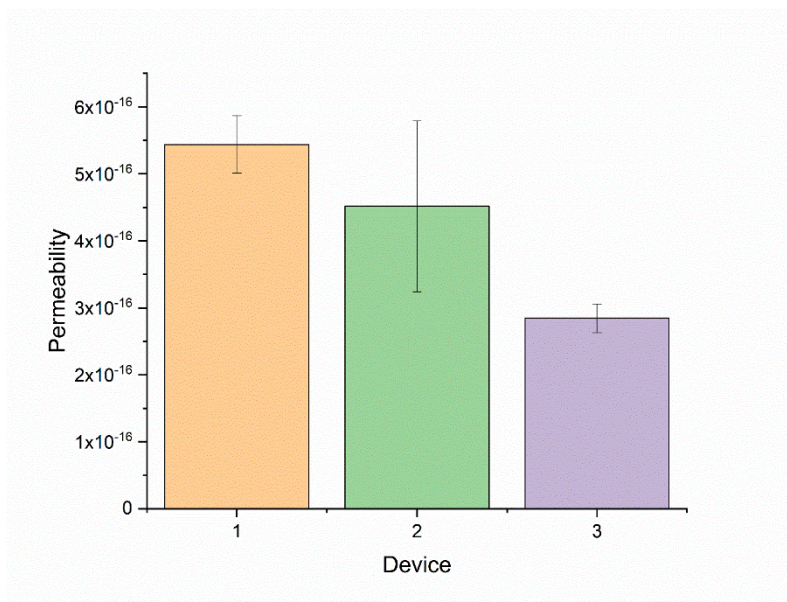


Figure 4: Permeability of three packed devices measured using water at 0.1, 0.2 and 0.4 mL/min. The average permeability and the standard deviation are plotted.

In addition to radial heterogeneity (section 3.3.1), the effect of axial heterogeneity on the local permeability was studied by applying a step gradient from 100% IPA to 100% water and recording the backpressure of the system. A device with a perfectly constant axial permeability is expected to lead to a linear decrease in the system backpressure from  $P_1$  (100% IPA) to  $P_2$  (100% Water), with slight non-linearity in the pressure profile being introduced by the packed flow distributor, device band broadening and axial mixing.

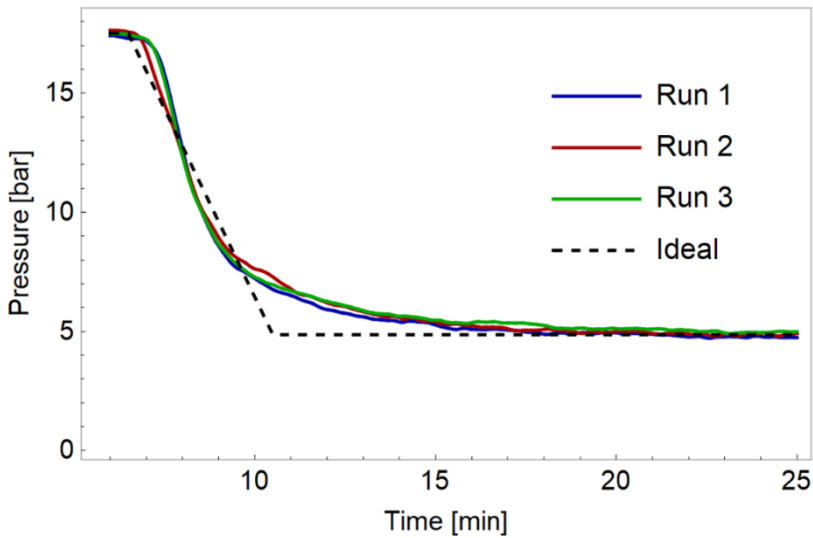


Figure 5: Pressure profile arising from a gradient from 100% IPA to 100% water in 0.1 min.

A significantly curved pressure profile at the start of the gradient indicates under-packed or heterogeneously packed regions within the flow distributor and prominent tailing at the end of the pressure profile indicates heterogeneities in the separation region. The measured profiles shown in Figure 5 show an initial steep decline (4 to 5 min) when the gradient passes the flow distributor. The curvature is relatively minor, which may be due to a homogeneous packing and/or the relatively small volume of the flow distributor. The steep decline is followed by a shallow part when the gradient passes through the separation region. The curvature of this part of the curve is indicative for heterogeneities in the packed bed.

### 3.3.3 Separation of peptide standards

The device was envisioned to be the third dimension of a separation space. We attempted the separation of four peptides under reversed-phase gradient conditions. The separation bed was only 7 mm in length and a gradient of 10 min was programmed. The effluent of each outlet had to be measured individually, since a multi-channel detector was not available. To obtain correct results, a detector was needed that did not alter the flow distribution between the four outlets.

Initially, the flow output of the device was recorded in each outlet and then one of the outlets was connected to a mass spectrometer (MS). The flow output from the three remaining channels was measured again to determine the influence of the MS on the flow profile. A comparison between the free outlets and one outlet connected to the MS can be seen in supplementary information (figure S11 and table S2). We observed no change in backpressure caused by the MS and no influence on the flow distribution across the four channels. Therefore, the MS was deemed a good option for detection.

The separation of the peptide mixture can be seen in figure 6. The peptides separated were Gly-Tyr, Val-Tyr-Val, Met-Enkephalin and Leu- Enkephalin (structures shown in figure S13, supplementary information). The elution order of the four peptides was the same in all four outlets but a shift in retention time was observed, which could be correlated with the flow through each outlet. Outlet 4 exhibits the highest linear velocity. Therefore, the composition gradient will arrive earlier and be steeper, leading to faster elution and sharper peaks. Outlet 1 showed broader peaks and the longest retention times, due to a relative flow of only 11%. The peaks were not baseline separated. However, with MS detection we were able to use extracted ion currents (EIC) to easily identify the four peptides. The repeatability of the separation was investigated for the fourth outlet. The same gradient was run

three times and the EICs plotted as overlays (see figure S14 in supplementary information).

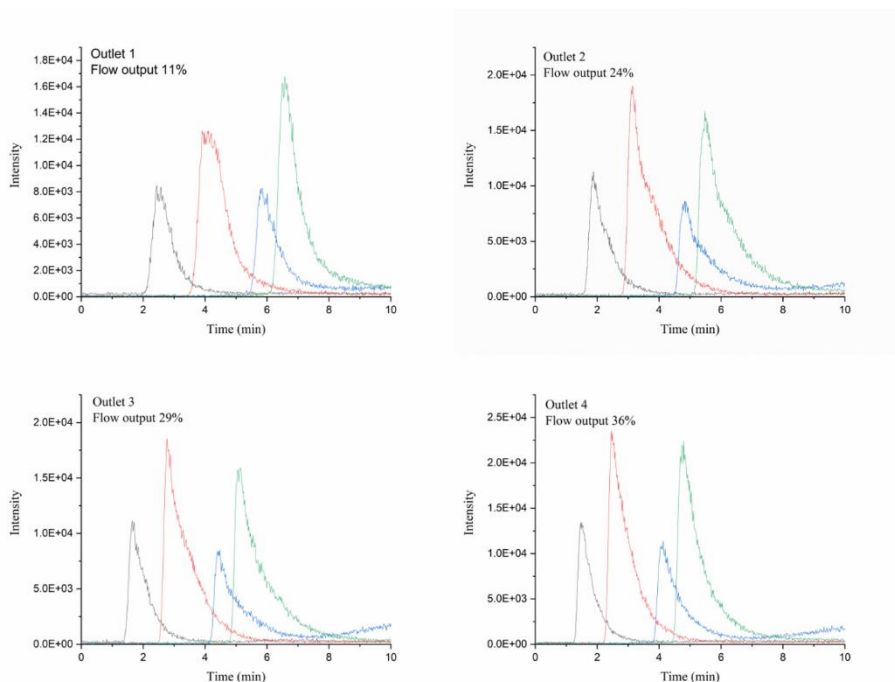


Figure 6: Separation of four peptides using a gradient from 15% to 50% ACN in 10 min at a flow rate of 0.3 mL/min with MS detection at each of the 4 outlets. Peptides in order of elution: Gly-Tyr (black), Val-Tyr-Val (red), Met-Enkephalin (blue) and Leu-Enkephalin (green).

In all outlets severe peak tailing was observed. This may possibly be attributed to dead zones in the corners of the cube. Even in a cylindrical column, it has been shown that the mobile-phase velocity can be 2 to 5% lower close to the wall [30]. When the separation space is a cube, the linear velocity in the corners may be even lower. This will then lead to distortion of the peaks. Such “wall effects” will have less influence for a device that features a larger array of outlets.

The peak capacity for this imperfect device was calculated based on equation 2 [31]:

$$n_c = \frac{t_g}{1.7 \times w_{\frac{1}{2}h}} + 1 \quad (2)$$

Where  $n_c$  is the peak capacity,  $w_{\frac{1}{2}h}$  is the peak width measured at half height (min) and  $t_g$  the gradient time (min). And a value of  $n_c = 9$  was obtained.

In a perfect multidimensional system, the total peak capacity may be obtained by multiplying the peak capacities obtained in each dimension [11]. When using a limited number of channels, this puts a limited on the actual achievable peak capacity. Also, the effective peak capacity is limited by the orthogonality of the different separations. The time needed for the separation is determined by the sum of the analysis times in each dimension. Assuming a final device with 16 outlets between the first and second dimension (hence, an assumed <sup>1</sup>D peak capacity of  $^1n_c = 16$ ), and 16 outlets between each second-dimension channel and the third dimension (<sup>2</sup> $n_c = 16$ ), and with <sup>3</sup> $n_c = 9$ . The anticipated total peak capacity of the device would be 2304.

## 4. Conclusions

A device was designed so as to mimic a unit in a three dimensional separation space. Such devices were successfully created in this work using a Form 2 3D-printer (Formlabs) using Durable as resin, resulting in a good solvent stability, transparency, and flexibility. The latter property allowed connections to be made to fritted capillaries, providing a barrier for the particles. We succeeded in packing C18 porous particles suspended in 50% IPA under constant-flow conditions (0.2 mL/min). Monitoring of the pump pressure during packing was found to offer an indication of the completion of the packing process. Therefore, the procedure is also applicable to non-transparent devices,

allowing the possibility to use metal printing. The use of metal printing would allow for a wider range of organic solvents and the devices may withstand higher pressures.

When investigating the flow stability and uniformity through the device, highly repeatable measurements were obtained for each single outlet, but there were large variations between the four outlets. The latter could be caused by errors in printing (*e.g.* unequal channels in the flow distributor), differences in the inner diameters of outlet capillaries, differences in length and/or permeability between different frits, or differences in particle consolidation. In spite of all this, the repeatability of the device promises future gains in separation power by adding a third-dimension separation.

A proof-of-principle separation of peptides using the device was obtained by loading the sample from the flow distributor. In future experiments separations of samples will be developed in the plane above the separation space and different analytes will be sent to each outlet. In the present case we obtained the same chromatogram from all the outlets with some variation in retention times, that could be correlated with differences in the flow output. The separation of the four peptides was repeatable, but peak tailing was observed due to dead zones in the device, most likely in the corners of the separation space. This situation may be improved by smoothing the corners of the separation space and by creating more outlets. The detection was performed for each outlet separately by connection to the MS. In the future, other detection methods will be employed to monitor all channels simultaneously or to store fractions of each outlet before detection (droplet collection). If droplet collection is employed detection could then be performed by scanning (*e.g.* fluorescence spectroscopy) or matrix-assisted laser-desorption/ionization (MALDI) mass spectrometry.

## **5. Acknowledgments**

The authors would like to acknowledge Sven Koot for technical assistance and Andrea F.G. Gargano for valuable discussions.

## **6. Compliance with Ethical Standards**

Funding: The STAMP project is funded under Horizon 2020 – Excellent Science – European Research Council (ERC), Project 694151. The sole responsibility of this publication lies with the authors. The European Union is not responsible for any use that may be made of the information contained therein.

Conflict of interests: The authors declare that they have no known conflict of interests.

Ethical approval: This article does not contain any studies with human participants or animals performed by any of the authors.

## **7. Statements and Declarations**

The STAMP project is funded under Horizon 2020 – Excellent Science – European Research Council (ERC), Project 694151. The sole responsibility of this publication lies with the authors. The European Union is not responsible for any use that may be made of the information contained therein.

The authors have no relevant financial or non-financial interests to disclose.

## **8. References**

Supplementary material:



- [1] K. Sandra, P. Sandra, Lipidomics from an analytical perspective, *Curr. Opin. Chem. Biol.* 17 (2013) 847–853. doi:10.1016/j.cbpa.2013.06.010.
- [2] P. Miggels, B. Wouters, G.J.P. van Westen, A.C. Dubbelman, T. Hankemeier, Novel technologies for metabolomics: More for less, *TrAC - Trends Anal. Chem.* 120 (2019) 115323. doi:10.1016/j.trac.2018.11.021.
- [3] W.H. McDonald, J.R. Yates, Shotgun proteomics and biomarker discovery, *Dis. Markers.* 18 (2002) 99–105. doi:10.1155/2002/505397.
- [4] G. Guiochon, N. Marchetti, K. Mriziq, R.A. Shalliker, Implementations of two-dimensional liquid chromatography, *J. Chromatogr. A.* 1189 (2008) 109–168. doi:10.1016/j.chroma.2008.01.086.
- [5] J.R. Mazzeo, U.D. Neue, M. Kele, R.S. Plumb, Advancing LC performance with smaller particles and higher pressure, *Anal. Chem.* 77 (2005) 460–467. doi:10.1021/ac053516f.
- [6] M. Gilar, A.E. Daly, M. Kele, U.D. Neue, J.C. Gebler, Implications of column peak capacity on the separation of complex peptide mixtures in single- and two-dimensional high-performance liquid chromatography, *J. Chromatogr. A.* 1061 (2004) 183–192. doi:10.1016/j.chroma.2004.10.092.
- [7] J.M. Davis, J.C. Giddings, Statistical Theory of Component Overlap in Multicomponent Chromatograms, *Anal. Chem.* 55 (1983) 418–424. doi:10.1021/ac00254a003.
- [8] P. Dugo, F. Cacciola, T. Kumm, G. Dugo, L. Mondello, Comprehensive multidimensional liquid chromatography: Theory and applications, *J. Chromatogr. A.* 1184 (2008) 353–368. doi:10.1016/j.chroma.2007.06.074.
- [9] M. Gilar, P. Olivova, A.E. Daly, J.C. Gebler, Orthogonality of separation in two-dimensional liquid chromatography, *Anal. Chem.* 77 (2005) 6426–6434. doi:10.1021/ac050923i.
- [10] D.J.D. Vanhoutte, S. Eeltink, W.T. Kok, P.J. Schoenmakers, Construction and initial evaluation of an apparatus for spatial comprehensive two-dimensional liquid-phase separations, *Anal. Chim. Acta.* 701 (2011) 92–97. doi:10.1016/j.aca.2011.06.004.
- [11] B. Wouters, E. Davydova, S. Wouters, G. Vivo-Truyols, P.J. Schoenmakers, S. Eeltink, Towards ultra-high peak capacities and peak-production rates using spatial three-dimensional liquid chromatography, *Lab Chip.* 15 (2015) 4415–4422. doi:10.1039/c5lc01169h.
- [12] T. Adamopoulou, S. Deridder, T.S. Bos, S. Nawada, G. Desmet, P.J. Schoenmakers, Optimizing design and employing permeability differences to achieve flow confinement in devices for spatial multidimensional liquid chromatography, *J. Chromatogr. A.* 1612 (2020) 1–10. doi:10.1016/j.chroma.2019.460665.

## Chapter 5

- [13] M. Passamonti, I.L. Bremer, S.H. Nawada, S.A. Currivan, A.F.G. Gargano, P.J. Schoenmakers, Confinement of monolithic stationary phases in targeted regions of 3d-printed titanium devices using thermal polymerization, *Anal. Chem.* 92 (2020) 2589–2596. doi:10.1021/acs.analchem.9b04298.
- [14] N. Abdulhussain, S. Nawada, S. Currivan, M. Passamonti, P. Schoenmakers, Fabrication of polymer monoliths within the confines of non-transparent 3D-printed polymer housings, *J. Chromatogr. A.* 1623 (2020) 461159. doi:10.1016/j.chroma.2020.461159.
- [15] F. Matheuse, K. Vanmol, J. Van Erps, W. De Malsche, H. Ottevaere, G. Desmet, On the potential use of two-photon polymerization to 3D print chromatographic packed bed supports, *J. Chromatogr. A.* 1663 (2022). doi:10.1016/j.chroma.2021.462763.
- [16] F. Gritti, S. Nawada, On the road toward highly efficient and large volume three-dimensional-printed liquid chromatography columns?, *J. Sep. Sci.* (2022). doi:10.1002/jssc.202100962.
- [17] G. Guiochon, Monolithic columns in high-performance liquid chromatography, *J. Chromatogr. A.* 1168 (2007) 101–168. doi:10.1016/j.chroma.2007.05.090.
- [18] G. Guiochon, T. Farkas, H. Guan-Sajonz, J.H. Koh, M. Sarker, B.J. Stanley, T. Yun, Consolidation of particle beds and packing of chromatographic columns, *J. Chromatogr. A.* 762 (1997) 83–88. doi:10.1016/S0021-9673(96)00642-5.
- [19] D. Zelenyánszki, N. Lambert, F. Gritti, A. Felinger, The effect of column packing procedure on column end efficiency and on bed heterogeneity – Experiments with flow-reversal, *J. Chromatogr. A.* 1603 (2019) 412–416. doi:10.1016/j.chroma.2019.05.040.
- [20] A.E. Reising, J.M. Godinho, J. Bernzen, J.W. Jorgenson, U. Tallarek, Axial heterogeneities in capillary ultrahigh pressure liquid chromatography columns: Chromatographic and bed morphological characterization, *J. Chromatogr. A.* 1569 (2018) 44–52. doi:10.1016/j.chroma.2018.07.037.
- [21] A.E. Reising, S. Schlabach, V. Baranau, D. Stoeckel, U. Tallarek, Analysis of packing microstructure and wall effects in a narrow-bore ultrahigh pressure liquid chromatography column using focused ion-beam scanning electron microscopy, *J. Chromatogr. A.* 1513 (2017) 172–182. doi:10.1016/j.chroma.2017.07.049.
- [22] R.D. Oleschuk, L.L. Shultz-Lockyear, Y. Ning, D.J. Harrison, Trapping of bead-based reagents within microfluidic systems: On-chip solid-phase extraction and electrochromatography, *Anal. Chem.* 72 (2000) 585–590. doi:10.1021/ac990751n.
- [23] S. Thurmann, A. Dittmar, D. Belder, A low pressure on-chip injection strategy for high-performance chip-based chromatography, *J. Chromatogr. A.* 1340 (2014) 59–67. doi:10.1016/j.chroma.2014.03.009.

- [24] N.P. Macdonald, J.M. Cabot, P. Smejkal, R.M. Guijt, B. Paull, M.C. Breadmore, Comparing Microfluidic Performance of Three-Dimensional (3D) Printing Platforms, *Anal. Chem.* 89 (2017) 3858–3866. doi:10.1021/acs.analchem.7b00136.
- [25] H.K. Versteeg, W. Malalasekera, *An Introduction to Computational Fluid Dynamics - the finite volume method*, 2007.
- [26] C. Lv, J. Heiter, T. Haljasorg, I. Leito, Covalent attachment of polymeric monolith to polyether ether ketone (PEEK) tubing, *Anal. Chim. Acta.* 932 (2016) 114–123. doi:10.1016/j.aca.2016.05.026.
- [27] F. Capriotti, I. Leonardis, A. Cappiello, G. Famiglioni, P. Palma, A fast and effective method for packing nano-*lc* columns with solid-core nano particles based on the synergic effect of temperature, slurry composition, sonication and pressure, *Chromatographia.* 76 (2013) 1079–1086. doi:10.1007/s10337-013-2514-7.
- [28] C.A. Cramers, J.A. Rijks, C.P.M. Schutjes, Factors determining flow rate in chromatographic columns, *Chromatographia.* 14 (1981) 439–444. doi:10.1007/BF02262882.
- [29] H.M. Quinn, A Reconciliation of Packed Column Permeability Data: Column Permeability as a Function of Particle Porosity, *J. Mater.* 2014 (2014) 1–22. doi:10.1155/2014/636507.
- [30] T. Farkas, G. Guiochon, Contribution of the Radial Distribution of the Flow Velocity to Band Broadening in HPLC Columns, *Anal. Chem.* 69 (1997) 4592–4600. doi:10.1021/ac970530m.
- [31] X. Li, D.R. Stoll, P.W. Carr, A Simple and Accurate Equation for Peak Capacity Estimation in Two Dimensional Liquid Chromatography, *Anal. Chem.* 81 (2009) 845–850. doi:10.1021/ac801772u.

# Chapter 6

## Future outlook

### Contents

1.	The STAMP project.....	156
2.	Computational tools.....	158
3.	Microfluidic devices .....	160
4.	Conclusion.....	161
5.	References .....	161

## Abstract

A few aspects of the research described in this thesis are discussed in the present chapter, with focus on future prospects. The main investigational routes are described in the quest for a peak capacity of one million, as formulated in the “Separation Technology for A Million Peaks” (STAMP) project. The main challenges that need to be tackled are manufacturing of devices, introduction of stationary phases, flow confinement and control, retention mechanisms (orthogonality), and detection. Retention modelling has been studied extensively in the context of the present thesis, specifically for hydrophilic-interaction liquid chromatography (HILIC). Retention modelling is essential for developing and optimizing complex separation methods in an efficient and successful manner. A brief outlook on the computational tools required for this purpose is presented in this chapter. All the efforts to realize spatial two- and three-dimensional separations have involved small separation devices, aiming at flow rates well below 1 mL/min. Hence, we aim to use microfluidic devices. A discussion on these and their impact on liquid-chromatographic separations is also provided in this chapter. Finally, some general considerations, recommendations and conclusions are presented.

## 1. The STAMP project

The continuous improvement of separation and detection techniques have inspired scientists to strive for the complete elucidation of highly complex samples. For this to be an attainable goal, a very high peak capacity is essential. Therefore, we made it our goal in the Separation Technology for A Million Peaks (STAMP) project to work towards a peak capacity of one million.

The STAMP project was focused on tackling the most-important challenges from different directions. The answers to these, when brought together, would pave the road towards extremely high peak capacities, which could then serve to complete the puzzle of identifying and understanding the properties of highly complex samples. The main directions in the STAMP project and the progress towards the one million peak capacity goal can be seen in Table 1.

*Table 1: Summary of challenges confronted and results achieved in the STAMP project.*

	<b>Challenge</b>	<b>Main achievements</b>	<b>Ref.</b>
(i)	creation of multidimensional separation devices by the use of 3D-printing and computer-aided design	3D-Printed modular device for 2D separations	Adamopoulou <i>et al.</i> [1] EU patent: EP3598125A1
(ii)	3D-printing technology	Hybrid stereolithography	Nawada <i>et al.</i> [2] EU patent: EP 9170376.8-1022
(iii)	design optimization and flow control, both in practice and	Band broadening investigation by CFD, and testing of 3D printed devices	Adamopoulou <i>et al.</i> [3]

Table 1: Summary of challenges confronted and results achieved in the STAMP project.

<b>Challenge</b>	<b>Main achievements</b>	<b>Ref.</b>
through computational simulations	Temperature controlled flow confinement by creation of freeze-thaw valves	Nawada <i>et al.</i> [4]
	Flow confinement in 3D-LC devices by employing permeability differences between dimensions	Adamopoulou <i>et al.</i> [5]
(iv) introduction of stationary phases and testing of devices	Creation of monolithic stationary phase in 3D-printed polypropylene columns	Abdulhussain <i>et al.</i> [6]
	Confinement of monolithic stationary phases in desired zones of 3D-printed titanium devices	Passamonti <i>et al.</i> [7]
	Creation of monolithic frits and introduction of particles in a glass chip	Abdulhussain <i>et al.</i> [8]
	Introduction of particles in transparent 3D -printed device with multiple outlets	Roca <i>et al.</i>
(v) understanding and optimizing (combinations of) retention mechanisms	Retention modelling for the separation of peptides in HILIC	Roca <i>et al.</i> [9]
	Comprehensive two-dimensional separation of peptides by HILIC×RPLC	Roca <i>et al.</i> [10]
(vi) detection techniques suitable for the analytes and devices in use	Parallel electrochemical detection for 3D printed device with multiple channels	Komendova <i>et al.</i> [11]

## Chapter 6

In this thesis, we have focused on understanding recent developments in liquid chromatography (LC) and how these can be applied to improve two-dimensional separations (Chapter 2). The main advances that were of interest for the design of a 3D separation device were those in column technology, instrument capabilities and miniaturized separation devices. We proceeded with an investigation into the miniaturization of comprehensive two-dimensional LC (LC×LC) for the analysis of peptides by direct coupling with a high-resolution mass spectrometer (HR-MS) (Chapter 4). In choosing the best combination of retention mechanisms for the LC×LC system, we have investigated computational programs for the prediction of retention and the optimization of peptide separations in hydrophilic-interaction liquid chromatography (HILIC) and reversed-phase liquid chromatography (RPLC) (Chapter 3). Finally, we investigated the introduction of particles in a 3D-printed device as a model for a future 3D-spatial-separation device (Chapter 5).

To reach the ultimate goal of a 3D-spatial-separation device with the capability of achieving a peak capacity of one million, further research is still required. The future outlook following the research in this thesis is described in the following sections.

## **2. Computational tools**

In Chapter 2, we showed the use of retention modelling to predict elution of peptides under various conditions and to predict a pareto-optimal separation. A computational approach to data analysis is highly desirable, especially when dealing with multidimensional separations and/or complex samples. One way of tackling the retention-time-prediction challenge was named inverse methods of chromatography [12]. The term “inverse” refers to the

experimental set-up, *viz.* initial separations are performed either in the form of a few scouting (or “scanning”) experiments or following a design of experiments and the resulting data are used to train a gradient model that can predict retention times under various conditions. The advantage of this approach is a faster optimization based on a limited number of runs and on the extensive underlying studies into different retention mechanisms in LC, in which various models have been evaluated [13–16]. Practical limitations of such a model are the need to input the instrument hold-up volume and the dwell volume, the accurate determination of which can cause difficulties when using multiple set-ups, the assumption that gradients are strictly linear without any effects from the column chemistry, the eluents or the instrument, and the use of empirical retention models that are not always validated for the exact experimental conditions.

Looking forward, the introduction of artificial intelligence (AI) is being advocated as an alternative for retention-time prediction and optimization of separations in liquid chromatography. Multiple approaches using AI were reported for retention-time prediction and/or optimization in LC separations in recent years. Some of the approaches are quantitative structure–retention relationship (QSRR) methods [17], least-squares support-vector machines (LSSVM) [18] and ANNs [19]. The use of AI would require large amounts of data to train the algorithm. However, the results would be independent of fundamentals and principles of LC. The most accurate artificial neural network (ANN) reported had a relative error of 5% for the training set and about 9% in the validation set [20]. Generally, such errors are not acceptable, as a 5% difference in (net) retention time may change the results from fully overlapping (*e.g.* retention factors  $k_1 = k_2 = 3$ , resolution  $R_s = 0$ ) to well separated ( $k_1 = 3$  and  $k_2 = 3.15$ ,  $R_s = 1$ ) for two analytes in typical HPLC operation ( $N = 12,000$ ).

### 3. Microfluidic devices

Miniaturization of LC separations, often referred to as capillary LC (capLC), is a powerful tool in analytical chemistry. The attractiveness of capLC is based on its ability to analyse very small amounts of sample, and to obtain higher sensitivity and greater compatibility when coupled to MS. Packed capillary columns can be divided into micro (0.8–0.15 mm ID) and nano (20–100  $\mu\text{m}$  ID) columns, which utilize flow rates of 2–20  $\mu\text{L}/\text{min}$  and 100–1000  $\text{nL}/\text{min}$ , respectively. The use of low flow rates also greatly reduces the solvent consumption [21].

A further development towards miniaturization in analytical chemistry has been the creation of microfluidic devices. This field is often referred to as  $\mu$ -TAS (micro total-analysis system) or as Lab-on-a-chip, and applications can be found, for example, in chemical, biochemical and biomedical domains.

In line with the advantages of capLC, microfluidic devices utilize smaller samples and solvent volumes. A further advantage compared to capLC is the possibility to create various designs with multiple channels or chambers. Therefore, microfluidic devices have become of great interest also for separation science, thanks to its potential for creating a multidimensional separation device on one chip.

Initial microfluidic devices were fabricated in glass, quartz, or silicon substrates by etching, photolithography or deposition techniques. However, the high cost of the substrates, the time-consuming fabrication process, and limitations in channel design made these devices unfavourable [22]. A more suitable alternative was found by the use of polymers. Fabrication of polymeric microfluidic devices can be achieved by various techniques such as micro-milling [23], laser ablation [24], casting [25], 3D-printing [26], *etc.*

Several microfluidic chips have been developed and commercialized for nano-LC separations with MS detection in a plug-and-play format [27–29]. The chips contain a nano-column that can be coupled to a nano-LC pump. Optionally, such chips can have an integrated electrospray emitter for easier coupling to MS detection.

An alternative commercial microfluidic device is the pillar-array column. De Malsche *et al.* [30] proposed the construction of a silicon-based microfluidic device, with ordered pillars that are coated with a hydrophobic monolayer. The use of such a highly ordered system can drastically reduce plate heights and flow resistance, allowing, in principle, very long columns to be used [31]. Reported drawbacks of the current pillar-array columns were a low sample loadability and an increase in band broadening due to imperfect wall etching.

## 4. Conclusion

The work presented in this thesis was focused on investigating retention mechanisms and multidimensional separations for the elucidation of complex samples, such as those found in the field of proteomics. Improvements described in this thesis can be applied in the future also to other fields (for instance, pharmaceutical, food science *etc.*). Future improvement in computational tools for method development, technology for building devices (e.g. 3D-printing) and their operation (e.g. low volume connections), and detection methods are some of the challenges still faced to achieve the goal of one million peaks.

## 5. References

- [1] T. Adamopoulou, S. Deridder, G. Desmet, P.J. Schoenmakers, Two-dimensional insertable separation tool (TWIST) for flow confinement in spatial separations, *J. Chromatogr. A.* 1577 (2018) 120–123. doi:10.1016/j.chroma.2018.09.054.

## Chapter 6

- [2] S.H. Nawada, T. Budel, Novel 3D-Printing Method to Create Liquid Chromatography Columns, *LCGC North Am.* (2021) 414–417.
- [3] T. Adamopoulou, S. Nawada, S. Deridder, B. Wouters, G. Desmet, P.J. Schoenmakers, Experimental and numerical study of band-broadening effects associated with analyte transfer in microfluidic devices for spatial two-dimensional liquid chromatography created by additive manufacturing, *J. Chromatogr. A.* 1598 (2019) 77–84. doi:10.1016/j.chroma.2019.03.041.
- [4] S.H. Nawada, T. Aalbers, P.J. Schoenmakers, Freeze-thaw valves as a flow control mechanism in spatially complex 3D-printed fluidic devices, *Chem. Eng. Sci.* 207 (2019) 1040–1048. doi:10.1016/j.ces.2019.07.036.
- [5] T. Adamopoulou, S. Deridder, T.S. Bos, S. Nawada, G. Desmet, P.J. Schoenmakers, Optimizing design and employing permeability differences to achieve flow confinement in devices for spatial multidimensional liquid chromatography, *J. Chromatogr. A.* 1612 (2020) 1–10. doi:10.1016/j.chroma.2019.460665.
- [6] N. Abdulhussain, S. Nawada, S. Currivan, M. Passamonti, P. Schoenmakers, Fabrication of polymer monoliths within the confines of non-transparent 3D-printed polymer housings, *J. Chromatogr. A.* 1623 (2020) 461159. doi:10.1016/j.chroma.2020.461159.
- [7] M. Passamonti, I.L. Bremer, S.H. Nawada, S.A. Currivan, A.F.G. Gargano, P.J. Schoenmakers, Confinement of monolithic stationary phases in targeted regions of 3d-printed titanium devices using thermal polymerization, *Anal. Chem.* 92 (2020) 2589–2596. doi:10.1021/acs.analchem.9b04298.
- [8] N. Abdulhussain, S.H. Nawada, S.A. Currivan, P.J. Schoenmakers, Fabrication of monolithic frits and columns for chip-based multidimensional separation devices, *J. Sep. Sci.* 45 (2022) 1400–1410. doi:10.1002/jssc.202100901.
- [9] L.S. Roca, S.E. Schoemaker, B.W.J. Pirok, A.F.G. Gargano, P.J. Schoenmakers, Accurate modelling of the retention behaviour of peptides in gradient-elution hydrophilic interaction liquid chromatography, *J. Chromatogr. A.* (2019) 460650. doi:10.1016/j.chroma.2019.460650.
- [10] L.S. Roca, A.F.G. Gargano, P.J. Schoenmakers, Development of comprehensive two-dimensional low-flow liquid-chromatography setup coupled to high-resolution mass spectrometry for shotgun proteomics, *Anal. Chim. Acta.* 1156 (2021) 338349. doi:10.1016/j.aca.2021.338349.
- [11] M. Komendová, S. Nawada, R. Metelka, P.J. Schoenmakers, J. Urban, Multichannel separation device with parallel electrochemical detection, *J. Chromatogr. A.* 1610 (2020). doi:10.1016/j.chroma.2019.460537.

- [12] F. Gritti, Perspective on the Future Approaches to Predict Retention in Liquid Chromatography, *Anal. Chem.* 93 (2021) 5653–5664. doi:10.1021/acs.analchem.0c05078.
- [13] L.M. Blumberg, Theory of gradient elution liquid chromatography with linear solvent strength: Part I. migration and elution parameters of a solute band, *Chromatographia*. 77 (2014) 179–188. doi:10.1007/s10337-013-2555-y.
- [14] L.R. Snyder, H. Poppe, Mechanism of solute retention in liquid—solid chromatography and the role of the mobile phase in affecting separation: Competition versus “sorption,” *J. Chromatogr. A*. 184 (1980) 363–413. doi:10.1016/S0021-9673(00)93872-X.
- [15] U.D. Neue, H.J. Kuss, Improved reversed-phase gradient retention modeling, *J. Chromatogr. A*. 1217 (2010) 3794–3803. doi:10.1016/j.chroma.2010.04.023.
- [16] E. Tyteca, J. De Vos, N. Vankova, P. Cesla, G. Desmet, S. Eeltink, Applicability of linear and nonlinear retention-time models for reversed-phase liquid chromatography separations of small molecules, peptides, and intact proteins, *J. Sep. Sci.* 39 (2016) 1249–1257. doi:10.1002/jssc.201501395.
- [17] C. Veenaas, A. Linusson, P. Haglund, Retention-time prediction in comprehensive two-dimensional gas chromatography to aid identification of unknown contaminants, *Anal. Bioanal. Chem.* 410 (2018) 7931–7941. doi:10.1007/s00216-018-1415-x.
- [18] K. Yu, Y. Cheng, Discriminating the Genuineness of Chinese Medicines Using Least Squares Support Vector Machines, *Chinese J. Anal. Chem.* 34 (2006) 561–564. doi:10.1016/S1872-2040(06)60029-7.
- [19] X.C. Xiong, X. Fang, Y.Z. Ou, Y. Jiang, Z.J. Huang, Y.K. Zhang, Artificial neural networks for classification and identification of data of biological tissue obtained by mass-spectrometry imaging, *Fenxi Huaxue/ Chinese J. Anal. Chem.* 40 (2012) 43–49. doi:10.1016/S1872-2040(11)60525-2.
- [20] T.S. Bos, W.C. Knol, S.R.A. Molenaar, L.E. Niezen, P.J. Schoenmakers, G.W. Somsen, B.W.J. Pirok, Recent applications of chemometrics in one- and two-dimensional chromatography, *J. Sep. Sci.* (2020) 1–50. doi:10.1002/jssc.202000011.
- [21] J. Abian, M. Carrascal, Quantitative Peptide Determination Using Column-Switching Capillary Chromatography Interfaced with Mass Spectrometry, in: 2003: pp. 39–73. doi:10.1016/S0301-4770(03)80006-4.
- [22] S.M. Scott, Z. Ali, Fabrication methods for microfluidic devices: An overview, *Micromachines*. 12 (2021). doi:10.3390/mi12030319.
- [23] B. Wouters, J. De Vos, G. Desmet, H. Terryn, P.J. Schoenmakers, S. Eeltink, Design of a microfluidic device for comprehensive spatial two-dimensional liquid chromatography, *J. Sep. Sci.* 38 (2015) 1123–1129. doi:10.1002/jssc.201401192.

## Chapter 6

- [24] D.L. Pugmire, E.A. Waddell, R. Haasch, M.J. Tarlov, L.E. Locascio, Surface characterization of laser-ablated polymers used for microfluidics, *Anal. Chem.* 74 (2002) 871–878. doi:10.1021/ac011026r.
- [25] S.M. Langelier, E. Livak-Dahl, A.J. Manzo, B.N. Johnson, N.G. Walter, M.A. Burns, Flexible casting of modular self-aligning microfluidic assembly blocks, *Lab Chip*. 11 (2011) 1679–1687. doi:10.1039/c0lc00517g.
- [26] S. Waheed, J.M. Cabot, N.P. Macdonald, T. Lewis, R.M. Guijt, B. Paull, M.C. Breadmore, 3D printed microfluidic devices: Enablers and barriers, *Lab Chip*. 16 (2016) 1993–2013. doi:10.1039/c6lc00284f.
- [27] H. Yin, K. Killeen, The fundamental aspects and applications of Agilent HPLC-Chip, *J. Sep. Sci.* 30 (2007) 1427–1434. doi:10.1002/jssc.200600454.
- [28] A. Kecskemeti, A. Gaspar, Particle-based liquid chromatographic separations in microfluidic devices - A review, *Anal. Chim. Acta.* 1021 (2018) 1–19. doi:10.1016/j.aca.2018.01.064.
- [29] D.A. Vargas Medina, E.V.S. Maciel, F.M. Lanças, Miniaturization of liquid chromatography coupled to mass spectrometry. 3. Achievements on chip-based LC–MS devices, *TrAC - Trends Anal. Chem.* 131 (2020) 116003. doi:10.1016/j.trac.2020.116003.
- [30] W. De Malsche, H. Eghbali, D. Clicq, J. Vangeloooven, H. Gardeniers, G. Desmet, Pressure-driven reverse-phase liquid chromatography separations in ordered nonporous pillar array columns, *Anal. Chem.* 79 (2007) 5915–5926. doi:10.1021/ac070352p.
- [31] W. De Malsche, J. Op De Beeck, S. De Bruyne, H. Gardeniers, G. Desmet, Realization of  $1 \times 10^6$  theoretical plates in liquid chromatography using very long pillar array columns, *Anal. Chem.* 84 (2012) 1214–1219. doi:10.1021/ac203048n.



## Overview of co-authors' contributions

### Chapter 1 Introduction

**Liana S Roca:** Wrote the introduction focusing on the importance of multidimensional separations.

**Peter J Schoenmakers:** Guidance for chapter structure, reviewed the chapter and made suggestions for improvement.

### Chapter 2 How two-dimensional liquid chromatography can benefit from recent technological advances

**Liana S Roca:** Wrote the literature review on progress in two-dimensional liquid chromatography thanks to the technological advances.

**Peter J Schoenmakers:** Guidance for chapter structure, reviewed the chapter and made suggestions for improvement

### Chapter 3 Accurate modelling of the retention behavior of peptides in gradient-elution hydrophilic-interaction liquid chromatography

**Liana S. Roca:** Co-developed the idea, planned and performed experiments, performed the modelling work, wrote the manuscript.

**Suzan E. Schoemaker:** Performed a significant part of the experiments.

**Bob W. J. Pirok:** Helped with bringing the idea to fruition, supported the modelling work, reviewed the manuscript and made suggestions for improvement.

**Andrea F. G. Gargano:** Consulted on various aspects of HILIC, reviewed the manuscript and made suggestions for improvement.

**Peter J. Schoenmakers:** General support and supervision, reviewed the manuscript and made suggestions for improvement.

**Chapter 4** Development of comprehensive two-dimensional low-flow liquid- chromatography setup coupled to high- resolution mass spectrometry for shotgun proteomics

**Liana S. Roca:** Co-developed the idea, planned and performed experiments, wrote the manuscript.

**Andrea F.G. Gargano:** Co-developed the idea, supported the experimental work, reviewed the manuscript and made suggestions for improvement.

**Peter J. Schoenmakers:** General support and supervision, reviewed the manuscript and made suggestions for improvement.

**Chapter 5** Introduction of octadecyl-bonded porous particles in 3D-printed transparent housings with multiple outlets

**Liana S. Roca:** Co-developed the idea, planned and performed experiments, wrote the manuscript.

**Theodora Adamopoulou:** Co-developed the idea, performed the 3D printing work, reviewed the manuscript and made suggestions for improvement.

**Suhas H. Nawada:** Consulted on various aspects of calculations for the device parameters, realization of one of the figures, reviewed the manuscript.

**Peter J. Schoenmakers:** General support and supervision, reviewed the manuscript and made suggestions for improvement.

## **Chapter 6** Conclusion/ Future outlook

**Liana S Roca:** Wrote the future outlook on retention modelling and microfluidic devices.

**Peter J Schoenmakers:** Guidance for chapter structure, reviewed the chapter and made suggestions for improvement

## Summary

Increasing peak capacity has become a critical need for the analysis of complex samples, such as those encountered in the field of proteomics. State-of-the-art one-dimensional liquid chromatography (1D-LC) can provide a limited peak capacity, constrained by the time of analysis and the maximum permissible pressure of the column and system. To circumvent the limitations of 1D-LC, further separation dimensions can be added to increase peak capacity. Comprehensive column-based two-dimensional LC has already become a widely used tool. However, it still requires great knowledge and complex setups.

The desired multidimensional separation device would employ spatial separations. The peak capacity could be greatly improved, while the simultaneous development all separations in the second and the eventual third dimension would allow for short analysis times. Such a device, even at modest pressures, could yield peak capacities in the order of one million.

The objectives of the research described in this thesis were to explore implementation of multidimensional separations for peptides, combinations of retention mechanisms, optimization of separations, and operation of 3D-printed devices.

In Chapter 1 an introduction is given to the need of multidimensional separations and the critical aspects needed to be considered for improvements.

Chapter 2 provides a comprehensive review of the latest advancements in one-dimensional liquid chromatography (1D-LC) that have impacted the development of column-based two dimensional LC. The main need for advancing LC×LC was deemed to be speed of the second dimension

separation. Several improvements in column and system technology have proven useful for realizing fast separations in the timeframe of seconds. These include stationary-phase development (sub-2- $\mu\text{m}$  particles, core-shell particles, monoliths, temperature-stable packings), systems that can operate at ultra-high pressures, use of supercritical fluids, and advances in the field of microfluidics.

In Chapter 3 the separation of peptides by hydrophilic-interaction LC (HILIC) was investigated. An experimental data set was created using three HILIC columns and different mobile-phase modifiers, using various gradient conditions and mass-spectrometric (MS) detection. The data set was used to test several retention models in order to predict retention times and optimize the separation of a model sample (BSA digest). It was shown that accurate prediction of retention times was possible for peptides in HILIC, using a small set of experiments.

Chapter 4 describes the construction of a low-flow comprehensive two-dimensional separation setup for peptides. Due to the small amounts of samples typically available in proteomics studies, miniaturized 1D-LC separations have become the gold standard. To improve the separation capacity, we proposed a two-dimensional separation using HILIC $\times$ RPLC coupled to high-resolution MS (HR-MS). Complete transfer of all fractions of the first-dimension effluent to the second dimension was achieved by active modulation with C18 trap columns. We demonstrated an increase in peak capacity and in the number of peptides identified without an increase in total analysis time.

In Chapter 5 the introduction of C18 particles in a 3D-printed device was investigated. Unlike a 1D column, the envisioned multidimensional separation devices come with challenges, such as flow distribution, multiple outlets, large

separation blocks, *etc.* The work in Chapter 5 shows a proof-of-principle device containing a flow distributor, four outlets and a cuboid separation space. The proposed device was used to investigate packing methods for transparent 3D-printed housings, containment of particles, and separation in a cuboid space with multiple outlets. Successful packing of the device with C18 particles was achieved. Separation of peptide standards was demonstrated by coupling of the device to a mass spectrometer.

In Chapter 6 the future outlook of the work described in the above chapters is discussed, with some general recommendations for optimization tools and microfluidics.

## Samenvatting

Een hogere piekcapaciteit is een kritische noodzaak geworden voor de analyse van complexe monsters, zoals die die zich aandienen op het gebied van *proteomics*. Met de huidige stand van de techniek kan ééndimensionale vloeistofchromatografie (1D-LC) een beperkte piekcapaciteit bieden, doordat de analysetijd en de maximum druk begrensd worden door de kolom en het instrument. Om de beperkingen van 1D-LC te omzeilen en om de piekcapaciteit te verhogen kunnen meer scheidingsdimensies worden toegevoegd. Alomvattende (“*comprehensive*”) tweedimensionale LC (LC×LC) is een al veelgebruikte techniek, die echter nog wel veel kennis en complexe apparatuur vereist.

Het gewenste multidimensionale systeem zou gebaseerd moeten zijn op ruimtelijke scheidingen. Daardoor zou de piekcapaciteit sterk verhoogd kunnen worden, terwijl de gelijktijdige ontwikkeling van alle scheidingen in de tweede en eventuele derde dimensie korte analysetijden mogelijk zouden maken. Een dergelijk systeem zou zelfs met een bescheiden druk piekcapaciteiten van de orde van een miljoen mogelijk moeten maken.

De doelen van het in dit proefschrift beschreven onderzoek betroffen de exploratie van meerdimensionale scheidingen van peptiden, combinaties van verschillende retentiemechanismen, de optimalisering van scheidingen en het gebruik van met 3D-printing vervaardigde apparaten.

Hoofdstuk 1 bevat een inleiding in multidimensionale scheidingen, de noodzaak daarvan en de kritische aspecten waarmee rekening gehouden moet worden om de systemen te verbeteren.

Hoofdstuk 2 omvat een uitgebreid overzicht van de meest recente ontwikkelingen op het gebied van ééndimensionale LC die de ontwikkeling van op kolommen gebaseerde tweedimensionale chromatografie hebben beïnvloed. De snelheid van de scheiding in de tweede dimensie werd geïdentificeerd als de belangrijkste behoefte. Verschillende verbeteringen in kolom- en instrumenttechnologie zijn nuttig gebleken om snelle scheidingen – binnen het tijdsbestek van enkele seconden – te realiseren. Daaronder vallen ontwikkelingen op het gebied van stationaire fasen (sub-2- $\mu\text{m}$  deeltjes, deeltjes met een harde kern en een poreuze buitenlaag, monolieten en temperatuur-stabiele deeltjes), systemen die een ultrahoge druk leveren, superkritische mobiele fasen en “*microfluidics*”.

In Hoofdstuk 3 werd de scheiding bestudeerd van peptiden met behulp van “*hydrophilic-interaction*” LC (HILIC). Een experimentele data set werd gecreëerd voor drie HILIC kolommen en verschillende oplosmiddelen in de mobiele fase, bij verschillende gradiëntcondities en met massaspectrometrische (MS) detectie. De data set werd gebruikt om verscheidene retentiemodellen te testen, zodat retentietijden voorspeld konden worden en scheidingen van een modelmengsel (BSA digest) konden worden geoptimaliseerd. Aangetoond werd dat een juiste voorspelling van retentietijden van peptiden in HILIC mogelijk was op basis van een klein aantal experimenten.

In Hoofdstuk 4 wordt de constructie beschreven van een LC $\times$ LC systeem voor de scheiding van peptiden met lage vloeistofdebieten. Vanwege de kleine hoeveelheden monsters die doorgaans beschikbaar zijn in onderzoek op het gebied van *proteomics* zijn geminiaturiseerde 1D-LC systemen uitgegroeid tot de “gouden standaard”. Om het scheidend vermogen te vergroten hebben wij een tweedimensionaal systeem voorgesteld, bestaande uit HILIC $\times$ RPLC in combinatie met hoge-resolutie MS (HR-MS). De volledige transfer van alle

fracties van het effluent van de eerste dimensie naar de tweede dimensie werd bereikt door “actieve modulatie” met C18 trap-kolommen. We hebben een toename in de piekcapaciteit en in het aantal geïdentificeerde peptiden aangetoond, zonder de analysetijd te laten toenemen.

In Hoofdstuk 5 werd het inbrengen van C18 deeltjes in 3D-geprinte apparaatjes bestudeerd. In vergelijking met eendimensionale kolommen biedt dit uitdagingen, zoals een goede verdeling van de vloeistofstroom, meerdere uitgangen, een relatief groot scheidingsblok, enzovoort. Het in Hoofdstuk 5 beschreven werk toont een principemogelijkheid voor een apparaat met een stroomverdeler, vier uitgangen en een kubusvormig scheidingsdomein. Het voorgestelde ontwerp werd gebruikt om methoden te bestuderen om deeltjes te pakken in transparante omhulsels vervaardigd met behulp van 3D-printing, om de deeltjes daar vast te houden en om scheidingen te verrichten. C18 deeltjes werden met succes gepakt in het apparaat. De scheiding van peptiden werd gedemonstreerd door het apparaat te koppelen aan een massaspectrometer.

In Hoofdstuk 6 worden vooruitzichten besproken voor het in eerdere hoofdstukken besproken werk, waarbij enkele algemene aanbevelingen worden geformuleerd voor optimaliseringsprogramma's en *microfluidics* systemen.

## List of Publications

- [1] B.W.J. Pirok, S.R.A. Molenaar, L.S. Roca, P.J. Schoenmakers, Peak-Tracking Algorithm for Use in Automated Interpretive Method-Development Tools in Liquid Chromatography, *Anal. Chem.* 90 (2018) 14011–14019. doi:10.1021/acs.analchem.8b03929.
- [2] A.F.G. Gargano, L.S. Roca, R.T. Fellers, M. Bocxe, E. Domínguez-Vega, G.W. Somsen, Capillary HILIC-MS: A New Tool for Sensitive Top-Down Proteomics, *Anal. Chem.* 90 (2018) 6601–6609. doi:10.1021/acs.analchem.8b00382.
- [3] L.S. Roca, S.E. Schoemaker, B.W.J. Pirok, A.F.G. Gargano, P.J. Schoenmakers, Accurate modelling of the retention behaviour of peptides in gradient-elution hydrophilic interaction liquid chromatography, *J. Chromatogr. A.* (2019) 460650. doi:10.1016/j.chroma.2019.460650.
- [4] A.F.G. Gargano, O. Schouten, G. Van Schaick, L.S. Roca, J.H. Van Den Berg-verleg, R. Haselberg, M. Akeroyd, N. Abello, G.W. Somsen, Profiling of a high mannose-type N-glycosylated lipase using hydrophilic interaction chromatography-mass spectrometry, *Anal. Chim. Acta.* 1109 (2020) 69–77. doi:10.1016/j.aca.2020.02.042.
- [5] L.S. Roca, A.F.G. Gargano, P.J. Schoenmakers, Development of comprehensive two-dimensional low-flow liquid-chromatography setup coupled to high-resolution mass spectrometry for shotgun proteomics, *Anal. Chim. Acta.* 1156 (2021) 338349. doi:10.1016/j.aca.2021.338349.
- [6] L.S. Roca, T. Adamopoulou, S.H. Nawada, P.J. Schoenmakers, Introduction of Octadecyl - Bonded Porous Particles in 3D - Printed Transparent Housings with Multiple Outlets, *Chromatographia.* (2022). doi:10.1007/s10337-022-04156-w.

## Acknowledgements

The end of this thesis also represents an end of a wonderful chapter and a start to many more. It has been a time that formed me as a scientist and all of this would not have been possible without the many people around me.

The first thanks that I would like to give is to my family, so I will switch to Romanian:

Cel mai mare multumesc si multa apreciere o am pentru familia mea. Ati fost mereu alaturi de mine si mi-ati oferit support oricand am avut nevoie. Nu as fi ajuns aici fara ajutorul vostru, incurajarile, compania voastra si multele conversatii la telefon care mi-au adus intodeauna zambetul pe buze. Parinti, Cristina si Alex va multumesc din suflet!

To my promoter, Peter Schoenmakers, I would like to say a big thank you for giving me this opportunity, for the constant support, valuable lessons and a constant push to network and present our work. I would like to thank also my co-promoter, Andrea Gargano, for all the support and invaluable lab skills.

A big thank you goes to all my co-authors for a big support and exciting discussions.

I send a big thank you to my committee for agreeing to be part of my last day as a PhD student and for their great work that has been a source of inspiration throughout my PhD.

I would also like to acknowledge all the friends that I met since arriving in Amsterdam and all the friends that came before. I strongly believe that life is always sweeter with some fun and some distraction, not only work. You have all been a great help during these years. My paranymphs, Alan and Dorina,

were a great part of this, incredibly supportive both in my personal life and at work.

Dorina, you will always be the best roommate ever and I will never forget coming up with the idea for our last paper during our morning coffee, filled with excitement.

Alan, I will always miss our scientific and philosophical discussions (and constantly disagreeing with you). Oh, and not to forget, playing cards.

Tom, thank you for being there for me.

And finally, a thank you to all the people at UvA, VU and lately at Janssen that I had the pleasure to meet during this time.